EXPERIMENTAL INVESTIGATION OF ULTRA-HIGH VACUUM ADHESION AS RELATED TO THE LUNAR SURFACE

FOURTH QUARTERLY PROGRESS REPORT
AND 1ST YEAR SUMMARY

1 APRIL THROUGH 30 JUNE 1965
DOUGLAS REPORT SM-47914

EXPERIMENTAL INVESTIGATION OF ULTRA-HIGH VACUUM ADHESION AS RELATED TO THE LUNAR SURFACE

FOURTH QUARTERLY PROGRESS REPORT AND 1ST YEAR SUMMARY

1 APRIL THROUGH 30 JUNE 1965
DOUGLAS REPORT SM-47914

PREPARED BY: J.A. RYAN
PRINCIPAL INVESTIGATOR
R&D/LUNAR AND PLANETARY
SCIENCES BRANCH

PREPARED FOR:
NASA/OFFICE OF
ADVANCED RESEARCH & TECHNOLOGY
WASHINGTON, D.C.

CONTRACT NAS7 307

DATE OF ISSUE:
26 JUNE 1964
A-830-BBK3-9

DOUGLAS MISSILE & SPACE SYSTEMS DIVISION

TABLE OF CONTENTS

TABLE OF CONTENTS Cont'd

ABSTRACT

33849

This report presents the results obtained during the past year on the ultra-high vacuum adhesion of silicates as related to the lunar surface. Silicates, such as may exist at the lunar surface, were contacted with silicates and with engineering materials which may be used at the lunar surface. The adhesion was measured as a function of load force, temperature, and type of material. Load forces up to about 1000 grams were applied; temperature was varied from about 100°K to about 400°K, approximately the lunar temperature range. Adhesion as small as 20μg could be detected. Materials used were orthoclase, albite, bytownite, hornblende, hypersthene, and obsidian among the silicates; aluminum, magnesium, titanium alloy, Stainless Steel, and beryllium among the metals; a ceramic (alumina) and a commercial glass. A definite load dependence for the adhesion was detected. For some samples no adhesion was detected at low loadings, but as load was increased the adhesion increased rapidly to relatively large values (generally hundreds of milligrams). All evidence indicates that this behavior is produced by the action of the normal atomic bonding forces. For other samples, however, adhesion was present at low loading, but it increased only slightly with increasing load, reaching a maximum value of only a few milligrams at most. The evidence indicates that the dispersion forces were responsible for this behavior. No effect of temperature on the adhesion was detected.

Author

1.0 INTRODUCTION

1.1 General

This report presents a summary of work accomplished during the period July 1, 1964 through July 1, 1965 on the study of the ultra-high vacuum frictional-adhesional behavior of silicates as related to the lunar surface.

1.2 Purpose and Importance of Program

The primary purpose of this program is to obtain quantitative experimental data concerning the ultra-high vacuum adhesional-frictional behavior of the materials which may presently exist at the lunar surface (primarily silicates), and between these and engineering materials which may be placed upon this surface. Additional purposes are to analyze these data with regard to the possible reactions of granular lunar materials to engineering operations, and to investigate means by which the problems, if any, posed by these reactions may be minimized.

The importance of this program is that adhesional-frictional phenomena may pose serious problems to lunar surface operations.

1.3 Approach

The approach used during the first year of this study has been to obtain quantitative data relating to the adhesion force as a function of load force, temperature, type of silicate, crystalline orientation, and surface preparation; and then to use these data to analyze the possible behavior of silicates at the lunar surface and the problems this may pose to lunar operations.

Single crystals of each mineral were used since this allows one to obtain understanding as to the basic physics of silicate behavior in ultra-high vacuum. Load forces were applied by means of an electromagnet; adhesion force was measured by means of a torsion microbalance. Details of the experimental techniques employed are given in following sections.

2.0 THE SILICATES

It is of interest, since the majority of effort during this study is concentrated upon the silicates, to outline briefly the physical nature of silicate systems such as occur in terrestrial and meteoritic materials.

The silicates are as a whole highly stable structures. The basic building unit of all silicates is the silica tetrahedron consisting of a silicon atom (at the center) surrounded by four oxygens (at the vertices). The silicon-oxygen bond is intermediate between a pure covalent and pure ionic type. The wide diversity within the silicate family can be explained by the varying degrees to which these oxygen atoms are shared by a second silicon, also by the fact that there are a number of other atoms which can either substitute for the silicon (such as aluminum) or can enter into the general lattice (such as potassium, sodium, calcium, barium, aluminum, and OH^- radical). On the basis of oxygen sharing the silicates are generally grouped into six classes: independent tetrahedral groups (the orthosilicates); double tetrahedral structures (dimers); ring structures; chain structures; sheet structures; and three dimensional networks. A wide variety of mineral types are found within each class due to the introduction into the lattice of various different atoms.

The general characteristics of each class are as follows:

(1) Independent Tetrahedral Groups

No oxygens are shared and each silica tetrahedron is in this sense independent of all others. The crystal integrity is maintained by bonding between the oxygens and cations other than silicon. Examples of this type of structure are olivine (an important constituent of meteorites) and the epidote group of minerals.

(2) Double Tetrahedral Structures

The tetrahedra occur in pairs with a single oxygen per pair being shared. Each pair is separated from all other pairs, the remaining oxygens bonding with cations other than silicon. An example of this type of structure is shown by hemimorphite.

(3) Ring Structures

Two oxygen atoms per tetrahedron are shared. The tetrahedra form rings containing two, three, four or six tetrahedra per ring. The remaining oxygens bond with cations other than silicon. An example of this class is beryl (six tetrahedra per ring).

(4) Chain Structures

(a) Single Chain

Two oxygens per tetrahedron are shared and the tetrahedra are joined into chains of "infinite" extent. The chains normal to their length are bonded by means of linkages between the remaining oxygens and cations other than silicon. An example of this type of structure is given by the pyroxene group of

minerals, relatively important constituents of terrestrial igneous rocks, particularly the more basic varieties, and meteorites.

(b) Double Chains

The tetrahedra share alternately two and three oxygens forming double linked chains of "infinite" extent. The chains, normal to their length, are bonded by means of linkages between the remaining oxygens and cations other than silicon. An example of this type of structure is given by the amphibole group of minerals.

(5) Sheet Structures

Three oxygen atoms are shared per tetrahedron, the remaining oxygen bonding with cations other than silicon. The silicon bonded oxygens form parallel planes of "infinite" extent. An outstanding example of this type of structure is given by the micas, relatively common constituents of terrestrial igneous rock.

(6) Three-Dimensional Networks

All oxygens of each tetrahedra are shared with adjacent tetradehra. The diversity of minerals in this class results from the replacement of some of the silicon atoms and the introduction of additional atoms into the structure to maintain charge neutrality. An example of this type of structure is given by the feldspars, most important rock and meteorite constituents.

The silicates are characterized by significant variation in bond strengths and bond types. The ionic-covalent type bonds dominate, and within any given mineral two or more bond types (within the ionic-covalent extremes) are common. Cleavage, a characteristic feature of many silicates, is thus explained as being due to the presence of weaker (ionic) bonding in certain directions; also of course in part to the geometric configurations of the atoms in the lattice.

It is of interest, in the light of these comments, to consider what the ultra-high vacuum frictional-adhesional behavior of silicates may be. First, since the silicate bonding varies within degrees of being more ionic or more covalent, and several different types of bonds can exist in a single mineral crystal, this implies that the strength of adhesion for silicates should be sensitive both to type of crystal and to crystal orientation (assuming of course that the structure of a surface reflects to some degree the structure of the crystal interior).

Second, ionic-covalent bonds are more directional than metallic bonds and this implies that, to the degree to which this difference is important, the adhesional forces between silicates should be significantly less than those between metals (it also implies a decided crystal orientation sensitivity). Finally, the relative hardness and brittleness of silicates also implies some significant degree of elastic recovery upon removal of load. This also indicates that silicate adhesion may be less than that of the metals, at least for those metals found to adhere.

In any comprehensive treatment of the ultra-high vacuum frictional-adhesional

behavior of silicates, representatives from each of the classes noted in this section should be investigated. However, for the present study it is of more importance to investigate the common silicate minerals such as may predominate at the lunar surface. This is used as the primary criterion for sample choice. The samples chosen for study, as well as the reasons for their choice, are discussed in a following section. It is worthwhile noting, however, that the above structural groups which contain the most common igneous and meteoritic-contained silicates are: the independent tetrahedral groups, the chain structures, the sheet structures, and in particular the three dimensional networks.

3.0 SUMMARY OF PREVIOUS WORK

3.1 Concepts of Friction and Adhesion

The generally accepted theory of friction is the so-called "adhesional" or "weld junction" theory developed by Bowden and many others. It is so well known that only the barest outline of it need be given. This theory states that when two surfaces are placed in contact the load is borne by a few contacting surface asperities. The high pressures developed cause plastic flow until the true area of contact is sufficient to support the load. At these points of contact atoms of one surface are within range of the attractive forces of the atoms of the other surface and adhesive bonds are formed. The strength of these bonds depends upon whether the interactions are between atoms of the bulk material or between surface contaminants, being greatest in the absence of contamination. This leads immediately to the concept that friction is produced by the force required to shear these bonds.

This theory, developed principally for metals, has been applied with a

reasonable degree of success to the non-metals as well (see for instance the list of references to this work given by Walton [1962]). Regardless of the success achieved to date, the theory remains as an incomplete, and in certain cases a somewhat dubious, solution to the friction (and adhesion) question. This is not completely unexpected, however, since friction and adhesion phenomena relate to surface interactions and bulk reactions, many of which are not well understood. It is worth enumerating (and discussing where applicable) some of the uncertainties involved.

An important concept in the "adhesion" theory is that of plastic flow. By assuming plastic flow at the few contacting asperities, and that the yield and shear strengths of the material remain constant, it is possible to satisfy Amonton's Laws (which are themselves, it should be noted, not of universal validity). However, it has been noted by Archard (1961) and others that the invoking of plastic flow is not necessary to explain these Laws. According to Archard, if one permits multiple contacts (significantly greater than three), Amonton's Laws can be satisfied with purely elastic asperity deformation. The possible reality of this effect in certain cases has received partial verification from the work of Dyson and Hirst (1954). Nevertheless, it does not appear that Archard's mechanism could be generally operative, since it depends upon what could be called a certain "regularity" (in height) in the surface roughness. However, it is possible that under certain conditions of surface preparation (for instance during polishing) such regularity could well be produced. This possibility points out one variable of frictional phenomena not explicitly considered in the adhesion theory: surface preparation.

There are two other important factors relating to surface preparation. These are the degree of surface roughness and the effect of surface preparation upon the physico-chemical state of the surface and near surface layers. The significant frictional role played particularly by extreme surface roughness is obvious. For most engineering applications the roughness is such that it is generally disregarded as a separate frictional term. However, for the understanding of soil behavior it becomes of considerable importance. Significant physico-chemical changes can be produced by polishing. In particular, a glassy or crypto-crystalline state can be formed in the immediate surface layers. This effect, though of considerably less importance for silicates than for metals, must be taken into account. Its importance to frictional phenomena will become evident shortly when the roles played by crystalline structure and the nature and types of atomic bonding are discussed.

One consequence of the "adhesion" theory of friction is that a finite force should be required to separate contacting surfaces. This force has indeed been detected, but only under certain conditions. One such condition is vacuum where with suitable surface cleaning many, but not all, materials have been found to adhere, some quite strongly. Unfortunately, despite these findings, essentially no quantitative data are available. Another condition under which materials on occasion have been found to adhere is when one or both is of sufficiently low hardness (or the load force sufficiently high) for a large amount of bulk plastic flow to occur. The lack of observable adhesion in many cases has been ascribed variously as being due to the action of released elastic stresses, the presence of oxide layers, the presence of adsorbed gases, and/or the general incompatibility of the materials comprising the surfaces.

It is reasonable to expect that for contacting surfaces, unless the materials are quite soft, upon release of load some degree of elastic recovery will occur. This elastic recovery will tend to break junctions formed during the prior loading. The introduction of elastic recovery brings a whole host of new variables into the frictional-adhesional phenomena. These relate directly to the bulk physical properties of the material such as hardness, the elastic and plastic parameters, and strength (tensile, yield, shear, compressional, and theoretical); and to such considerations as junction geometry (relating particularly to stress concentrations) and temperature.

It has been found (see for instance Walton [1962]) that elastic recovery is not sufficient to account for the often noted lack of observable adhesion. Calculations indicate that if this were the only factor operative then easily measurable adhesion should remain in essentially all cases, at zero load. This difficulty led in part to consideration of the role played by oxide films (on metals: metallic friction historically having received most attention). One possible role of oxide films had been known for some time, the argument being that increased elastic recovery occurs in the presence of an oxide layer (harder than underlying metal) and hence in the presence of such a layer the adhesion, under zero load, would be much less than that of the pure metal alone. However, a new possible role was uncovered, this pertaining to the type of atomic bonds formed across the interface. The metallic bond, being highly non-directional, can tolerate a significant amount of atomic mis-match across the interface and yet still produce strong adhesion. The oxide bonds, on the other hand, are considerably more directional, and hence unless a perfect or near-perfect atomic match were made across the interface the resultant

adhesion may be quite weak. A similar role has been postulated for adsorbed gas films. These films when present are believed to keep the materials separated to the extent that the normal atomic bonding forces cannot come into play across the interface. The only remaining active forces are then the weak attractive forces between the absorbed gas molecules (alternatively, under certain conditions, the dispersion forces). These concepts, which appear to be valid, add additional variables to frictional phenomena: atomic bond type(s) present and acting (directionally and strength) and crystalline structure. The importance of the physico-chemical natures of the surface and near-surface structure, as well as alterations in these through surface preparation, noted earlier, and exposure to the atmosphere now become apparent.

These concepts led to the introduction of the "work of adhesion" by Rabinowitz (1961), a quantity associated with the surface free energy which in turn is some function of the atomic bond types, crystal structure, and crystalline orientation. This concept and the problems associated with it have been discussed by Spalvins and Keller (1962). Experimental data relating to this concept and indicating the importance of the contained variables have been obtained by Spalvins and Keller (1962), Riesz and Weber (1962), Duwell (1962), Steijn (1963), Roshon (1964) and others. Unfortunately, a considerable amount of work remains to be done before a detailed understanding of these variables can be achieved.

The various variables of frictional-adhesional phenomena are listed, for convenience, in Table 1. Though these may appear to cover the entire list of possible variables, there is no assurance that this is actually

the case. Also, it is difficult at present to weigh the relative importance of each.

TABLE I

Variables Relating to Frictional-Adhesional Phenomena

Atomic Related Variables

Bonding forces acting - type, strength, directionality

Crystalline structure

Interface Related Variables

Roughness (including roughness regularity)

Contamination (type and degree of)

Junction Geometry

Crystalline Orientations

Chemical Composition

Physico-Chemical Surface State

Bulk Related Variables

Hardness

Elastic and Plastic Properties

Strength Properties

Miscellaneous

Temperature

3.2 Experimental Evidence for Silicate Adhesion

The earliest work of interest appears to be that by Tomlinson (1928, 1930) and by Stone (1930). Tomlinson measured adhesion between glass and quartz (not strictly, at least historically, a silicate) balls and fibers, detecting forces between the spheres as large as one gram. Tomlinson's results, particularly his interpretations of the adhesion as being atomic were challenged by Stone, but apparently no satisfactory resolution of their differences was achieved. It should be noted, however, that the work was done in air and even though careful cleaning techniques were used, a reasonably large amount of surface contamination, particularly adsorbed water, was undoubtedly present. More recently, Harper (1955) performed adhesion experiments with quartz spheres, in air, finding adhesional forces as large as 0.15 gm. Though he presented convincing arguments that these forces were not due to surface charging, it is likely that at least a mono-layer of adsorbed water was present and hence it is difficult to say what fraction of this adhesion force was indeed due to atomic quartz-quartz interactions. A few additional experiments with micas have been performed but these are of no particular use to the present problem.

It has not been until the last few years that the first experiments in vacuum were performed. These have demonstrated the presence of silicate adhesion. Salisbury et al. (1964) conducted experiments with polycrystalline silicate powders at a vacuum in the mid 10^{-10} mm Hg range. They found adherence of the powder grains ($\approx$5 microns in diameter) and made a rough calculation that the adhesion force was $\approx 2\text{-}3 \times 10^{-7}$ gm. In these experiments there was no high temperature or other (e.g., ionic-electronic) outgassing

attempted and the adhesion was that under essentially zero prior load. This work was followed by that of Stein and Johnson (1964) who studied larger grains (up to 140 microns in diameter) at pressures of 6.3×10^{-10} to 1.3×10^{-9} mm Hg and with one day outgassing at about 100°C. They found that the force of adhesion (with no prior loading) increased with particle size, being in excess of $\approx 30\mu g$ for the larger particles. They noted that if prior loading had been used the adhesion force may have been significantly greater than this. Additional experiments have been performed by Halajian (1964), also upon powders, using grains of about 40 microns in diameter. The pressures obtained were in the high 10^{-10} mm Hg range and the system was maintained continuously at 200°C. From Halajian's results one can make a rough calculation as to the adhesion force, utilizing the method applied by Salisbury, finding that it was at least $30\mu g$.

4.0 POSSIBLE ADHESION PRODUCING FORCES

The primary bonding forces for the silicates are of the ionic-covalent type (e.g., intermediate between the ionic and covalent extremes). In addition to these there are forces such as the London-Van der Waals (dispersion) and surface electrostatic which though playing no significant role in silicate bonding can be of importance to investigations of silicate adhesion.

4.1 Ionic-Covalent Bonding Forces

As noted above, these are the primary binding forces of the silicate lattice. They are also the primary binding forces for the various metal oxides. These forces are highly directional and hence should show a significant crystalline orientation dependence. They are also, in general, the only

forces of sufficient strength to produce surface disruption and material transfer. These forces have the shortest range of effective action of all forces considered here, and hence their effectiveness is highly sensitive to the degree of surface contamination present.

4.2 Dispersion Forces (London-Van der Waals)

The London-Van der Waals forces can contribute significantly to silicate adhesion, as evidenced by the work of Bradley (1932), Lowe and Lucas (1953), Jordan (1954), and Derjaguin et al. (1954). Though these forces, between two atoms, are quite small and decrease in strength rapidly with atomic separation, they are additive and hence in solid specimens can provide detectable (at least by the techniques used in the present experiment) adhesion.

These forces have a range of effectiveness much greater than that of the ionic-covalent forces, but less than that for the forces produced by electrostatic surface charging. The force-distance relationships for these dispersion forces have been calculated theoretically and verified experimentally (for surface separations greater than about a tenth of a micron). This experimental verification of theory is of particular interest since it indicates that even though the theory was developed for molecular solids, it is more or less applicable to silicates (most of the experiments were performed upon quartz and fuzed silica).

For two parallel plates, the equations expressing the dispersion force behavior are

$$F \text{ (dynes cm}^{-2}) = \frac{2.6 \times 10^{-15}}{h^3 \text{ (cm)}} \qquad h < 200A^\circ$$

$$F \text{ (dynes cm}^{-2}) = \frac{10^{-19}}{h^4 \text{ (cm)}} \qquad h > 2000A^\circ$$

where F = attractive force per unit area and h = separation of the surfaces. The magnitude of the adhesion produced by dispersion forces is then, for various surface separations (assuming atomically flat surfaces):

h (microns)	F (dynes cm^{-2})	Experimental Verification
2×10^{-4} ($2A^\circ$)	3×10^{8}	No
5×10^{-4} ($5A^\circ$)	2×10^{7}	No
10^{-3} ($10A^\circ$)	2.6×10^{6}	No
10^{-2} ($100A^\circ$)	2.6×10^{3}	No
10^{-1}	1.5	Yes
0.5	1.6×10^{-2}	Yes
1.0	10^{-3}	Yes
2.0	6×10^{-5}	No

4.3 Surface Electrostatic Charging

Harper (1955) has shown that the contacting of quartz surfaces produces surface electrostatic charges. This can result in a net positive or negative charge. In general, these charges produce long range forces, the longest range of any considered in this study, so that if sufficient charging occurs, detectable (by the techniques used in the present experiment) attraction or repulsion can be present, even when the surfaces are not in

contact. This phenomenon shall henceforth be called "homogeneous" surface charging as did Overbeek and Sparnaay (1954). Another type of surface charging, denoted as "mosaic charging" has been postulated by Derjaguin (1954) to explain the anomalously high attractive forces detected by Overbeek and Sparnaay (1954). According to Derjaguin, no surface being perfect with respect to atomic arrangement, lack of localized impurities, etc., a mosaic distribution of charges (of opposite signs) could be generated, with the net surface charge remaining zero or near zero. If a certain amount of surface mobility of these charges is allowed, then forces could act between two dielectrics brought into close proximity or contact. Because of the mosaic distribution of these charges, the range of effectiveness of the forces produced would be much less than those produced by homogeneous surface charging, but greater than the range of effectiveness of the ionic-covalent and dispersion forces. Though there is no completely convincing evidence as to the existence of mosaic charging, particularly for single mineral samples, this must be considered a possible source of adhesive force in the present study.

4.4 Discrimination of Forces Acting

It is of interest to consider the methods by which the nature of the measured adhesional forces may be determined. The following techniques were available in this study:

A. Studies in dry nitrogen at atmospheric pressure; also studies at moderate vacuum.

B. Studies relating to evidence of surface damage produced by adhesion.

C. Studies relating to the effects of crystalline orientation (for like faces in contact) upon the adhesion force.

D. Studies relating to the load dependence of the adhesion.

E. Studies relating to the temperature dependence of the adhesion.

F. Studies relating to the mineral dependence of the adhesion.

G. Studies relating to surface preperation (in particular, roughness).

For Technique A, experience has shown that the short range ionic-covalent forces are not generally effective at these pressures. Hence, only surface electrostatic forces or London-Van der Waals forces should be detectable. Detection of adhesion in UHV, but not under the conditions of Technique A, provides strong evidence that homogeneous surface electrostatic charging is not playing a significant role in the adhesion.

Technique B is one of the most important for determining whether or not the ionic-covalent forces have been brought into play. If evidence of surface disruption (plastic deformation and rupture rather than simple fracturing) after contact is observed, the evidence that the normal bonding forces of the silicate lattice were acting becomes overwhelming, since none of the other forces are sufficiently strong.

Technique C is a very valuable one. Electrostatic forces, whether uniform or mosaic, should not in general be affected by crystalline orientation, particularly for a given crystal face. This is even more true for the London-Van der Waals forces. On the contrary, the magnitude of the ionic-covalent forces should be highly orientation dependent (provided complete atomic disorder of the surface is not produced during preparation)

since they are, particularly the covalent bonds, quite directional in nature.

Technique D, if resulting in a load dependent behavior for the adhesion, serves to exclude homogeneous surface electrostatic charges from contributing significantly. Study of the load force-adhesion relations can give information as to which of the others may be primarily responsible.

Technique E, particularly if a temperature dependence exists, can provide evidence as to the elastic-plastic processes acting and hence to the type of forces contributing to the adhesion. Techniques F and G also serve to provide auxiliary information helpful in discriminating between the possible forces.

5.0 SAMPLE CHOICE AND PREPARATION

5.1 Choice of Samples

(a) Silicates

Five criteria were used in the choice of the silicate samples. These were first, that the samples be representative of the more commonly occurring igneous rock and meteorite silicate minerals; second, that in so far as possible the mineral suite should encompass the igneous rock range of acidic to ultrabacic (which includes the meteorites); third, that each sample be as perfect (as regards competency, purity) an example of the chosen mineral as can be obtained; fourth, that in so far as possible at least one example of each important crystal class be studied; and finally, that the sample physical properties be such that the sample can withstand the forming operations required in sample preparation.

A set of minerals which appeared to satisfy these criteria to a reasonably good degree were chosen. These were: orthoclase, microcline, albite, and bytownite (alternatively labradorite or anorthite) representing the feldspars; hornblende, augite, and hypersthene representing the amphibole and pyroxene groups; and epidote. Of these, samples of orthoclase, albite, bytownite, labradorite, hornblende, enstatite, and hypersthene were successfully fabricated. Adhesion data were obtained for all of these except for the labradorite and enstatite samples which were not run due to time limitations.

In addition to these samples, it was considered desirable to study at least one silicate glass, since such glass might well be present at the lunar surface. Accordingly, two samples of naturally occurring obsidian were fabricated and adhesional data were obtained for these.

It is worth noting at this time the mineralogic and chemical chacteristics of the particular samples for which adhesion data were obtained. Orthoclase is a member of the Feldspar Group with a composition of approximately $KAlSi_3O_8$. It belongs to the monoclinic crystal system and has a Mohs hardness of 6. Orthoclase is one of the most common minerals in igneous rock, particularly the more acidic types, and is also found as a minor constituent in meteorites. The source localities for the orthoclase samples used in this study are Poona, India and Itrongahy, Madagascar. The sample identity has been checked with the petrographic microscope, and by X-Ray flurscence and emission spectroscopic analysis. The

results of the analysis are:

	Weight Percent	
Oxide	India	Madagascar
SiO_2	48	48
Al_2O_3	36	30
K_2O	15	19
Fe_2O_3	0.1	0.1
TiO_2	0.1	0.1
CaO	1.0	2.0

The orthoclase plane chosen for the initial studies was the (001) plane. This is a "perfect" cleavage plane and represents the plane along which fracture, during comminution, occurs most readily.

Albite is a member of the Feldspar Group of minerals and has a composition of approximately NaAl Si_3O_8. In particular, it is a plagioclase feldspar forming one end member of an isomorphous series varying in composition from that of albite to that of anorthite ($CaAl_2$ Si_2O_8). It belongs to the triclinic crystal system and has a Mohs hardness of six. The plagioclase feldspars are common constituents of igneous rock. Albite is found principally in the acidic rocks, anorthite principally in the basic varieties; both are found in the stony phase of some meteorites. The source locality for the albite sample used is Madagascar. The sample identity has been checked with the petrographic microscope, and by X-Ray fluorescence and emission spectroscopic analysis. The results of the analysis are:

Oxide	Weight Percent
SiO_2	50
Al_2O_3	32
Na_2O	≈15*
Fe_2O_3	0.5
CaO	2.0
K_2O	1.0

* by emission spectroscopy

The albite plane chosen for the initial studies was the (001) plane. This is a "perfect" cleavage plane and represents the plane along which fracture, during comminution occurs most readily.

Bytownite is a member of the same isomorphous series as albite falling, in composition, near the anorthite end. It is triclinic with a Mohs hardness of six. It tends to occur preferentially in the more basic varieties of igneous rock. The source locality for the bytownite used is Casa Grande, Chihuahua, Mexico. The results of the chemical analysis are:

Oxide	Weight Percent
SiO_2	40
CaO	40
Na_2O	10

(Cont'd)

Oxide	Weight Percent
Fe_2O_3	4
K_2O	3
MgO	2
TiO_2	<1

The bytownite plane chosen for the initial studies was the (001) plane. This is a "perfect" cleavage plane and represents the plane along which fracture, during comminution, occurs most readily.

Hornblende is a member of the Amphibole Group of minerals. Its composition is highly variable. It belongs to the monoclinic crystal system and has a Mohs hardness of between five and six. Hornblende is an important constituent of the more basic varieties of igneous rock. The source locality for the sample used is Kragero, Norway. The results of the chemical analysis are:

Oxide	Weight Percent
SiO_2	35
Al_2O_3	30
Fe_2O_3	15
CaO	10
Na_2O	9.0
K_2O	1.5
TiO_2	0.8

The hornblende plane chosen for the initial studies was the (101) plane. This is the only silicate mineral sample studied to date for which the surface was not that of a cleavage plane. The "perfect" cleavage plane (prismatic cleavage) for hornblende is the (110) plane.

Hypersthene is a member of the Pyroxene Group of minerals and has a composition of approximately $(Mg,Fe)_2\ Si_2O_6$. It belongs to the orthorhombic crystal system and has a Mohs hardness of between five and six. It is closely related to enstatite, differing principally by the presence of additional iron. It, along with enstatite, is a common constituent of basic and ultrabasic igneous rock and the stony phase of meteorites. The source locality for the hypersthene used in this study is Bamle, Telemark, Norway. The results of the chemical analysis are:

Oxide	Weight Percent
SiO_2	38
MgO	18
CaO	16
Fe_2O_3	15
Al_2O_3	9.0
TiO_2	2.0
K_2O	0.5

The presence of significant magnesium and calcium indicates the sample should more properly be called hedenbergite, or manganhedenbergite, rather than hypersthene.

The hypersthene plane chosen for the initial studies was the (110) plane. This is a "good" cleavage plane and represents the direction along which fracture, during communication, occurs most readily.

Obsidian is a silicate glass formed by the rapid chilling of a silicate melt, the rapid chilling preventing formation of any long-range atomic ordering. The source locality for the sample used is Alturas, California, on the Modoc Plateau. The composition, based on the type of extrusives in the area, should be rhyolitic. The results of the chemical analysis are:

Oxide	Weight Percent
SiO_2	50
Al_2O_3	15
Na_2O	10
MgO	10
K_2O	5
Fe_2O_3	4.5
CaO	4
TiO_2	1

It is seen that the composition is somewhat more basic than rhyolite. Also, the sodium content is a bit on the high side.

(b) Engineering Samples

The engineering samples used, were chosen on the basis of 1) the materials might be used on lunar missions and exposed to the lunar surface environment and/or 2) the materials provided interesting cases for study to better understand the mechanics of adhesion. The samples chosen for study and studied were: "pure" aluminum; "pure" magnesium; "pure" beryllium; titanium alloy (6Al, 4V); stainless steel (304); ceramic (alumina); and aluminosilicate glass (Corning #1723). The metals chosen range in hardness from very soft (Al, Mg) to very hard (Be), and from very ductile (Al, Mg) to quite brittle (Be). The ceramic and glass used were chosen solely because of their possible lunar applications.

Chemical analyses were performed on all samples. The results obtained are:

1. Aluminum

Furnished by Johnson, Matthey and Co., Limited, London, England. A spectrographic analysis of the sample was made by the supplier. The impurities present are as follows:

Element	Estimate of Quantity Present (parts per million)
Mg	30
Fe	5
Si	3

(Cont'd)

Element	Estimate of Quantity Present (parts per million)
Cd	2
Sn	1
Na	1
Ag	< 1

Forty-three additional elements were specifically sought for but not detected.

2. Magnesium (emission spectroscopy)

Element	Weight Percent
Al	3.6
Mn	0.28
Cu	0.04

3. Titanium Alloy (emission spectroscopy)

Element	Weight Percent
Al	6.0
V	3.8

4. 304 Stainless Steel (emission spectroscopy)

Element	Weight Percent
Cr	18.0
Ni	8.8
Si	0.98
Mn	0.84

5. Beryllium

Furnished by The Brush Beryllium Company. A spectrographic analysis of the sample was made by the supplier. The impurities present are as follows:

Element (or compound)	Weight Percent
BeO	1.49
C	0.100
Fe	0.1070
Al	0.0900
Mg	0.0080
Si	0.0350
Mn	0.0135
Other	$<$ 0.04

6. Corning Glass #1723

Information furnished by the Corning Glass Company.

Material	Weight Percent
Silica	60
Alumina	15
B_2O_3	5
CaO	10
BaO + MgO	Remainder

5.2 Sample Preparation Techniques

(a) Silicates

The sample preparation techniques for the silicates were as follows. An excellent specimen of the mineral type to be used was chosen. Each sample was then cleaved, using a razor blade and hammer, to give good exposure to the principal cleavage planes (by good exposure is meant large areal extent along each cleavage plane with no large cleavage steps). The crystal axes were then determined by means of a petrographic microscope and marked. Cylinders of each sample, about 0.5 cm in diameter, were then cut by means of a Raytheon Ultrasonic Impact Grinder. During this cutting, the samples were oriented so that the face of interest for the adhesion studies was essentially perpendicular to the axis of the cylinder. Next, the cylinders were inserted in the cleavage device shown in Figure 1, and cleaved into disks, 0.32 cm long, by impacting the chisel shown (for the few samples where the face of interest was not a cleavage plane, the formation of the disks was also done ultrasonically). With practice, it was found possible to obtain excellent cleavage faces in this manner. The samples were then returned to the ultrasonic cutter and intersecting perpendicular holes were drilled. The position of these holes is shown in Figure 2. Their purpose was to fasten the samples to the experimental apparatus. A copper slug was inserted into the larger, dead-ended, hole. A fine tungsten wire was then inserted into the small cross hole, being passed through a hole in the copper slug to lock the slug to the sample. The slug and cross-pin are shown in the figure.

The samples, after cutting of the holes, were then washed carefully with distilled water, vacuum oven dried, and stored in degreased, sealed glass containers.

Each sample, immediately prior to use was removed from its container, the holding slug and cross-pin installed, and the sample given a light, 10 second, etch with a mixture of approximately 30% (by volume) hydrofluoric, 30% glacial acetic, and 40% fuming nitric acid. The purpose of this etch was to remove surface dust contamination. It was found that this technique was the only effective way to remove the smallest particles on the surface. This particular etch was chosen because previous work had shown it does not leave an insoluble residue on the silicate surface. This etch was followed immediately by distilled water washes and then by oven drying in an "almost sealed" glass container. When the sample appeared to be sufficiently dried, it was inserted into the vacuum system and pumpdown begun. A number of checks were made to determine whether the short exposure to the laboratory air was sufficient to cause a significant amount of surface particulate contamination. It was found that generally no significant contamination occurred during this period (about 2-3 minutes maximum), though it was necessary to discard a few experimental runs due to the obvious presence of surface dust contamination.

Photomicrographs of the faces to be contacted were taken for all samples prior to each run. These are shown in Figures 3-15. Also, surface roughness traces were made using a Bendix Proficorder.

These traces are shown in Figures 16-44.

(b) Engineering Materials

All the metal samples were fabricated by standard machine shop techniques. The glass and ceramic samples were, however, cut ultrasonically. It was found necessary, due to the presence of undesirable ridges, to give the Al, Mg, Ti alloy, and 304 SS a light polish with 3 micron aluminum oxide powder. All samples, except the ceramic sample, were, immediately prior to use, cleaned with detergent, rinsed then with water, cleaned again with trichlorethylene (electronic grade) followed by acetone (electronic grade) and distilled water. They were then oven dried and inserted into the vacuum system. The ceramic sample was cleaned in a manner similar to that used for the silicates.

Photomicrographs of the faces to be contacted, prior to contact, are shown in Figures 3-15. Roughness plots are shown in Figures 16-44.

A few comments should be made regarding the roughness plots for both the engineering materials and the silicates. First, there are significant differences in the degree of surface roughness between the samples, varying from optically flat for the Corning glass to highly irregular for most of the silicates. Second, when considering these plots it should be noted carefully that the horizontal scale is much compressed over the vertical scale, and hence that the surfaces are actually not as jagged as they appear. Finally, these plots are only an approximate representation of the true surface roughness

due to 1) the limitations in sensitivity of the diamond stylus used in obtaining these, and 2) the surface damage produced by this stylus (there is a tendency for the stylus to plough across the surface, particularly for the softer samples, so that some of the fine structure is lost). Hence, these plots can only be used to indicate surface roughness; they cannot be used to determine true contact area.

6.0 INSTRUMENTATION

6.1 Vacuum System

The vacuum system consists of four major parts: forepump, liquid nitrogen cold trap, ion pump, and the experimental chamber. The system is shown schematically in Figure 45. The mechanical forepump provides the initial pumping down to a pressure of about 10^{-3} mm Hg, the pressure being monitored by a thermocouple gage. The cold trap is utilized to prevent migration of oil vapors into the experimental chamber during the initial pumpdown (the time between when the mechanical pump is turned on and when the UHV part of the system is isolated from this pump is usually about ten minutes). The low vacuum part of the system is degreased prior to every pumpdown. The basic unit for obtaining ultra-high vacuum is the ion pump. It has a pumping speed of about 200 liters sec^{-1} at a pressure of 10^{-8} mm Hg. Its speed decreases slowly through the 10^{-9} and mid 10^{-10} mm Hg range, more rapidly thereafter. Pressure is monitored by a "nude" Bayard-Alpert ionization gage. This gage is shielded from direct exposure to the sample surfaces to be contacted. Good agreement has been found between readings given by this gage and the pressure indicated by the ion pump current into the low 10^{-10} mm Hg range.

The experimental chamber, along with the ion pump itself, constitutes the ultra-high vacuum part of the system. This section is separated from the forepump and cold trap by means of an ultra-high vacuum bakeable valve. This valve is closed during operation of the ion pump. The UHV section is of all-metal construction, principally 304 Stainless Steel, with the vacuum seals being made by means of copper and gold gaskets. The chamber itself consists of a six inch (diameter) tee and a six inch cross upon which is mounted the adhesion measuring system (see Figure 46). Two viewing ports are provided to permit observation of the experiment. An additional viewport, along with a bellows-mounted adjustable arm, is provided to adjust the zero point of the adhesion measuring system (these are not shown in the figure). One linear motion feedthrough and an eight pin electrical feedthrough are installed on the top flange of the tee. These are used in conjunction with the adhesion measuring system. Four additional electrical feedthroughs (not shown) are mounted on the side of the tee. These are used for the mounting of thermocouples (for measurement of sample temperature). The bottom flange of the tee contains the sample holder (Figures 47 and 48). This consists (see Figure 47) of a machined copper baseplate and a stainless steel bellows whose orientation is adjustable by means of three micrometer screws.

Due to restrictions imposed by the adhesion measuring system, bakeout of the completely assembled experiment is limited to 110°C. However, bakeouts to higher temperatures, for general system cleaning, have been made with the adhesion measuring device removed.

Heating is accomplished by aluminum foil shielded electrical tapes which

are wrapped about the system. All bakeouts are performed with the bakeable valve closed. Due to the relatively low temperatures involved, bakeout normally extends for a period of two to three days after which time the system pressure is about 3-4 x 10^{-8} mm Hg. Following bakeout, it generally takes the system four to five hours to reach the low 10^{-10} mm Hg range.

After each run the system is backfilled with nitrogen. This nitrogen is obtained from the top of a large Linde liquid nitrogen tank located adjacent to the laboratory building. The lines leading from this tank to the vacuum chamber are flushed (with nitrogen from the tank) immediately prior to each backfilling.

System vibration provides a serious problem to adhesion studies. Hence, the entire ultra-high vacuum section of the system has been suspended from "soft" springs with oil-vane pots used for damping. By use of these springs it has been possible to reduce the natural frequency of the suspended system, in its three oscillation modes, to about 0.5 cps. This technique has served to reduce the background vibration to an acceptable level (it should be noted that the low vacuum part of the system is disconnected and the mechanical pump turned off prior to adhesion measurement).

6.2 Load Application System

The load application system provides the load force to press the samples together. It is shown best in Figure 47. The system employs an electromagnet outside the vacuum chamber and a steel bucket inside the chamber. The bucket, resting on the upper sample, has been designed to meet the conditions that its weight should not overload the adhesion measurement

system, that it at no time contacts any other components, that load forces up to≈1000 gms. can be applied, and that the geometric configuration be such that the bucket remains stable (in orientation) during operation and allows observation of the contacting surfaces.

Load force is applied by first raising the electromagnet to the position shown in Figure 47. Note that the magnet is slightly out of contact with the system. Current through the magnet is then slowly increased to the desired level. This attracts the bucket toward the magnet and hence applies a load force to the contacting sample faces. As the current is increased, the vacuum system (spring mounted) moves into contact with the face of the electromagnet slug. The desired current is maintained for a few seconds after which it is slowly reduced to zero. As the current is reduced, the vacuum system slowly separates from contact with the slug. The electromagnet is then removed, and the resulting adhesion measured with the adhesion measuring system.

A battery power supply was constructed for use with the electromagnet. It consists of eighteen, twelve volt wet-cell batteries. Included with this supply is a heavy-duty, variable resistor which permits uniform variation of the current. The maximum current which can be drawn by the electromagnet (with this system and when the magnet is cold) is about 12 amperes.

A number of calibrations of load force as a function of current drawn have been made. These were performed in the vacuum system at atmospheric pressure. The load force was measured by means of Chatillion precision

mechanical springs. It was found that the calibration did not vary appreciably (less than 5% for low currents to <2% for maximum current). The calibration curve used in transforming current to load force for all experimental runs is given in Figure 49.

Electromagnetic techniques have serveral major advantages for adhesion studies. First large load forces can be applied without affecting the adhesion measuring system. For instance, in the present study using this technique it has been possible to have the capability for measuring adhesion forces seven to eight orders of magnitude smaller than the applied load forces. Second, no mechanical contacts were made in vacuum with the possible undesirable secondary adhesions. This technique does have, however, a number of disadvantages. The major ones are those involved with residual magnetism. In the present system it has been found necessary to fabricate the base plate upon which the bottom sample rests (see Figure 47) out of copper. None of the stainless steels tried were sufficiently "non-magnetic." In addition, care had to be taken in the choice of the bottom sample, in particular it had to be non-magnetic. It was found that even some of the silicates had sufficient residual magnetism to require their mounting as a top sample.

6.3 Adhesion Measuring System

The adhesion measuring system is shown in Figure 48. The basic unit for measuring the force of adhesion is a modified Cahn Gram Microbalance. This balance is essentially a galvanometer movement. Current through the meter movement coil (suspended in a magnetic field) applies torque to the balance arm, which along with the coil is supported by means of

an elastic metal fiber. The adhesion force is then measured as the current which must be passed through the coil to cause separation of the samples. Separation is detected through movement of the microbalance beam from the zero reference line and through observation of the contacting surfaces by means of a cathetometer. The zero reference line consists of a fine wire attached to the flat face of a glass lens (in the vacuum system). A small lamp is used to project the image of the beam onto this face (which is frosted). The lens is observed through a one-inch view port using a small telescope. The microbalance itself is attached to a precision linear motion feedthrough with which the balance (and upper sample) can be raised or lowered, bringing the samples into contact prior to application of the load force, and keeping them separated during bakeout.

The balance was modified in two ways to make it conform to the requirements of the study. First, the balance head (that part which is inserted into the vacuum system) was stripped down to make it suitable for UHV use. Second, the step-potentiometer supplied with the balance control unit was replaced by a ten turn potentiometer. This permitted current to be varied smoothly over all scale ranges. Under optimum conditions this balance is capable of measuring forces as small as 0.1 micrograms. However, due primarily to the bucket weight, forces smaller than about 20 micrograms could not be detected. The maximum force which could be measured was about 0.4 gm.

The maximum temperature this balance can withstand is about 110-120°C. This then applied the basic constraint to bakeout temperature. It was found, during operation of the balance, that the zero point tended to drift. Hence, it was found necessary to provide a means for zeroing

the balance while at vacuum. The balance was then calibrated, in air, following each experimental run. The calibration techniques used were essentially the same as those recommended by the manufacturer.

There is one important point about the measurement of the adhesion force which should be noted. It was found, not unexpectedly, that the obtaining of good parallelism between the contacting sample faces was critical to the success of the experiment. The reason for this was that any deviation of the upper sample from its orientation when hanging free, caused by contact with the lower sample and the application of the load force, produced a restoring force in the sample support assembly sufficient, in many cases, to break any adhesion bonds formed. Because of this, means for adjusting the tilt of the base plate, upon which the lower sample was mounted, were incorporated into the system (see Figure 47). The procedure used then was to make preliminary parallelism adjustments with the tilting stage by observing the contacting sample faces with a cathetometer, and noting any sample movement produced when a step current pulse was applied to the electromagnet. It was found that this sufficed to reduce any restoring force to the degree that measurable adhesion remained. Final adjustment for parallelism was then made by adjusting the tilt stage until a maximum value of the adhesion was obtained (using a given load force). No further adjustments in the tilt stage were then made unless the data obtained indicated this was necessary. This arrangement worked quite well for the smaller adhesion forces (up to a few tens of milligrams). However, for the larger adhesion forces, it was found that the breaking of contact jarred the measuring system sufficiently so that in many cases parallelism was destroyed. After each such occurrence it was necessary to repeat the entire orientation procedure.

6.4 Sample Bakeout System

This system consisted of a heavy-duty insulated soldering iron. This iron was placed at the same point as the electromagnet shown in Figure 47 and its purpose was to heat the silicate samples up to temperatures in excess of 500°C for surface outgassing.

Unfortunately, this heating technique did not prove to be particularly successful since during heating the system pressure invariably rose into the 10^{-7} mm Hg range and the time required to pump down to the desired working pressure was sufficiently long so that much of what had been gained toward surface cleaning during the heating was almost certainly lost. This heating system is presently being replaced by electron gun techniques, as discussed in the third quarterly report on this study, but no data are as yet available using these techniques.

6.5 Temperature Control System

The system for varying the sample temperature in the adhesion versus temperature experiments is shown in Figure 50. It consists basically of a fluid tank which is inserted into the same vacuum chamber inset as are the high temperature heater and the electromagnet. Liquid nitrogen is pumped into the tank by means of a CVC Automatic Liquid Nitrogen Filler. Cooling of the samples is by conduction through the chamber walls (during the cooling, and between measurements, the samples were maintained in contact). Temperature was measured by means of a chromel/constantan thermocouple imbedded immediately below the surface (vacuum side) of the copper base plate, adjacent to the bottom sample. This thermocouple gave at best only a rough indication of sample temperature. Unfortunately,

due to the steel bucket, and considerations of microbalance operation, it was not possible to mount thermocouples to the samples themselves.

7.0 EXPERIMENTAL DATA

7.1 Adhesion versus Load

A total of over forty attempts were made to obtain adhesion versus load curves for various sample pairs. Of these, twelve were successful. The remainder, except for two, were discarded or aborted due to various problems such as the development of system leaks, the presence of surface contamination (principally particulate from the atmosphere) and/or equipment malfunction (this latter was particularly troublesome during the early stages of the program due to the necessary complexity of the system). Most of the unsuccessful attempts occurred during the early phase of the study. As the major problems were overcome, the frequency of success increased notably.

The twelve successful runs are outlined in Table II. Two additional runs Nos. 13 and 14, are also shown. These have been included since as best could be judged all conditions for a successful run were met but no adhesion could be detected. The table designates the sample pairs used with code numbers, notes the figures which show the roughness plots for each sample and the micrographs taken before and after contact (when applicable), denotes the degree of vacuum at which the measurements were made, and gives pertinent comments relating to the experimental conditions. Each run is discussed in detail in the following paragraphs.

TABLE II

Data Pertaining to Adhesion Versus Load Runs

TOP SAMPLE				BOTTOM SAMPLE					
Run No.	Type Code No.			Run No.	Type Code No.			Vacuum (mm Hg)	Comments
1	Orthoclase (001) [Os (//) 1T]	R* M*	16-18 3	1	Orthoclase (001) [Os (//) 1B]	R	19-20	4×10^{-10}	Orientation: a-axis/a-axis $\cong 80^{\circ}$
2	Orthoclase (001) [O (//) 2T]	R	21-22	2	Orthoclase (001) [O (//) 2B]	R	23-24	$2\text{-}3 \times 10^{-10}$	Orientation: a-axis/a-axis $\cong 10^{\circ}$
3	Hypersthene (110) [Hs (//) NP]	R M	25-26 6	3	Orthoclase (001) [O (//) 2T]	R	21-22	3×10^{-10}	Orientation: a-axis trace/a-axis $\cong 10^{\circ}$
4	Albite (001) [A (//) NP]	R M	27-28 4	4	Orthoclase (001) [O (//) 2T]	R	21-22	3×10^{-10}	Orientation: a-axis/a-axis $\cong 10^{\circ}$
5	Pure Al	R M	29 11	5	Orthoclase (001) [O (//) 2B]	R	23-24	3×10^{-10}	Oxide layer present on Al
6	Hornblende (101) [Hb ($\perp$) 1T]	R M	30-31 9	6	Bytownite (001) [B (//) NP]	R M	32-33 5	3×10^{-10}	
7	Ti Alloy	R M	34 13	7	Orthoclase (001) [O (//) 2B]	R	23-24	3×10^{-10}	Oxide layer present on Ti Alloy
8	Pure Mg	M	10	8	Orthoclase (001) [O (//) 3T]			$3\text{-}4 \times 10^{-10}$	Oxide layer present on Mg
9	Pure Be	R M	35 14	9	Orthoclase (001) [O (//) 1B]	R	36-37	3×10^{-10}	Oxide layer present on Be
10	Glass Corning #1723	R M	38 7	10	Orthoclase (001) [O (//) 1T]	R	39-40	3×10^{-10}	

- (Cont'd) -

TABLE II Cont'd

Data Pertaining to Adhesion Versus Load Runs

TOP SAMPLE				BOTTOM SAMPLE					
Run No.	Type Code No.			Run No.	Type Code No.			Vacuum (mm Hg)	Comments
11	Ceramic (Alumina)	R M	41 12	11	Orthoclase (001) [Os (//) 1T]	R M	16-18 3	5×10^{-10}	Slight vacuum leak
12	Obsidian [Ob 1T]	R M	42 15	12	Obsidian [Ob 1B]	R	43	6×10^{-10}	Slight vacuum leak
13	Stainless Steel (304)	R M	44 8	13	Orthoclase (001) [O (//) 2T]	R	21-22	2×10^{-10}	Oxide layer present on S. S.
14	Stainless Steel (304)	R M	44 8	14	Orthoclase (001) [O (//) 2T]	R	21-22	2×10^{-10}	Oxide layer present on S. S.

*R = Roughness Plot - Figure Numbers
*M = Micrograph - Figure Numbers

Run 1 - Orthoclase (001)/Orthoclase (001)

The samples were oriented so that their respective a-axes were approximately 80° from match in orientation. Prior to pumpdown, attempts were made to detect adhesion. None was detected. Evacuation of the system was then begun. During the time the system was being rough-pumped, the samples were maintained in contact. Then the system was baked out at temperatures between 100-200°C for two to three days. During this period, the bakeable valve was kept closed and the samples apart. The pressure at the end of the bakeout was in the low 10^{-8} mm Hg range. About four hours after bakeout was completed the pressure fell to about 6×10^{-10} mm Hg. The samples, still separated, were then baked to temperatures in excess of 500°C for one hour. The pressure, during this bakeout, rose to the mid 10^{-7} mm Hg range. Following bakeout, the pressure dropped slowly over a period of about ten hours to 4×10^{-10} mm Hg.

The experimental results are shown in Figure 51. It can be seen that no adhesion was detectable at low loadings but that for the higher loads the adhesion force increased quite rapidly. Attempts were made to determine whether any long range attractive forces (such as produced by surface electrostatic charging) were present. This was done by slowly lowering the upper sample toward the lower sample through varying the current into the microbalance, and observing the microbalance pointer line for any indications of an apparent increase in sample weight. Sample separation was monitored by means of a cathetometer. No long range forces were detected.

The system was then brought up to atmospheric pressure with tank nitrogen.

Attempts were then made to detect adhesion. None was detected. The system was then evacuated to about 10^{-3} mm Hg. Again, no adhesion was detected.

The sample contact faces were then studied by means of a Leitz Petrographic (polarizing) Microscope. Extensive surface damage was noted. Chips of orthoclase were scattered over both surfaces. Attempts to remove this debris mechanically (by means of rubbing with a chamois cloth, and scraping with a small metal probe) failed. Since the samples were of the same chemical composition, it was not possible to tell whether material transfer had occurred. The sample faces were then cleaned by means of the previously noted chemical etch. Following this, they were contacted in air with load forces up to several thousand grams. Repeated loadings failed to produce any detectable disruption. The surfaces were then rotated relative to each other while in contact and under load. This severe treatment produced some evidence of surface damage, but nothing even remotely approaching the degree of surface damage produced in vacuum.

Run 2 - Orthoclase (001)/Orthoclase (001)

The samples were oriented so that their respective a-axes were approximately 10° from match in orientation. The evacuation and bakeout procedures were similar to those used in Run #1, except that attempts were made to measure adhesion before the high temperature bakeout (at $\simeq 3 \times 10^{-10}$ mm Hg) as well as after. Adhesion was detected and it was found that the bakeout had no significant effect upon the magnitude of the adhesion.

The experimental results, obtained at pressures of 2-3 x 10^{-10} mm Hg, are shown in Figure 51. These, except at the highest loads, are similar to those for Run #1. There is some indication of a separation in the two curves at the highest loads, the magnitude of the adhesion forces for Run #2 tending to be greater than those for Run #1. No long range forces were detected.

The system was then brought up to atmospheric pressure with tank nitrogen. No adhesion was detectable. The system was opened and the samples studied with the petrographic microscope. The findings were the same as reported for Run #1.

Run 3 - Hypersthene (110)/Orthoclase (001)

These samples were oriented with the a-axis trace of the hypersthene approximately 10° from match in orientation with the a-axis of the orthoclase. The evacuation and bakeout procedures were similar to those used during Run #2.

The experimental results, obtained at a pressure of about 3 x 10^{-10} mm Hg, are shown in Figure 51. They are similar to those obtained for Runs #1 and 2, except for the adhesion force being of lower magnitude. No long range forces were detected. The system was then brought up to atmospheric pressure with tank nitrogen. No adhesion was detectable.

The sample surfaces were studied with the petrographic microscope. A large amount of surface disruption was evident. In addition, hypersthene was found to be present on the orthoclase surface and orthoclase on the

hypersthene (identified optically). A photomicrograph of the orthoclase surface is shown in Figure 52. The dark material is the hypersthene, the brightest material is orthoclase chips, oriented favorably for reflection, and the remaining light material is the orthoclase surface. This material could not be removed mechanically (by the techniques used for Run #1). Likewise, this surface disruption and material transfer could not be reproduced (in air) by loading the surfaces, and rubbing them together while in contact.

Run 4 - Albite (001)/Orthoclase (001)

These samples were oriented with their a-axes about 10° from match in orientation. The evacuation and bakeout procedures were similar to those used during Run #2.

The experimental results, obtained at a pressure of about 3×10^{-10} mm Hg, are shown in Figure 51. Their character is quite different from the results obtained from the previous runs, except at the highest loadings. Detectable adhesion was present at zero load and the load dependence was much less marked. No long range forces were detected.

The system was then brought up to atmospheric pressure with tank nitrogen. Contrary to the findings of the previous runs, it was found that measurable adhesion remained for about one hour after admission of the nitrogen. The measurements made are as follows:

Approximate time after backfilling (minutes)	30	30	50	80	80	80	90 →
Load force (gm)	750	750	750	750	750	800	800 →
Adhesion force (mg)	0.9	1.0	0.5	← Not detectable →			

In addition, measurements were made at zero load. The zero load adhesion dropped initially to 70μg, significantly less than the vacuum value. It then decreased slowly to below detectable ($<20\mu$g) in about half an hour.

The system was then opened and the sample surfaces studied with the petrographic microscope. Indications of very slight surface damage were found.

Run 5 - Pure Aluminum/Orthoclase (001)

The evacuation and bakeout procedures were similar to those used during Run #1 except that bakeout temperatures were all less than 200°C. No attempts were made to remove the oxide layer from the aluminum.

The experimental results, obtained at a pressure of about 3×10^{-10} mm Hg, are shown in Figure 53. Note the apparent two branches to the curve. At low loads the curve is similar to that obtained for albite contacting orthoclase in Run #4. For higher loads, however, the curve is similar to those obtained from Runs #1, 2, 3, and 4 (at highest loading). For intermediate loads (about 200-400 gms) both branches appear to be present, while the lower branch disappears for loads greater than 400 gm. This branching appears to be real, and will be discussed in a following section. No long range attractive force was detected.

The system was then brought up to atmospheric pressure with tank nitrogen. The upper branch of the adhesion-load curve immediately disappeared. However, forces of magnitude roughly comparable to that of the lower branch remained. Long range attractive forces were noted to be present on occasion. Measurements were made over a period of four hours. It was

found that any appreciable time delay between measurements resulted in a reduction in the magnitude of the adhesion force under zero load, but that applying a load force immediately raised the zero load adhesion to its previous value. After four hours, air was admitted to the system. All adhesion immediately disappeared.

The system was then opened and the sample surfaces studied with the petrographic microscope. Considerable surface disruption of both surfaces was noted, as well as transfer of aluminum to the orthoclase and orthoclase to the aluminum. A micrograph of the orthoclase surface, taken in transmitted light, is shown in Figure 54. The lighter material is the orthoclase, the dark material is the aluminum. Some orthoclase chips can be noted on the surface. This material could not be removed mechanically (by methods utilized in Run #1).

The surfaces were then cleaned and contacted in air. It was found that transfer of aluminum to the orthoclase occurred for load forces greater than about 300-400 grams. However, no transfer of the orthoclase to the aluminum was detected, nor was any damage to the orthoclase evident.

Run 6 - Hornblende (101)/Bytownite (001)

These samples were oriented with the a-axis trace of the hornblende about 10° from match in orientation with the a-axis of the bytownite. The evacuation and bakeout procedures were similar to those used during Run #2.

The experimental results, obtained at a pressure of about 3×10^{-10} mm Hg, are shown in Figure 51. They are similar to those found for the albite/orthoclase

run (Run #4), except that no indications of a second branch at highest load were obtained. No long range forces were detected.

The system was then brought up to atmospheric pressure with nitrogen. The source of the nitrogen for the previous runs was bottled tank nitrogen. However, for this and succeeding runs, the nitrogen was obtained from the top of a large Linde liquid nitrogen storage tank. It was found that detectable adhesion remained. Its magnitude was about the same as found in vacuum, but whereas the vacuum data had little scatter, the nitrogen data showed considerable scatter. A long range force was found to be present at times. After two hours, without any apparent decrease in the magnitude of the adhesion, the system was evacuated to about 30 microns. Adhesion remained and behaved in a manner similar to that in nitrogen. Air was then admitted to the system. All adhesion immediately disappeared.

The system was then opened and the sample surfaces studied with the petrographic microscope. No surface disruption or material transfer was detected.

Run 7 - Titanium Alloy/Orthoclase (001)

The evacuation and bakeout procedures were similar to those used during Run #5. No attempts were made to remove the oxide layers from the titanium.

The experimental results, obtained at a pressure of 3×10^{-10} mm Hg, are shown in Figure 53. They are similar to those found for Runs #4 and 6, exhibiting only a small load dependence, except for the highest loads

where there are indications of a sharp increase in the adhesion force. No long range forces were detected.

The system was then brought up to atmospheric pressure with nitrogen from the Linde liquid nitrogen tank. No adhesion could be detected.

Study of the surfaces with the petrographic microscope revealed a slight trace of metallic deposits on the orthoclase. A micrograph of some of these is shown in Figure 56. No other evidence of surface disruption or material transfer was observed. An electron microprobe analysis is being made on these deposits. However, the results are not as yet available.

Run 8 - Pure Magnesium/Orthoclase (001)

The evacuation and bakeout procedures were similar to those used during Run #5. No attempts were made to remove the oxide layer from the magnesium.

The experimental results, obtained at a pressure of $3-4 \times 10^{-10}$ mm Hg, are shown in Figure 53. They are similar to those obtained from Runs #1, 2, and 3 and the upper branch curve from the aluminum/orthoclase run (Run #5). No long range forces were detected.

The system was then brought up to atmospheric pressure with nitrogen from the Linde liquid nitrogen tank. The large magnitude adhesion forces measured in vacuum immediately disappeared. However, these were replaced by an adhesion force of about 300 μg which appeared to be essentially

independent of load force (there was quite a bit of scatter in the measured adhesion) and which was present at zero load (where no adhesion could be detected in vacuum). This adhesion remained for two hours at which time air was admitted to the system. An indication of a 300μg adhesion force, for an 850 gm load force, was detected immediately after admission of the air. However, this quickly disappeared and subsequently no adhesion could be detected at any loading.

The contacting faces were studied with the petrographic microscope. Extensive surface damage and material transfer were observed. A photomicrograph of the orthoclase surface is shown in Figure 57, and of the magnesium surface in Figure 55. The light spots scattered about on the orthoclase surface are magnesium. Some orthoclase chips can also be seen. The magnesium surface is extensively damaged. Pits and hillocks are present (that these were not present prior to the run, can be seen from Figure 10). Electron microprobe analysis of both surfaces (courtesy of Dr. Louis Walter, Goddard Spaceflight Center, NASA) confirmed that magnesium was present on the orthoclase and that orthoclase was present on the magnesium, in the damaged areas. The deposits could not be removed mechanically.

Magnesium and orthoclase samples were then contacted in air. It was found that for load forces greater than about 400-500 gm, transfer of magnesium to the orthoclase occurred. However, no damage to the orthoclase surface was evident, nor did any of the orthoclase appear to be transferred to the magnesium surface.

Run 9 - Beryllium/Orthoclase (001)

The evacuation and bakeout procedures were similar to those used during Run #5. No attempts were made to remove the oxide layer from the beryllium.

The experimental results, obtained at a pressure of 3×10^{-10} mm Hg, are shown in Figure 53. They are similar to those found for Runs #4, 6 and 7, exhibiting little load dependence. No long range forces were detected.

The system was then brought up to atmospheric pressure with nitrogen obtained from the Linde liquid nitrogen tank. Adhesion, of about the same magnitude as that found in vacuum, was observed. Air was then introduced into the system and all indications of adhesion immediately disappeared.

Study of the contacting surfaces with the petrographic microscope did not reveal any surface disruption or material transfer.

Run 10 - Corning Glass #1723/Orthoclase (001)

The evacuation and bakeout procedures used were similar to those used during Run #5. The experimental results, obtained at a pressure of about 3×10^{-10} mm Hg, are shown in Figure 58. It can be noted that a rapid increase in adhesion occurs as load force is increased, but that this increase is not as rapid as that observed in Runs #1, 2, 3, 5, and 8. No long range attractive force was detected.

The system was then brought up to atmospheric pressure with nitrogen from the Linde liquid nitrogen tank. Immediately thereafter, a 700μg

adhesion force was detected for a 700 gm applied load. However, following this measurement, all indications of adhesion disappeared.

Study of the contacting surfaces with the petrographic microscope revealed a small amount of surface disruption. However, it was not possible (due to the chemical similarities of the samples and the small amount of disruption present) to determine whether material transfer had occurred.

Run 11 - Ceramic/Orthoclase (001)

The evacuation and bakeout procedures used were similar to those used during Run #5. The experimental results, obtained at a pressure of about 5×10^{-10} mm Hg, are shown in Figure 58. These are similar to those obtained in Run #10, except for the adhesion forces being somewhat larger. No long range attractive force was detected. The system was then brought up to atmospheric pressure with nitrogen from the Linde liquid nitrogen tank.

Detectable adhesion remained, though its magnitude was somewhat less than half the vacuum values. After about one and a half hours, during which time only a slight drop in the magnitude of the adhesion occurred, air was admitted to the system. A slight indication of adhesion at highest load was detected initially, but thereafter no adhesion could be detected.

Study of the contacting faces revealed a small amount of surface disruption. However, it was not possible, for the same reasons as for Run #10, to determine whether material transfer had occurred.

Run 12 - Obsidian/Obsidian

The evacuation and bakeout procedures used were similar to those used during Run #5. The experimental results, obtained at a pressure of about 6×10^{-10} mm Hg, are shown in Figure 51. It can be noted that a rapid increase in the adhesion occurs as load force increases and that the shape of the curve is similar to that obtained for Runs #1, 2, 3, 5 and 8. No long range forces were detected.

The system was then brought up to atmospheric pressure with nitrogen from the Linde liquid nitrogen tank. No adhesion could then be detected.

Study of the contacting surfaces revealed that a small degree of surface disruption had occurred. Flakes of obsidian were distributed over both surfaces. These could not be removed by mechanical means (the same as those utilized for previous runs). However, since both samples were of the same material, it was not possible to determine whether or not material transfer had occurred. The samples were then cleaned and contacted in air with loading forces up to about 2000 gm. No evidence of surface disruption was detected.

Runs 13 and 14 - 304 Stainless Steel/Orthoclase (001)

The evacuation and bakeout procedures used were similar to those used during Run #5. No attempts were made to remove the oxide layer from the stainless steel. In Run #13, several hundred attempts were made to detect adhesion. Except for one possible indication of a very small adhesion force, no adhesion could be detected. The system was then opened and the contacting surfaces studied with the petrographic microscope.

No evidence for surface disruption or contamination was detected. The surfaces were then re-cleaned and inserted into the vacuum system. Several hundred attempts were again made (Run #14) to detect adhesion. No indications of adhesion were found. Study of the contacting surfaces with the petrographic microscope did not reveal any surface disruption or contamination.

7.2 Adhesion Versus Temperature

A number of attempts were made to obtain adhesion force versus temperature data. Only two of these attempts were completely successful. For the remainder, only a few isolated data points could be obtained before difficulties arose with the operation of the vacuum system, particularly as regards the formation of leaks.

The two complete runs are shown in Figures 59 and 60. The evacuation and bakeout procedures used were similar to those used during Run #2 of the adhesion versus load runs. The data do not indicate any load dependence of the adhesion as a function of temperature.

8.0 DISCUSSION OF EXPERIMENTAL DATA

8.1 Adhesion versus Load

8.1.1 General

The data for adhesion force versus load force are plotted in Figures 51, 53 and 58. The curves shown can be grouped into two and possibly three types. The first type, designated Type A, is characterised principally by a very rapid rise in adhesion force as load force is increased and the lack of detectable adhesion at lower loadings. In addition, the highest values of adhesion force detected are represented in this type.

This behavior was found for both orthoclase/orthoclase runs (#1 and 2), for the orthoclase/hypersthene run (#3), for the orthoclase/albite run (#4) at highest load, for the upper branch of the orthoclase/aluminum run (#5), possibly for the orthoclase/titanium run (#7) at highest load, for the orthoclase/magnesium run (#8) and for the obsidian/obsidian run (#12). To this might be added the orthoclase/Corning Glass and orthoclase/ceramic runs (#10 and 11 respectively).

The very rapid increase in adhesion force as load force increases cannot be explained on the basis of any simple model for elastic-plastic deformation relating to true contact area. There are, however, three factors which could cause this: surface roughness, surface contamination, and the production of sufficient distortion at the points of contact under high load to permit the formation of a significant amount of atomic bonding across the interface. Roughness could contribute through better mating being produced under load, causing increased area of intimate contact. This does not appear to be responsible in the present case, however, since as is noted in the next section there does not seem to be any correlation between roughness and the magnitude of the adhesion (also the rapidity of its increase with load). The effect of surface contamination would be to prevent intimate contact at lower loads. Higher loadings would cause penetration of the contamination (so long as there is not too much present) and thus allow the very short range atomic forces to act (the normal bonding forces). As noted in a previous section, the surface cleaning techniques were not as effective as had been hoped so that some surface contamination undoubtedly remained (this is not to say that if the cleaning techniques had been successful

a perfectly clean surface would have resulted). Hence, penetration of surface contamination must be considered to be a likely cause of the rapid increases in adhesion observed (as will be discussed in a following section; there are strong indications that Type A behavior is produced through the action of the normal atomic bonding forces). The final possibility is that only if a significant amount of distortion at the contact points occurs can significant bonding between the surfaces occur. That is, the normal silicate bondings are highly directional and it may be that only under the higher loads, where significant plastic distortion may occur, can the conditions of proper atomic configuration be achieved to any significant degree.

The second type, designated Type B, is characterized principally by the relative insensitivity of the adhesion to the load force, the presence of measurable adhesion at very low load, and the relatively low magnitude of the adhesion force. This type of behavior was found for the albite/orthoclase run (#4) except at highest load, for the lower branch of the orthoclase/aluminum run (#5), for the hornblende/bytownite run (#6), for the orthoclase/titanium run (#7) except possibly at highest load, and for the orthoclase/beryllium run (#9).

The possible third type consists of the curves obtained for the orthoclase/Corning Glass and orthoclase/ceramic runs (#10 and 11). For these, the adhesion increases rapidly with load, but not as rapidly as found for the Type A curves. However, relatively large values of the adhesion force were obtained. For present purposes these curves will be considered as belonging to Type A, though it should be noted that the evidence is not

completely convincing that these should be so grouped.

Of all the runs, only the orthoclase/aluminum, the orthoclase/albite, and possibly the orthoclase/titanium exhibited both Type A and Type B behavior. Further mention of this is made in a following section.

There are two other notable differences between these two types of curves in addition to those evident from the figures. First, it was found that when a Type A curve was obtained, study of the contacting surfaces revealed the presence of surface damage; also material transfer, where this could be determined. Also, it was found that the higher the magnitude of the adhesion detected, the greater the amount of surface damage. On the other hand, when only a Type B curve was obtained, study of the contacting surfaces did not reveal any evidence of surface damage. Second, Type A behavior was only found present at ultra-high vacuum. Admission of nitrogen or air to the system, or evacuation to moderate vacuum, resulted in the complete disappearance of the high magnitude adhesion forces associated with Type A behavior. This was not the case, however, with Type B behavior which disappeared only on the admission of air to the system.

8.1.2 Effects of Surface Roughness

The roughness plots for all the samples, save two, are given in Figures 16-44. The missing two are the orthoclase (001) [0 (//) 3 T] which was contacted with magnesium, and the magnesium. These are missing since the samples were sent out for electron microprobe analysis and have not as yet been returned.

The roughness plots have been studied carefully to determine whether surface roughness had any effect on the magnitude of the adhesion forces obtained. There is no correlation between roughness and the magnitude of adhesion for Type A behavior evident. In addition, there is no relation between roughness and whether the behavior was Type A or Type B. However, for Type B behavior there is some indication of a small increase in adhesion force as roughness increases.

8.1.3 Effects of Hardness

The hardness of all the silicates, the Corning Glass and the ceramic were about the same, so that for these no correlation between hardness and magnitude of adhesion could be obtained. The metal samples, on the other hand, covered a wide range of hardness. The Rockwell hardness of these samples was measured and the results are as follows, in order of decreasing hardness:

Sample	Rockwell Hardness
Beryllium	RC 50
Titanium Alloy	RC 29
304 Stainless Steel	RC 15
Magnesium	RB 19 ($\ll$RC 15)
Aluminum	Too soft for measurement.

Comparing these values with the magnitude of the adhesion for Type A behavior, it is seen that the order for decreasing adhesion, e.g., aluminum, magnesium, and titanium (slight indication of Type A behavior at highest load), is similar to the order of increasing hardness. This is not surprising since it is to be expected that the greatest degree of plastic flow will occur for the softest materials. The only troublesome

point about this is that no adhesion could be detected for the stainless steel sample, yet this is intermediate in hardness to the titanium and magnesium samples.

No correlation between hardness and the magnitude of adhesion for Type B behavior is evident.

8.1.4 Adhesion Producing Forces Acting in Vacuum

It is generally believed that four adhesion producing forces could act in vacuum. These, discussed previously, are those forces produced by homogeneous surface charging and mosaic surface charging, the normal atomic bonding forces, and dispersion forces (London-Van der Waals). In addition to these, forces produced by mating and interlocking-wedging of the surfaces under load could conceivably occur. It is of interest to consider which of these forces could have acted to produce the adhesion detected in the present study.

It appears quite definite that the forces involved in Type A behavior are principally the normal atomic bonding forces (ionic-covalent for the silicates, ceramic, Corning Glass, and metal oxides; metallic for the metals). There are a number of important lines of evidence leading to this conclusion: first, that Type A behavior could only be produced in ultra-high vacuum, and with prior loading; second, that in all cases where Type A behavior was observed, surface damage was produced, also material transfer was found in every case where the nature of the samples allowed the possibility of detecting transfer; third, the generally relatively large magnitude of the adhesion obtained; and finally the marked load dependence. It is of interest to consider these points:

a. Type A behavior present only at ultra-high vacuum.

The range of effectiveness of the normal bonding forces is the shortest of all the forces which could act. Hence, they are nost sensitive to the amount of surface contamination present. As noted previously, a significant amount of contamination was undoubtedly present at UHV, and it appears likely that only under high load could this be penetrated, resulting in the very rapid increase of the adhesion. Also, the complete disappearance of Type A behavior in nitrogen, air, and moderate vacuum, even under highest load, indicates that in these cases sufficient contamination was present to prevent the intimate surface contact required by the normal atomic bonding forces.

b. Surface disruption and material transfer noted only for Type A behavior.

Forces produced by surface charging, and the dispersion forces are incapable of producing these effects. On the other hand, the normal bonding forces are. Damage could also, however, be caused through strictly mechanical abrasion under load. Several experiments were performed to determine whether abrasion could be responsible. Samples exhibiting Type A behavior were rubbed together, in air, under loads greater than used in vacuum. It was found that, with the exception of the aluminum and magnesium samples, no surface disruption remotely approaching that obtained in vacuum could be obtained. For the aluminum and magnesium samples it was found that surface disruption did occur (note, however, that no adhesion force could be detected, in air, for these samples contacting silicates).

No material transfer was noted except, again, for transfer of aluminum and magnesium to the contacting silicates. Here, however, contrary to what was found in UHV, no disruption of the silicate surface occurred nor was any of the silicate transferred to the metal.

c. Relatively large magnitude of the adhesion for Type A behavior. The larger values of the adhesion force (greater than a few to a few tens of milligrams) cannot be explained on the basis of homogeneous surface charging. This conclusion is based on the results of previous work (referenced earlier), theoretical calculations relating to contact potentials, and the failure to obtain, experimentally, any indications of the presence of a long range attractive force at UHV. It also appears highly unlikely that wedging-interlocking could be responsible since no indications of these high magnitude adhesions could be detected at moderate vacuum, nitrogen or air. Mosaic charging and dispersion forces, particularly mosaic charging, could produce forces of the observed magnitude, but the complete disappearance in other than UHV argues against their effectiveness.

d. Marked load dependence of the adhesion for Type A behavior. The very rapid increase in the adhesion with load cannot be explained on the basis of homogeneous surface charging since the forces produced by such charging are long range and should be little affected by better mating of the contacting surfaces or penetration of surface contamination, both of which would cause a more intimate

surface contact. Surface wedging-interlocking can also be excluded since such rapid increases in the adhesion only appeared in UHV. Mosaic charge-produced and dispersion forces may likewise be excluded as being responsible since it appears that one or both of these remained active in nitrogen and moderate vacuum (after prior exposure to UHV). Type A behavior disappeared under these conditions. On the other hand, the normal bonding forces are quite sensitive to such things as surface contamination, and indeed penetration of the contamination probably contributes considerably to the rapid increase observed.

The evidence as to the nature of the forces producing Type B behavior is not as definitive. However, the most likely candidate for this appears to be the dispersion forces. The principal arguments are 1) the inability to detect any long range forces in vacuum, 2) the very small scatter in the experimental data (in vacuum), 3) the very small load dependence of the adhesion, and 4) the generally observed persistence of these forces in nitrogen.

Homogeneous charging could conceivably contribute to the relatively low magnitude adhesion forces detected for Type B behavior, but it does not appear too likely since no long range forces could be detected. The very small scatter in the vacuum data obtained indicates that neither mosaic nor homogeneous surface charging could be playing a significant role, since both of these, particularly mosaic charging, should produce highly erratic adhesional behavior. The very small load dependence of the adhesion would be expected if the dispersion forces were acting. Also,

the magnitude of the adhesion is easily explainable on the basis of dispersion forces. Finally, the general persistence of this adhesion in nitrogen is consistent with the known behavior of the dispersion forces, though the observations indicate that surface charging can be active under these conditions.

In summary, the evidence indicates strongly that Type A behavior is caused primarily or entirely by the action of the normal atomic bonding forces. Type B behavior, on the other hand, is most probably caused by the action of dispersion forces, though it is not possible at present to rule out the possibility that surface charging contributes.

8.1.5 Adhesion Producing Forces Acting in Nitrogen

It was found, as noted previously, that detectable adhesion remained in many cases after admission of nitrogen to the system. The magnitude of this adhesion was found to approximate that obtained for the Type B curves. However, differences in the behavior of the adhesion in nitrogen and at ultra-high vacuum were noted. First, a detectable long range attractive force was found occasionally in nitrogen; no such force was observed in vacuum. Second, the data generally exhibited quite a bit of scatter in nitrogen, whereas little scatter was found at vacuum. Finally, for some runs the magnitude of the adhesion in nitrogen showed a tendency to decrease with time, in other cases no such decrease was observed.

No correlation between the magnitude of the adhesion and the detection of a long range attractive force could be obtained. However, the presence of such a force indicates strongly that surface charging is playing a role

in the observed adhesion, at least during the times when the long range force was detected. This force was noted only on occasion (for a given run) so that presumably the amount of surface charging was highly variable. This could then explain the large degree of scatter observed. It is of interest to note in this regard that the large scatter in the nitrogen data occurred for those runs during which the long range force was detected.

The adhesion was found in some cases to decrease with time of exposure to nitrogen; in other cases, however, time of exposure appeared to have no effect. It has not as yet been possible to reach a firm conclusion as to why this difference in behavior existed. However, the most likely explanation is that during some of the backfillings a small amount of air was inadvertantly admitted to the system. This is a distinct possibility since the essentially immediate disappearance of all adhesion, when air was purposely admitted to the system, indicates that it would not take much air contamination to cause a noticeable decay of adhesion with time.

8.1.6 Discussion of Particular Runs

Three of the runs are of particular interest, and hence merit additional discussion. These are the aluminum/orthoclase (001) run (#5), the albite (001)/orthoclase (001) run (#4), and the stainless steel/orthoclase (001) runs (#13 and #14).

Aluminum/Orthoclase (001)

The data from this run are plotted in Figure 53. It is seen that both Type A and Type B behavior are present. Also, it is seen that there

appears to be some overlap in the curves representing each type, at moderate loads, and that above a certain load force the Type B behavior disappears. It is worth considering what could cause this.

The contacting surface of the aluminum is actually aluminum oxide. No means have yet been provided in the vacuum system for removing the oxide layers from the metal samples. This rather hard oxide layer is underlain by the very soft unoxidized aluminum. For low load forces it is quite possible that no penetration of the oxide layer occurs, so that contact is between the orthoclase and aluminum oxide. Here, as per previous discussions, the dispersion forces are probably the prime contributors to the adhesion. As the load force increases, however, penetration of the oxide layer occurs (aided considerably by the softness of the underlying aluminum), the normal atomic bonding forces become active, and Type A behavior is then observed. The overlap of the curves at moderate loading would then be produced by the transition to oxide penetration, in this region penetration not always occurring. Another possibility, probably not contributing greatly due to the softness of the aluminum, is that under low loads contamination remaining on the oxide surface prevents intimate contact so that only the dispersion forces are active. At higher loads, contamination penetration occurs and the normal bonding forces then become active (acting between the orthoclase and aluminum oxide). A final possibility, also probably not contributing greatly due to the softness of the aluminum, is that only under high loading does sufficient inelastic deformation occur to permit a significant amount of bonding between the highly directional bonds of the silicate and oxide.

Albite (001)/Orthoclase (001)

The data from this run are plotted in Figure 51. It is seen that, as for the aluminum run, two branches are present. This behavior cannot be ascribed, in this case, to a soft substrate. Rather it would appear that the most plausible explanations are the two alternatives noted for the aluminum run, e.g., that penetration of residual surface contamination occurs under higher loading, or that only under highest loading does sufficient inelastic deformation occur for a significant amount of bonding across the interface.

304 Stainless Steel/Orthoclase (001)

No adhesion was detected for these runs. As far as could be judged, these runs were normal in every respect: no evidence of contamination on the sample surfaces could be detected; study of the roughness plots revealed nothing unusual; and the hardness of the steel provided no clue, being intermediate to the magnesium and titanium alloy. Adhesion was detected in all previous runs. In addition, adhesion was detected in subsequent runs (to be reported in the next quarterly report). Hence, if something unusual occurred, such as increased contamination, it must have occurred only during these two particular runs, disappearing immediately afterwards. It will be necessary to study the adhesional behavior of 304 Stainless Steel further before it can be determined definitely whether or not this steel indeed does not adhere to silicates.

8.2 Adhesion versus Temperature

The adhesion force versus temperature data are plotted in Figures 59 and 60.

It can be noted immediately that, within the scatter of the data points, there is no indication of a temperature dependence for the adhesion. Additional isolated points obtained for the other, essentially unsuccessful, temperature runs also indicate no temperature dependence.

The two runs shown in the figures are of particular importance since the one, Figure 60, is for the orthoclase (001)/orthoclase (001) samples which displayed Type A behavior whereas the second, Figure 59, is for the hornblende (101)/bytownite (001) samples which exhibited Type B behavior. As discussed previously, evidence indicates strongly that Type A behavior is produced through the action of the normal atomic bonding forces, while Type B behavior (in vacuum) is probably caused by dispersion forces. The conclusion then is that the effectiveness of both the normal atomic and the dispersion forces in producing silicate adhesion is unaffected by temperature over a range roughly equivalent to the lunar temperature range.

There are still some uncertainties remaining, however. First, a basic problem in investigating the temperature behavior of adhesion is that a variable amount of contamination is present on the sample surfaces. That is, the cooling of the surfaces results in increased adsorption of gases in the chamber. Attempts were made to reduce the magnitude of this difficulty by cooling a relatively large portion of the vacuum chamber in addition to the sample, and by keeping the samples in contact during the cooling. It is not known how effective this procedure was though it is believed that the variable surface contamination did not significantly

affect the results. Second, none of the silicate-metal runs were successful. Hence, it is not known at present whether the metal behavior will be similar to that of the silicates. However, it is reasonable to believe that the harder metals should behave in about the same manner. Obviously, further data must be obtained to confirm this.

8.3 Major Remaining Questions and Problems

8.3.1 Surface Contamination

Surface particulate contamination from the atmosphere has been a major problem. In addition to the normal dust, it was found that there were a significant number of copper and aluminum particles in the air. The chemical etch discussed in a previous section was found to be best for removing this contamination. However, the experimental procedures required a short exposure to the laboratory air after cleaning and it was found that on occasion this exposure was sufficient to re-contaminate the surfaces. Since this could not be told until after the experimental run, considerable time was lost. Thought is being given to moving the experiment into a "dust-free" room to eliminate the problem.

8.3.2 Surface Cleaning and Preparation

The high temperature bakeout system, as noted previously, did not perform up to expectations. Hence, the sample surfaces were not as "clean" as had been hoped. Plans are underway to replace the present techniques by electron bombardment cleaning.

No attempts were made to remove the oxide layers from the metals. Hence, these runs represented the case of short duration lunar missions where

the only oxide removal would be for those surfaces experiencing abrasion. For long duration missions, the oxide layers on all exposed metal surfaces will be removed. Because of this, thought is being given to techniques for removal of the oxide layers. The two principal techniques are abrasion and ion bombardment. Though both techniques have inherent disadvantages, it is hoped that one or the other can be incorporated into the system in the future.

Consideration is also being given to the possibility of cleaving some of the silicate samples in vacuum. This technique has the advantage of reducing surface contamination and cleaning problems. It has the disadvantage not only in that it has serious experimental limitations, but also in that major changes in the present experimental system would be necessary.

8.3.3 Surface Roughness

It can be noted from study of the surface roughness plots included in this report that improvement is needed in the surface roughness control. Work is underway to achieve this. Even though very little effect of roughness on adhesion was found, it could conceivably be an important factor.

8.3.4 Type A versus Type B Behavior

Four important questions remain regarding the adhesion observed in vacuum during the past year. These are 1) why did not all samples show Type B behavior, 2) what, physically, determines whether or not Type A behavior will occur, 3) how reproducible are the data between separate runs, and 4) why was it not possible to detect any adhesion for the Stainless Steel.

It is of interest to discuss these questions.

If Type B behavior is indeed caused by the action of dispersion forces, then the detection of such behavior for some of the silicates implies that it should be detected for all, unless surface roughness variations played a role. The magnitude of dispersion force produced adhesion should decrease as surface roughness increases. However, no such tendency was detected. In fact, as noted previously, there was a slight tendency for the magnitude of the Type B adhesion to increase with increase in surface roughness. These same difficulties apply, in general, if Type B behavior were caused by surface charging. In addition, if the contacting surfaces were to be considered "perfect" atomically, and surface charging produced solely by contact potentials, e.g., the difference between the respective work functions, then if Type B behavior were caused by this, such behavior would only occur for unlike samples in contact. This is not what is found. Many more experimental data must be obtained before this problem can be resolved.

Work is underway regarding the question of why Type A behavior was not detected in all cases. This work presently consists of study of the available literature pertaining to the physico-chemical nature of surfaces, particularly for silicates, and the atomic arrangement in the samples. It is hoped that this can provide a clue as to when Type A behavior can be expected.

The answer to the question of reproducibility between runs must await the obtaining of more experimental data. The only information pertaining

to this question comes from the two orthoclase runs (#1 and #2). Here, good reproducibility has been obtained except at the higher loads. Since the samples were oriented differently in the two runs, this separation at high loads could be a crystal orientation effect. There are not sufficient data available as yet to determine whether or not this is the case.

More attempts to measure adhesion of 304 Stainless Steel are necessary before a definite answer to the last question can be given.

8.3.5 Additional

Additional questions that remain are worth noting briefly. These are 1) what is the cause of the observed behavior of the adhesion in nitrogen, and 2) are crystalline orientation effects present. Further work is necessary to answer these questions.

9.0 IMPLICATIONS OF THE RESULTS TO THE MOON AND LUNAR MISSIONS

It is much too early in the present program to reach any final conclusions as to the precise effects of ultra-high vacuum adhesion upon lunar missions. Indeed, the final answer to the question may not be obtained until lunar occupation becomes a reality. However, there are a number of implications given by this study as to what could occur. These relate principally to the evidence obtained that the normal atomic bonding forces of the silicates can indeed act in ultra-high vacuum.

9.1 Lunar Soil Mechanics

In order to discuss how a lunar soil may behave it is first necessary to

consider terrestrial soil behavior as described by the discipline of "soil mechanics." For illustrative purposes, it is of interest to consider one of the many equations of soil mechanics, that pertaining to soil shear strength. Shear strength is the stress required along a given plane in the soil to produce soil failure under load. The importance of this equation is that it is used as a basis for many theoretical analyses relating to the amount of load a surface can support (the ultimate bearing capacity). The shear strength equation is

$$s \cong p \tan \phi + c$$

where s is the shear strength, p is the load normal to the potential failure plane, ϕ is the angle of internal friction, and c is the cohesion. The quantity ϕ is primarily a function of grain shape, porosity, and mechanical friction; increasing as grain angularity increases, as porosity decreases, and as mechanical friction increases. The quantity c is the soil cohesion. In the terrestrial sense, this is the attractive interaction between soil grains due to the presence in the soil of water, with its various dissolved electrolytes. For engineering applications, c is found to be essentially independent of load.

Note that one side of the shear strength equation is only approximately equal to the other. Since soil behavior is complex and not completely understood, the equations of soil mechanics are at best only approximate representations. They tend to oversimplify the nature of soil behavior.

The terms "ϕ" and "c" are two of the important parameters in soil mechanics.

In general, as ϕ and c increase, the problems related to soil behavior under load decrease. These two parameters lead immediately to the two classical, extreme types of soil. The first is the cohesionless soil, where c is equal to zero. This soil has no tensile strength. It has what is called an "angle of repose." That is, the soil can repose at a certain maximum slope, beyond which it is unstable. A good example of such a soil is dry, clean sand. The second classical type is the cohesive soil for which ϕ is equal to zero. This soil possesses a tensile strength, and the concept of an angle of repose is, to a large degree, meaningless. A soil which approaches this theoretical concept is clay.

If vacuum adhesion occurs at the lunar surface, and the present study indicates that it should indeed occur unless a very large amount of surface contamination is present, then the lunar soils will possess a tensile strength. This tensile strength means that the soil is not strictly cohesionless, rather that $c \neq 0$. The present study has provided strong evidence that the normal atomic bonding forces do indeed act to produce UHV adhesion. Also, this adhesion force can reach relatively large values and is load dependent. The relatively large values indicate that the adhesion could be a significant contributor to lunar soil strength. The load dependence indicates that the cohesion (c) will be load dependent, and hence that the soil will behave in a manner unlike that of any known terrestrial soils.

It is of interest to consider how this variable "cohesion" could affect the soil behavior. As the soil surface is loaded, the areas of true contact between the grains increase. When the load is then removed, the

areas of true contact decrease, due primarily to elastic recovery. However, as is indicated in the present study, also to be expected on theoretical grounds, it is unlikely that the contact areas will decrease to the previous unloaded value. Hence, there will be residual contact areas which are greater in extent than the original areas and hence the tensile strength, or alternatively the cohesion, has been changed due to the impressed loading cycle. That is, the soil strength will depend, possibly critically, upon the loading history. Additionally, since the loading history will vary throughout the soil, so will the tensile strength. The importance of this is that the application of the shear strength equation to describing lunar soil behavior may involve considerable problems and uncertainties; and hence one must exercise great care in choosing equations from terrestrial soil mechanics to describe this behavior.

The present study has also indicated that dispersion forces can be active in UHV, as evidenced by Type B behavior. Very little load dependence of the adhesion is evident for this case. However, it should be noted that adhesion was measured after removal of the load force. While the load is being applied the dispersion forces can be expected to be somewhat greater than after removal, but since they are of considerably longer range effectiveness than the normal bonding forces, the load dependence should be very much smaller. Hence, for engineering purposes the dispersion force produced adhesion can probably be considered to be essentially constant. For this case, therefore, the shear strength equation would be applicable to lunar soils.

One final point is worth noting. Even though relatively large adhesion

forces could possibly exist at the lunar surface, this does not necessarily mean that there will be no bearing capacity problems. This adhesion could contribute, during soil formation, to a high porosity, higher than would be present if there were no adhesion. This could cause low soil strength, at least in the upper parts of the soil layer. However, compaction of these upper layers could then produce a very hard, stable surface.

9.2 Effects of Surface Material Adhesion on Lunar Missions

It is worth noting briefly some of the possible effects of silicate adhesion on lunar missions, and the implications as to this obtained in the present study.

The lunar surface layer can provide two principal locomotion problems. First, as noted previously, even with high adhesion forces some degree of sinkage appears likely (provided the upper soil layers have a very high porosity). This sinkage will provide resistance to motion requiring the expenditure of greater energy for propulsion than would be required if no sinkage occurred. It is, however, difficult to say at present how serious a problem this will be. Second, high adhesion means that a significant amount of soil material could adhere to the drive components, impeding motion. At the same time, however, this high adhesion would cause an increase in friction and thereby increase traction.

The proper functioning of many components of lunar missions will be quite sensitive to particulate contamination. These components include windows and viewing ports (in fact all optical systems exposed to the

surface material), solar cells, thermal control surfaces, the astronaut's clothing and equipment, and doors requiring vacuum tight sealing. Of particular note from the present study is the high degree of surface damage and material transfer that can occur, as well as the difficulties in removing this material. This means that great care must be taken to avoid contact between sensitive mission components (particularly optical systems and thermal control coatings) and the lunar surface material since adhesion could cause severe degradation in the proper functioning of the components.

10.0 SUMMARY AND CONCLUSIONS

During this past year a number of attempts have been made to determine the effects of load force and temperature upon the ultra-high vacuum adhesional behavior of silicates. Of these, fourteen have been successful: twelve for adhesion versus load, and two for adhesion versus temperature. Loading forces of $\approx$ 0-1000 gm have been applied; temperature has been varied over the range of roughly 100-400°K. Adhesion force as small as 20 μg could be detected. Vacuum, during the adhesion measurements has been maintained generally at about 2-4 x 10^{-10} mm Hg. Samples have been baked, in vacuum, to temperatures in excess of 500°C. Silicates have been contacted with other silicates, and with engineering materials such as metals (aluminum, magnesium, beryllium, titanium alloy, and Stainless Steel), ceramics (alumina), and commercial glass.

Adhesion has been detected for all samples except the Stainless Steel. It is not known definitely at present whether or not the apparent lack of adhesion for the Stainless Steel is real. For the other samples, it was found that the adhesion force was a definite function of load force.

This load dependence was very striking for some of the samples, no adhesion being detectable at low loads, the adhesion then increasing very rapidly with increasing loads up to relatively large magnitudes (hundreds of milligrams) in many cases. This behavior (designated Type A) was found to be present only in ultra-high vacuum, disappearing in moderate vacuum, nitrogen, and air. Also, for every case where Type A behavior was detected, inspection of the contacting surfaces revealed surface damage; additionally material transfer (when the nature of the surfaces permitted verification of material transfer). This disrupted surface material could not be removed mechanically. All evidence indicates strongly that Type A behavior was caused through the action of the normal atomic bonding forces of the silicate, metal, and oxide surfaces.

Some of the samples did not exhibit Type A behavior. Rather, the adhesion increased quite slowly with load, seldom reaching a magnitude greater than a few milligrams, and adhesion was detectable at low load. This behavior (designated Type B) was found to be present not only in ultra-high vacuum but also in nitrogen and moderate vacuum (after exposure to ultra-high vacuum), disappearing only after exposure to air. In addition, no evidence of surface disruption of the contacting surfaces, or material transfer, could be detected. The evidence indicates that the dispersion forces are probably responsible for Type B behavior, though it is possible that surface charging produced forces contributed to some degree in vacuum, quite probable that they did in nitrogen.

The adhesion force versus temperature studies have not indicated any effect of temperature upon adhesion. Though only two successful runs

were made, one was for a Type A adhesion versus load behavior, the other for a Type B. This indicates that, at least in the temperature range of 100-400°K (corresponding approximately to the lunar case) neither the normal atomic bonding nor the dispersion forces, for the silicates, vary appreciably. It could not be concluded whether this holds for silicate-metal contact due to the lack of data but, at least for the harder metals, it appears likely that it does.

The implications of this study to the moon are that 1) the behavior of lunar soils may very likely be quite different from any terrestrial soil, and 2) the surface disruption and material transfer, as well as the difficulty in removing the disrupted and transferred materials, can cause serious problems to lunar missions.

REFERENCES

Archard, J. F., Single Contacts and Multiple Encounters, J. Ap. Phys. 32, 1420-1425, 1961.

Bradley, M. A., The Cohesive Force Between Solid Surfaces and the Surface Energy of Solids, Phil. Mag. 13, 853-862, 1932.

Derjaguin, B. V., A. S. Titijevskaya, I. I. Abrocossova, and A. D. Malkina, Investigations of the Forces of Interaction of Surfaces in Different Media and Their Application to the Problem of Colloid Stability, Disc. Faraday Soc. 18, 24-41, 1954.

Derjaguin, B. V., "untitled," Disc. Faraday Soc. 18, 182-186, 1954.

Duwell, E. J., Friction and Wear of Single-Crystal Sapphire Sliding on Steel, J. Ap. Phys. 33, 2691-2698, 1962.

Dyson, J. & W. Hirst, The True Contact Area Between Solids, Proc. Phys. Soc. Lon. B 67, 309-312, 1954.

Halajian, J. D., The Case for a Cohesive Lunar Surface Model, Grumman Aircraft Engineering Corporation, Rept. No. ADR 04-04-64.2, June 1964.

Harper, W. R., Adhesion and Charging of Quartz Surfaces, Proc. Roy. Soc. Lon. 231, 388-403, 1955.

Jordan, D. W., The Adhesion of Dust Particles, Brit. J. App. Phys. 5, S 194-198, 1954.

Lowe, H. J. and D. H. Lucas, The Physics of Electrostatic Precipitation, Brit. J. Appl. Phys. 4, S 40-47, 1953.

Overbeek, J. Th. G., and M. J. Sparnaay, London-Van der Waals Attraction Between Macroscopic Objects, Disc. Faraday Soc. 18, 12-24, 1954.

Rabinowicz, E., Influence of Surface Energy on Friction and Wear Phenomena, J. Ap. Phys. 32, 1440-1444, 1961.

Riesz, C. H. and H. S. Weber, Mechanism of Wear of Nonmetallic Materials, Tech. Docum. Rept. No. WADC-TR-59-316, Armour Research Foundation, June 1962.

Roshon, D. D., Jr., Selected Area X-Ray Diffraction Studies of Surface Damage in Sliding on Single-Crystal Copper, J. Ap. Phys. 35, 1262-1269, 1964.

Spalvins, T. and D. V. Keller, Bulk Adhesion, in Adhesion Between Atomically Clean Metallic Surfaces, by D. V. Keller, Syracuse University Research Institute Rept. No. MET. E. 905-621 SA, Jan. 1962.

Salisbury, J. W., P. E. Glaser, B. A. Stein and B. Vonnegut, Adhesive Behavior of Silicate Powders in Ultra-High Vacuum, J. Geophys. Res. 69, 235-242, 1964.

Steijn, R. P., Sliding and Wear in Ionic Crystals, J. Ap. Phys. 34, 419-428, 1963.

Stein, B. A. and P. C. Johnson, Investigation of Soil Adhesion Under High Vacuum, in The Lunar Surface Layer, 93-105, Academic Press, New York, J. W. Salisbury and P. E. Glaser eds., 1964.

Stone, W., Some Phenomena of the Contact of Solids, Phil. Mag. 9, 610-620, 1930.

Tomlinson, G. A., Molecular Cohesion, Phil. Mag. 6, 695-712, 1928.

Tomlinson, G. A., Further Experiments on the Cohesion of Quartz Fibers, Phil. Mag. 10, 541-544, 1930.

Walton, O., Mechanism of Friction, J. Ap. Phys. 33, 519-526, 1962.

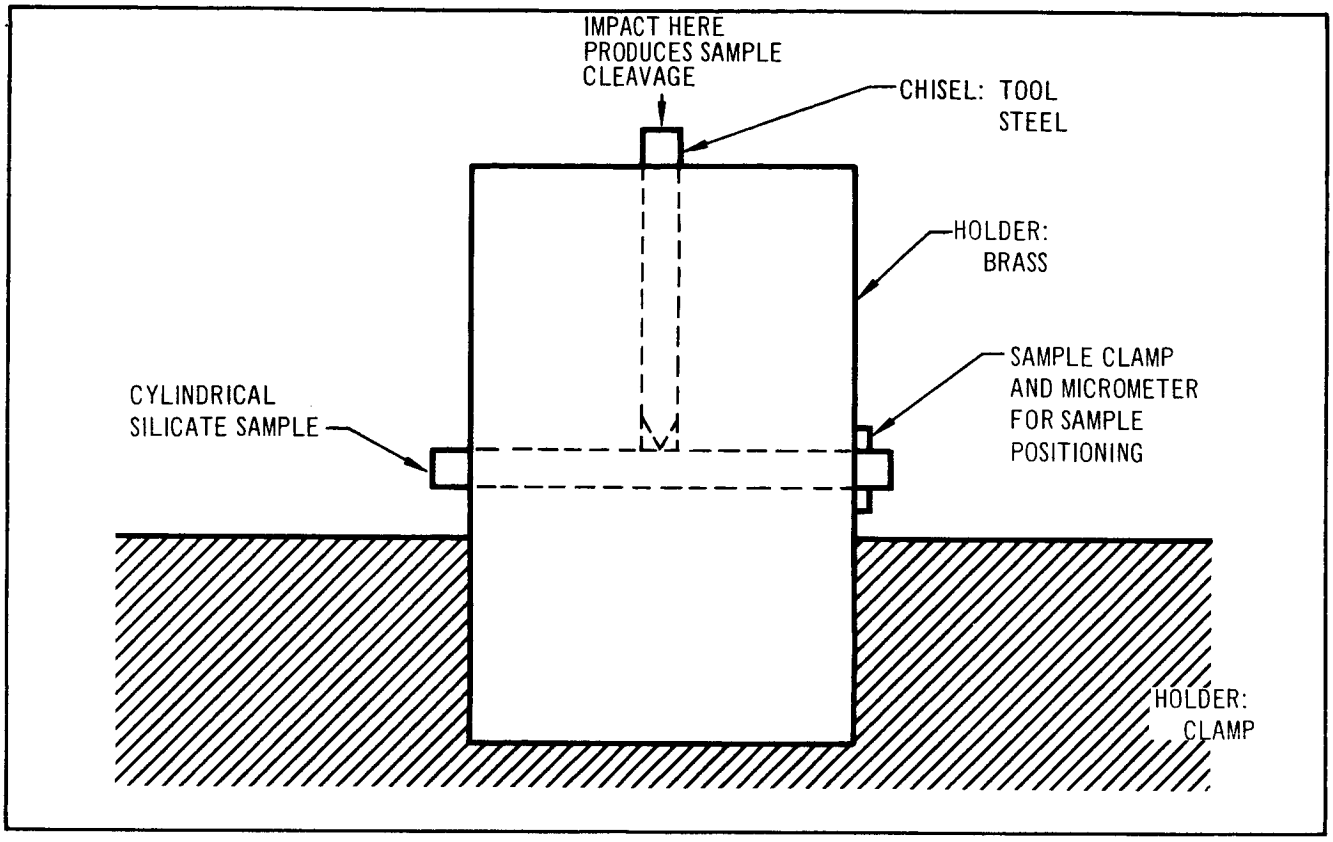

Figure 1. Sample Cleaving Device

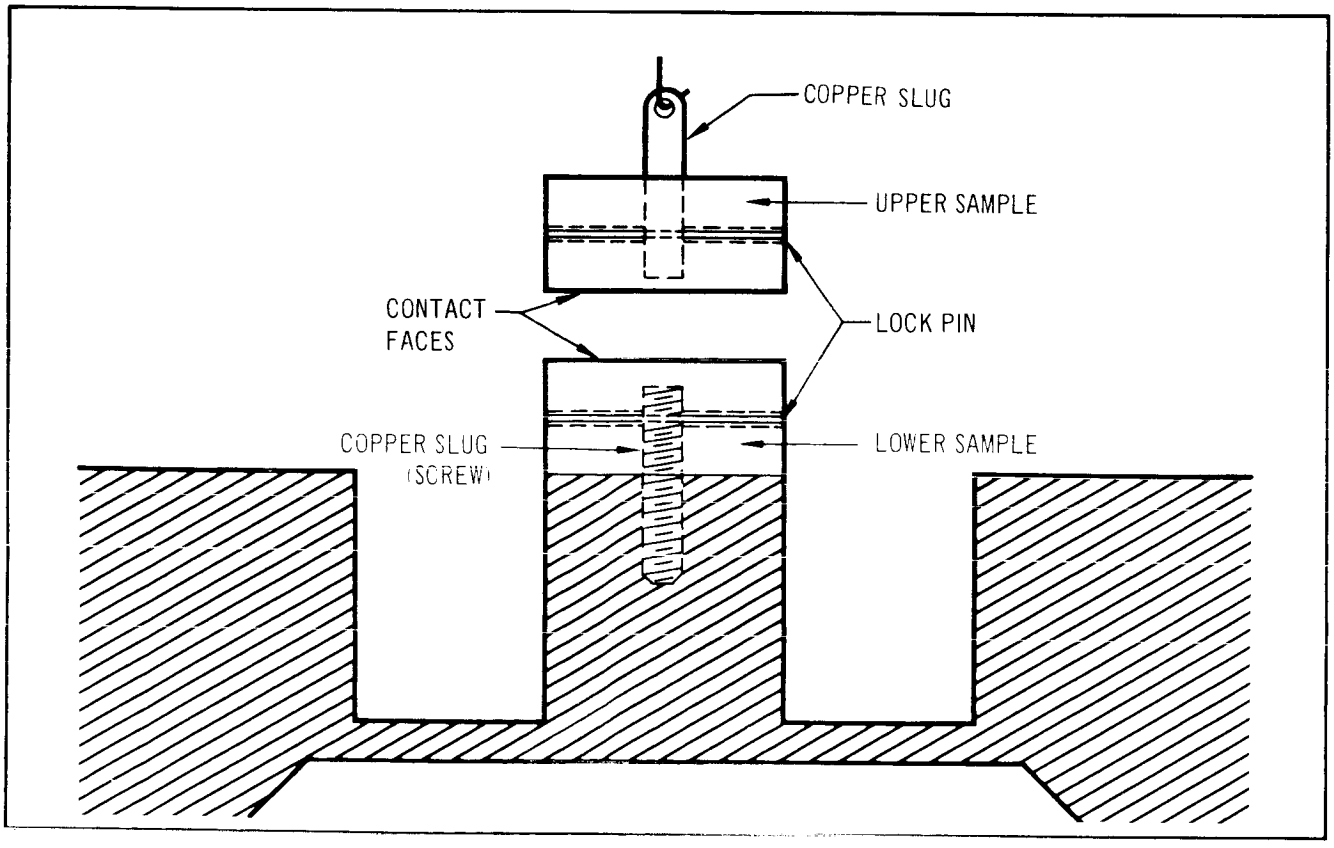

Figure 2. Technique for Securing Samples

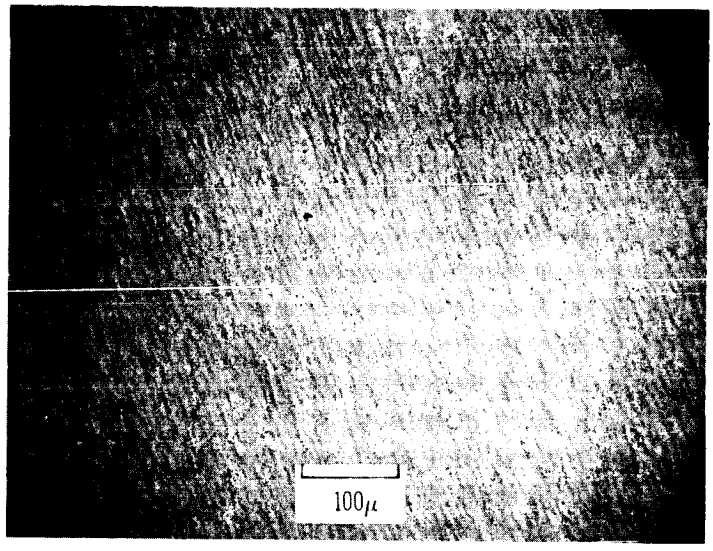

Figure 3. Orthoclase (001) Surface After Etching but Prior to Vacuum Contact

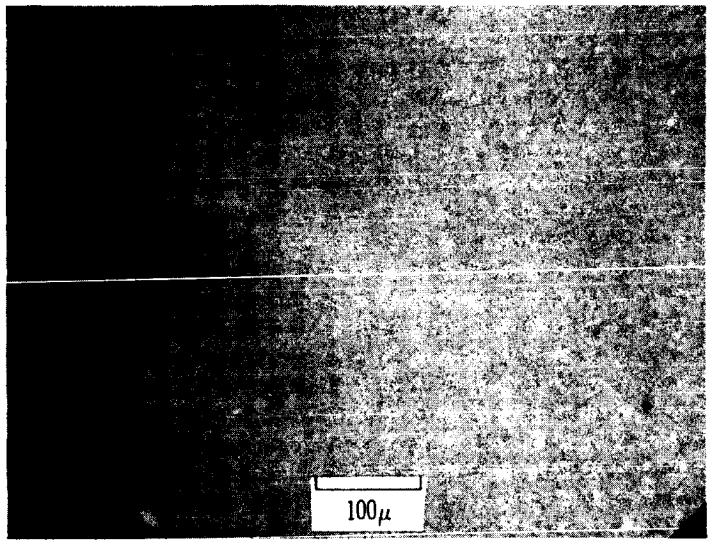

Figure 4. Albite (001) Surface After Etching but Prior to Vacuum Contact

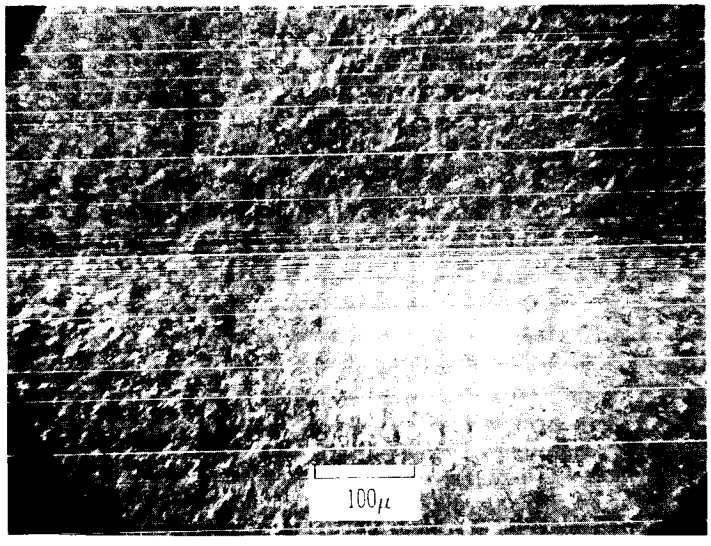

Figure 5. Bytownite (001) Surface After Etching but Prior to Vacuum Contact

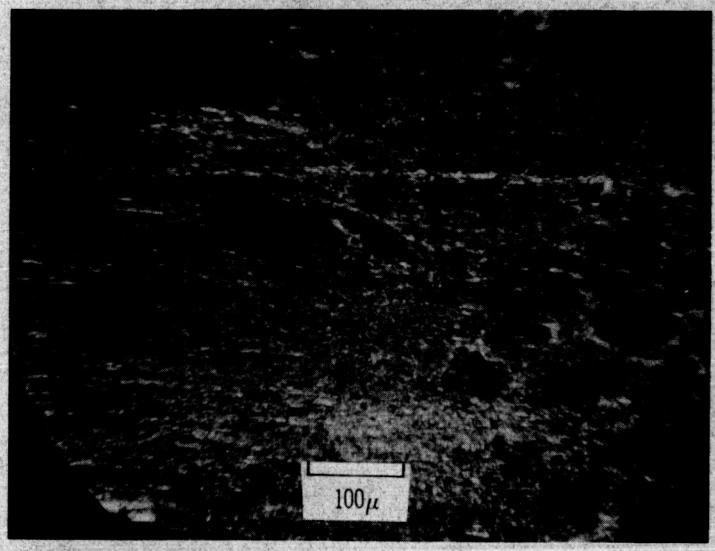

Figure 6. Hypersthene (110) Surface After Etching but Prior to Vacuum Contact

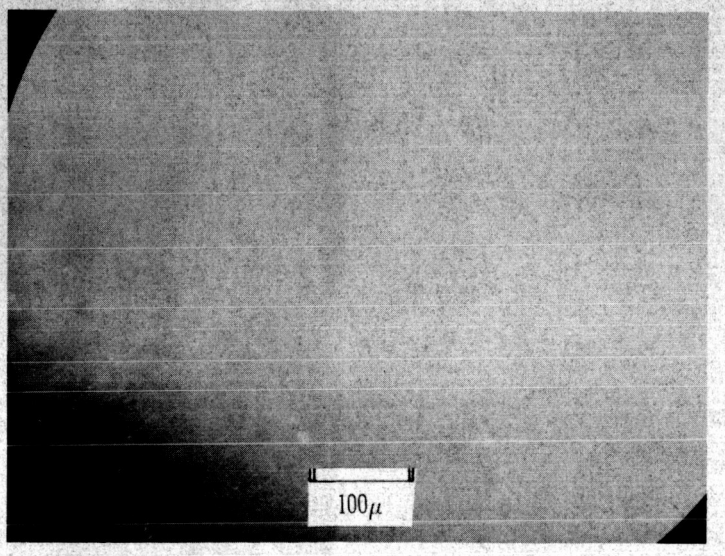

Figure 7. Glass (Corning No. 1723) Surface After Cleaning but Prior to Vacuum Contact

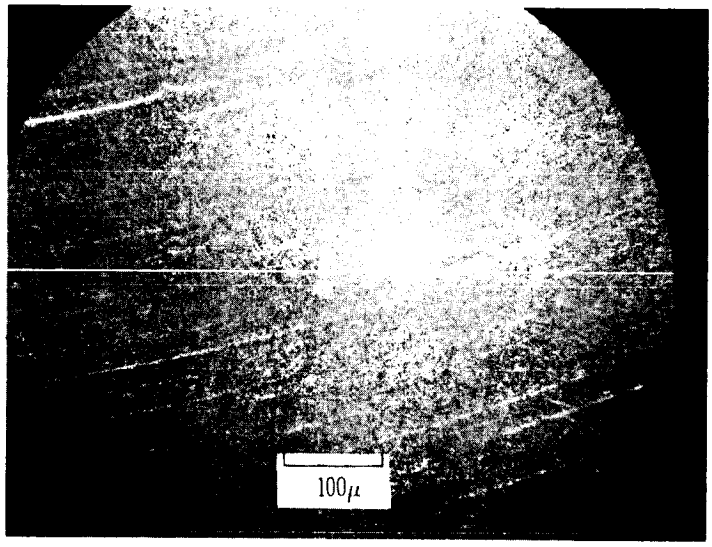

Figure 8. 304 Stainless Steel Surface After Cleaning but Prior to Vacuum Contact

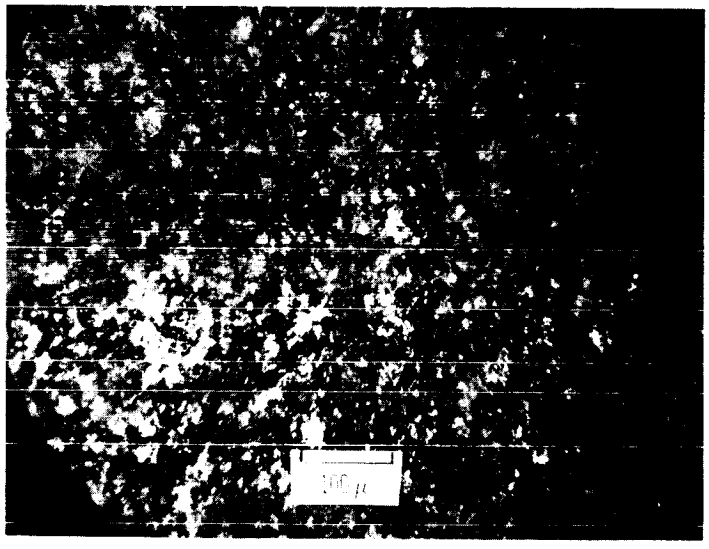

Figure 9. Hornblende (101) Surface After Etching but Prior to Vacuum Contact

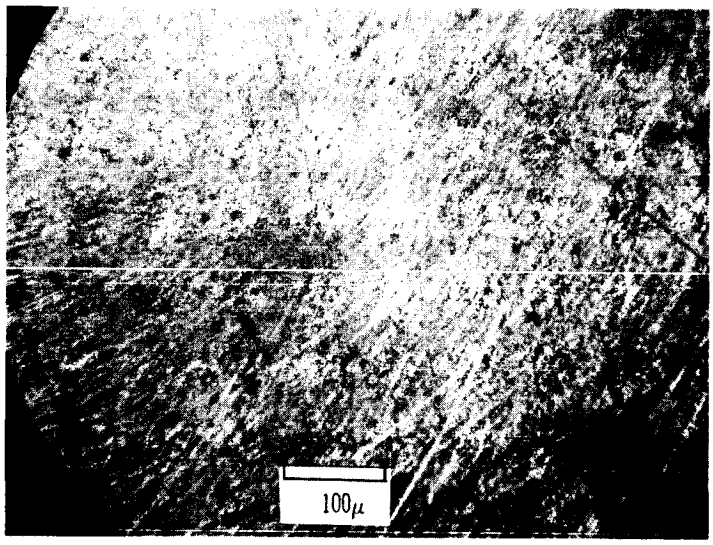

Figure 10. Pure Magnesium Surface After Cleaning but Prior to Vacuum Contact

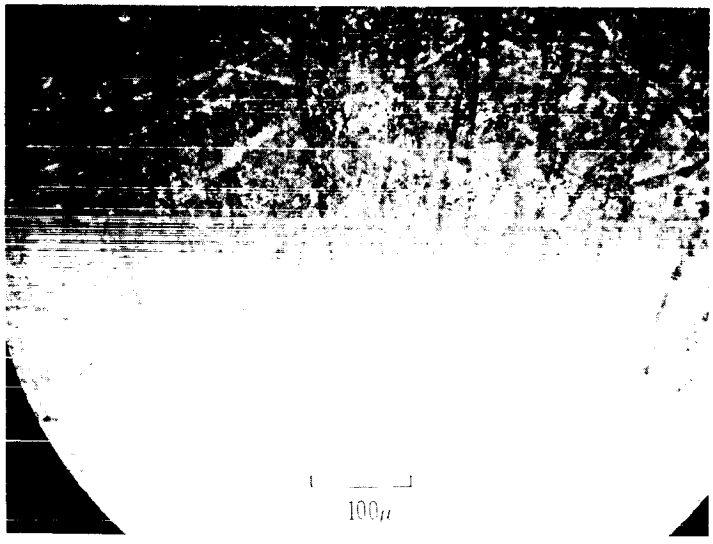

Figure 11. Pure Aluminum Surface After Cleaning but Prior to Vacuum Contact

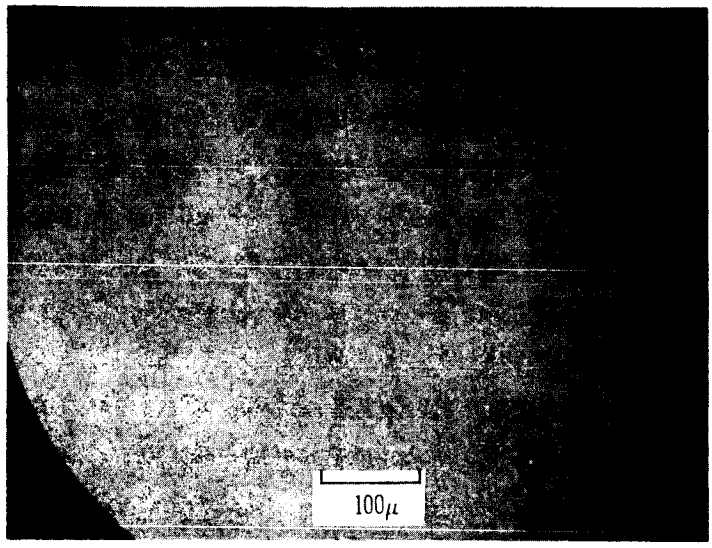

Figure 12. Ceramic Surface After Etching but Prior to Vacuum Contact

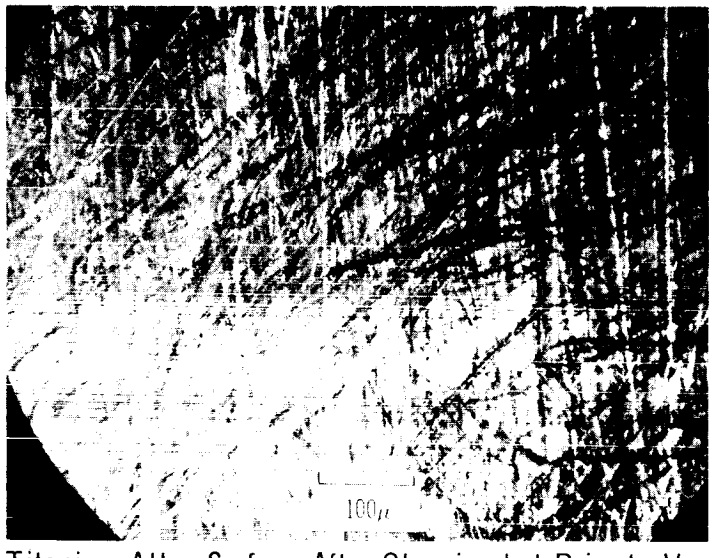

Figure 13. Titanium Alloy Surface After Cleaning but Prior to Vacuum Contact

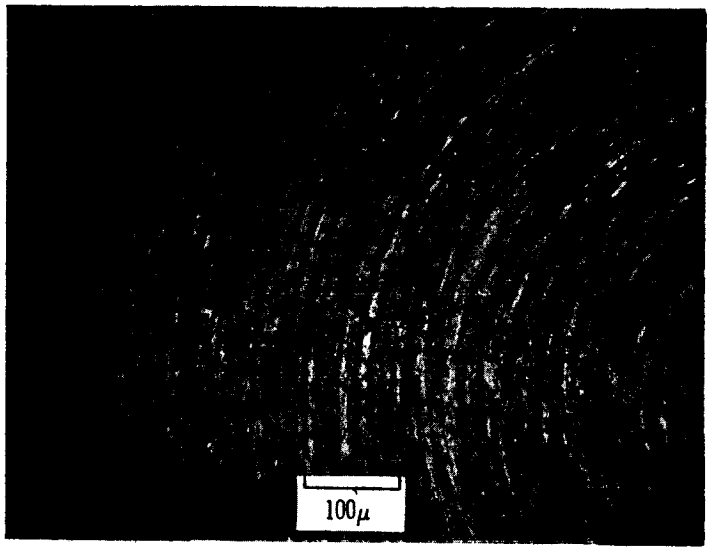

Figure 14. Pure Beryllium Surface After Cleaning but Prior to Vacuum Contact

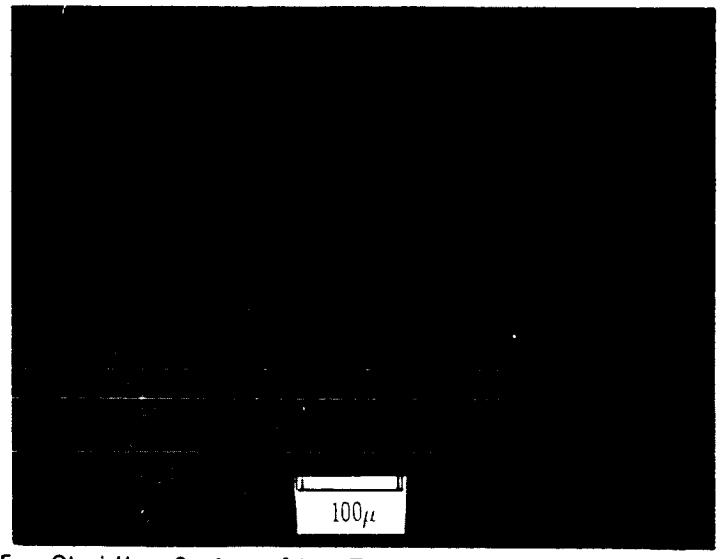

Figure 15. Obsidian Surface After Etching but Prior to Vacuum Contact

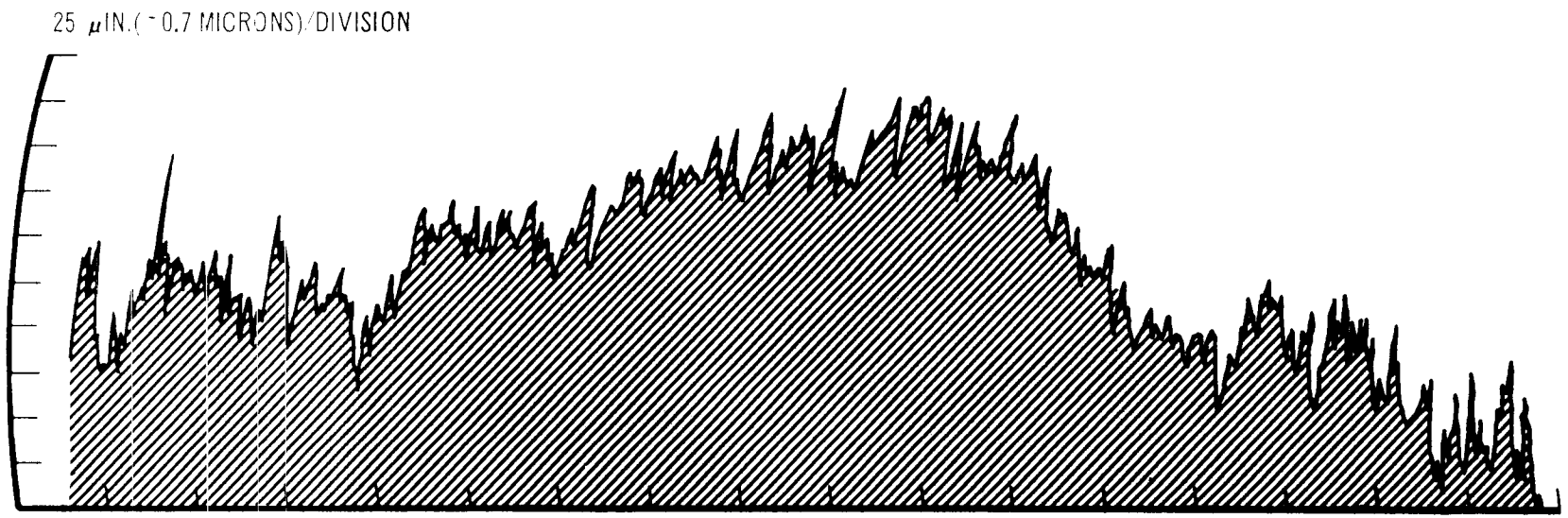

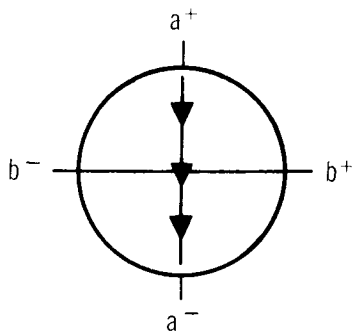

Figure 16. Orthoclase (001) [Os (||) 1T] Surface Roughness Along a-Axis

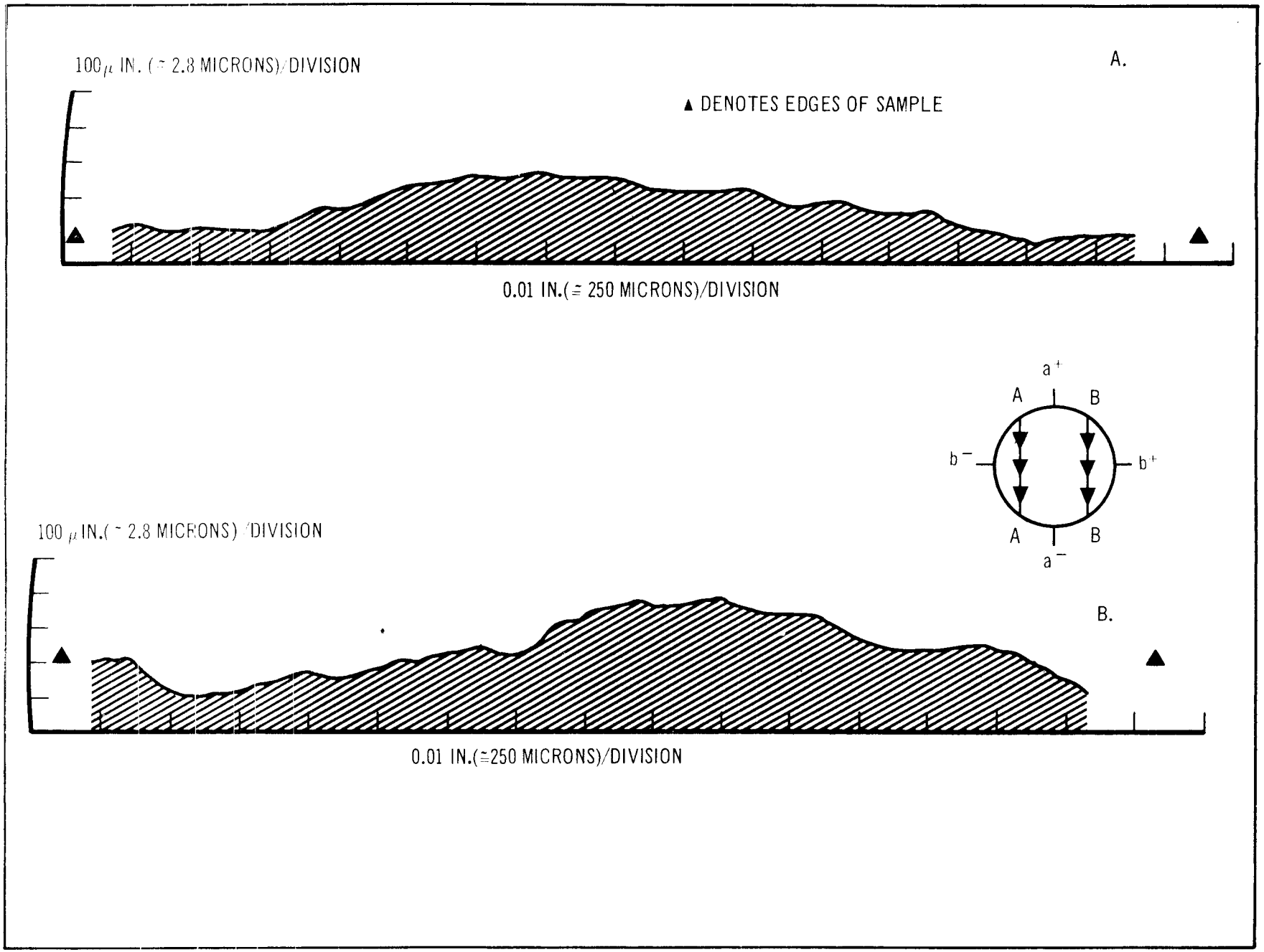

Figure 17. Orthoclase (001) [Os (II) 1T] Large Scale Surface Roughness Along a-Axis

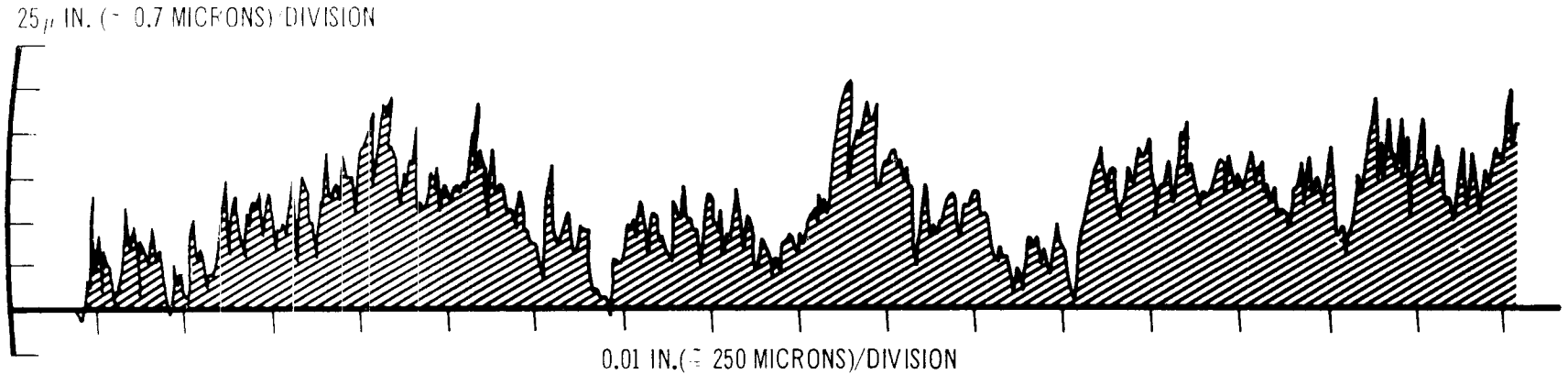

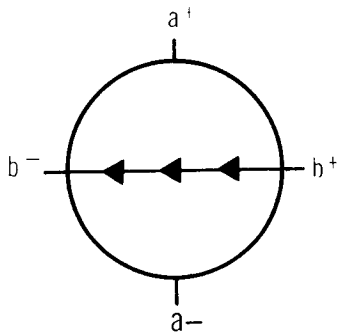

Figure 18. Orthoclase (001) [Os (II) 1T] Surface Roughness Along b-Axis

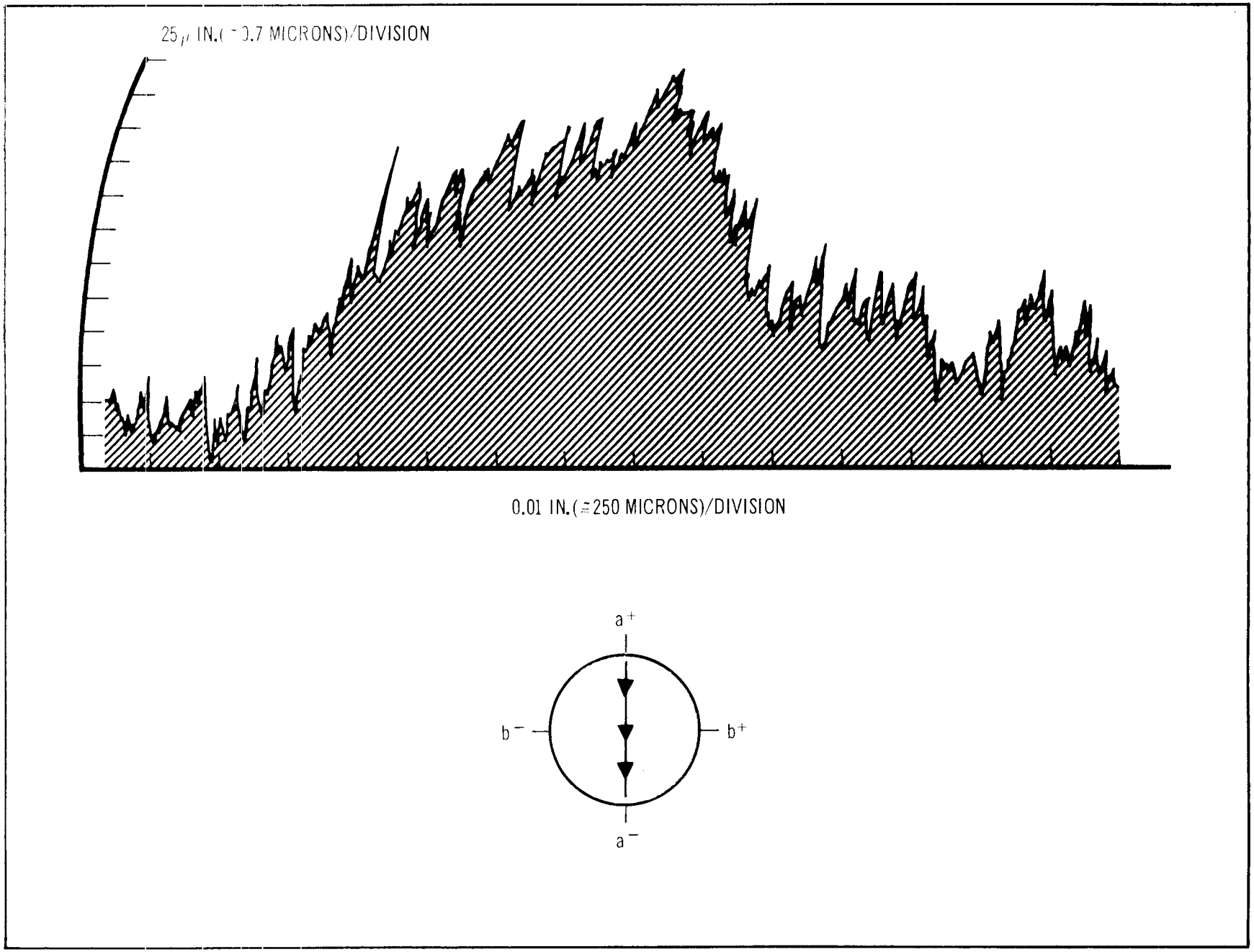

Figure 19. Orthoclase (001) [Os (II) 1B] Surface Roughness Along a-Axis

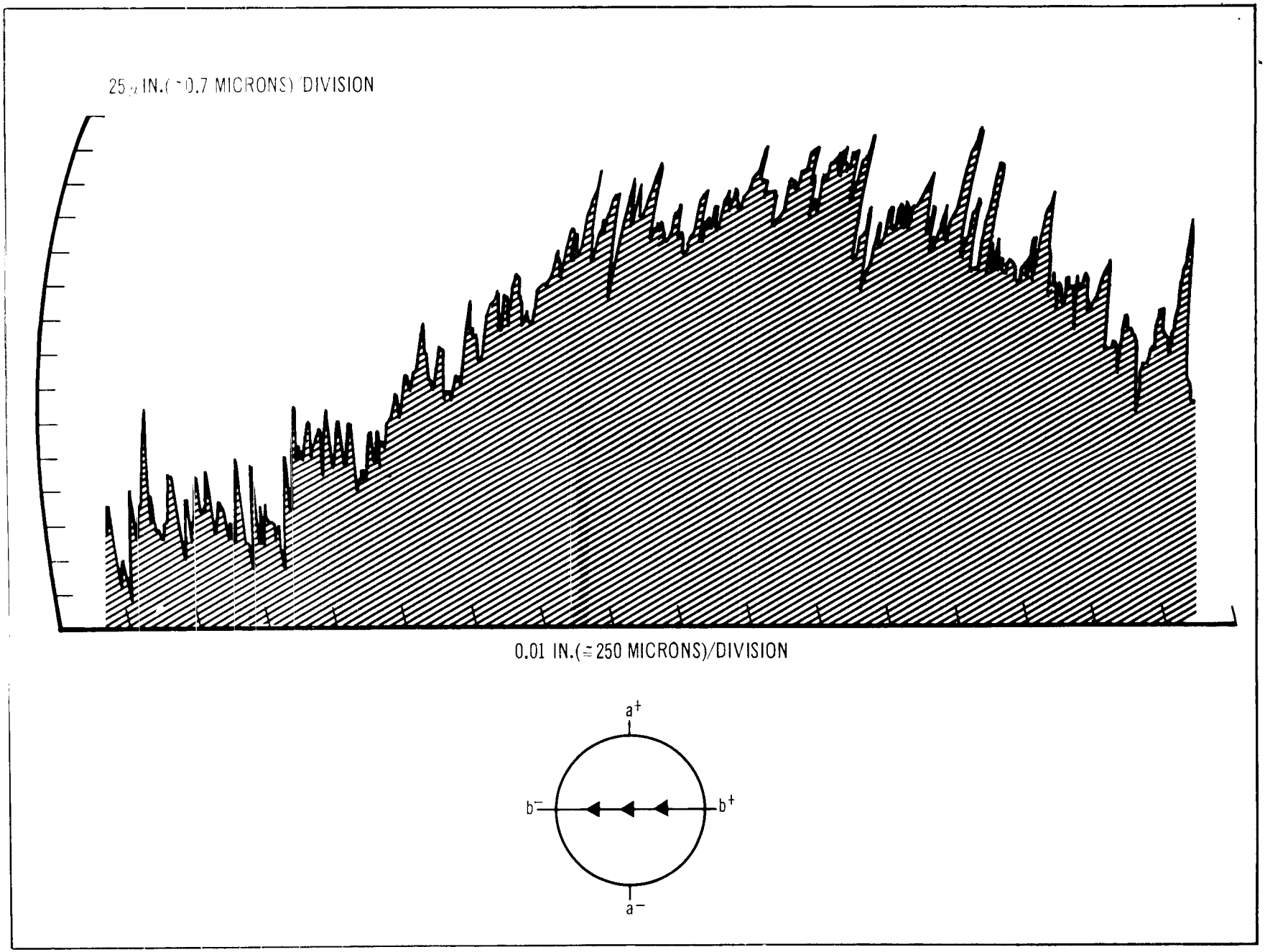

Figure 20. Orthoclase (001) [Os (II) 1B] Surface Roughness Along b-Axis

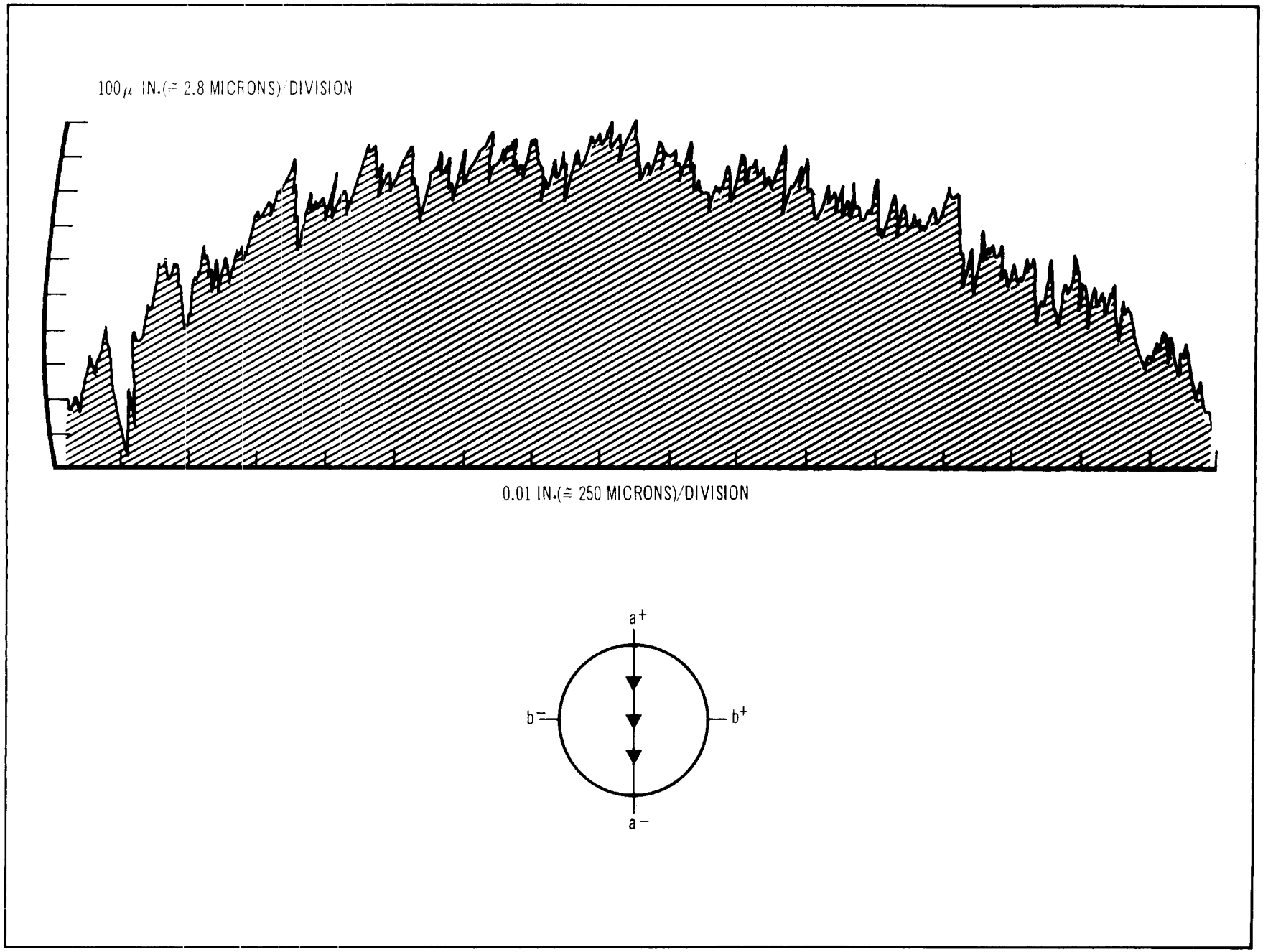

Figure 21. Orthoclase (001) [O (11)2T] Surface Roughness Along a-Axis

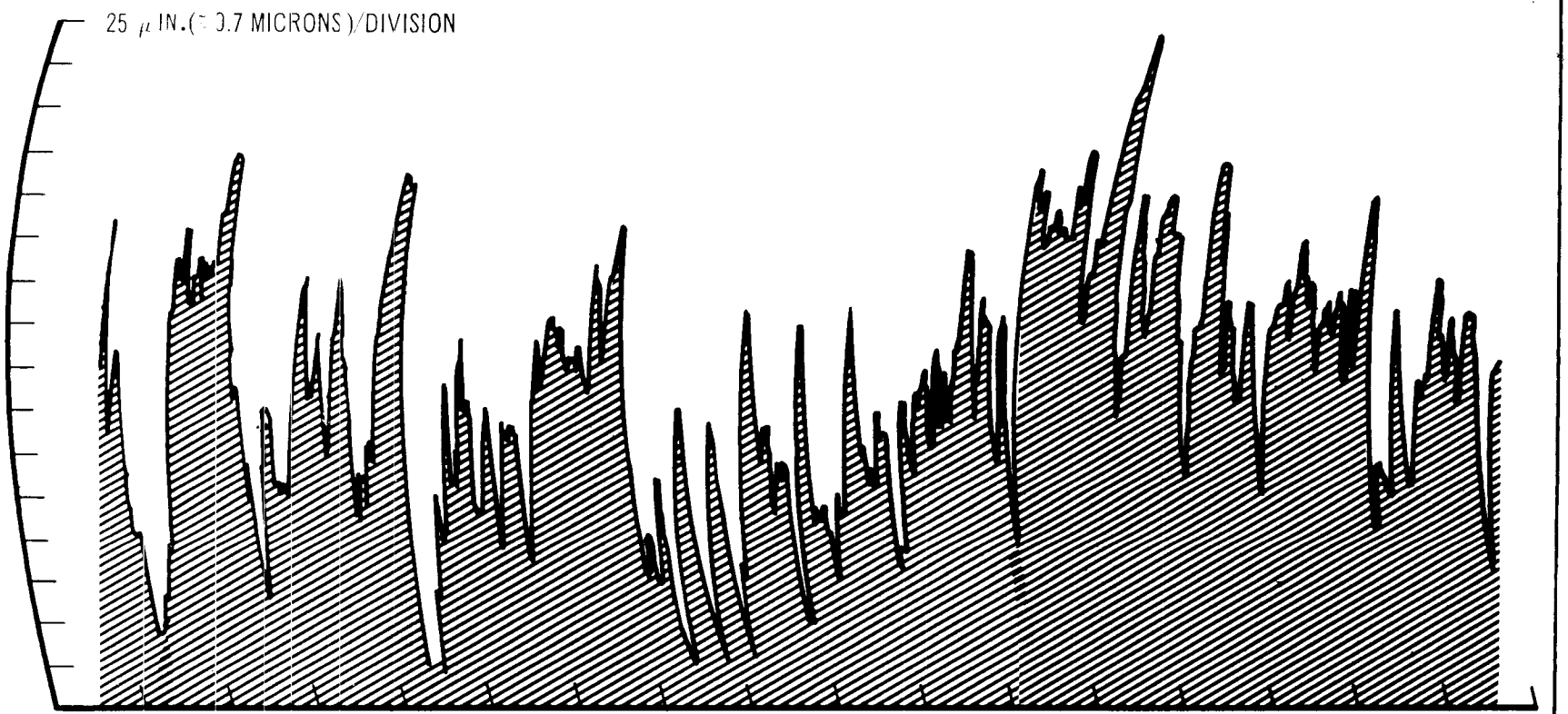

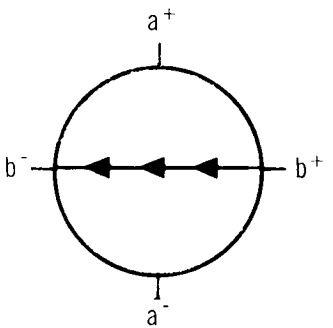

Figure 22. Orthoclase (001) [O (11) 2T] Surface Roughness Along b-Axis

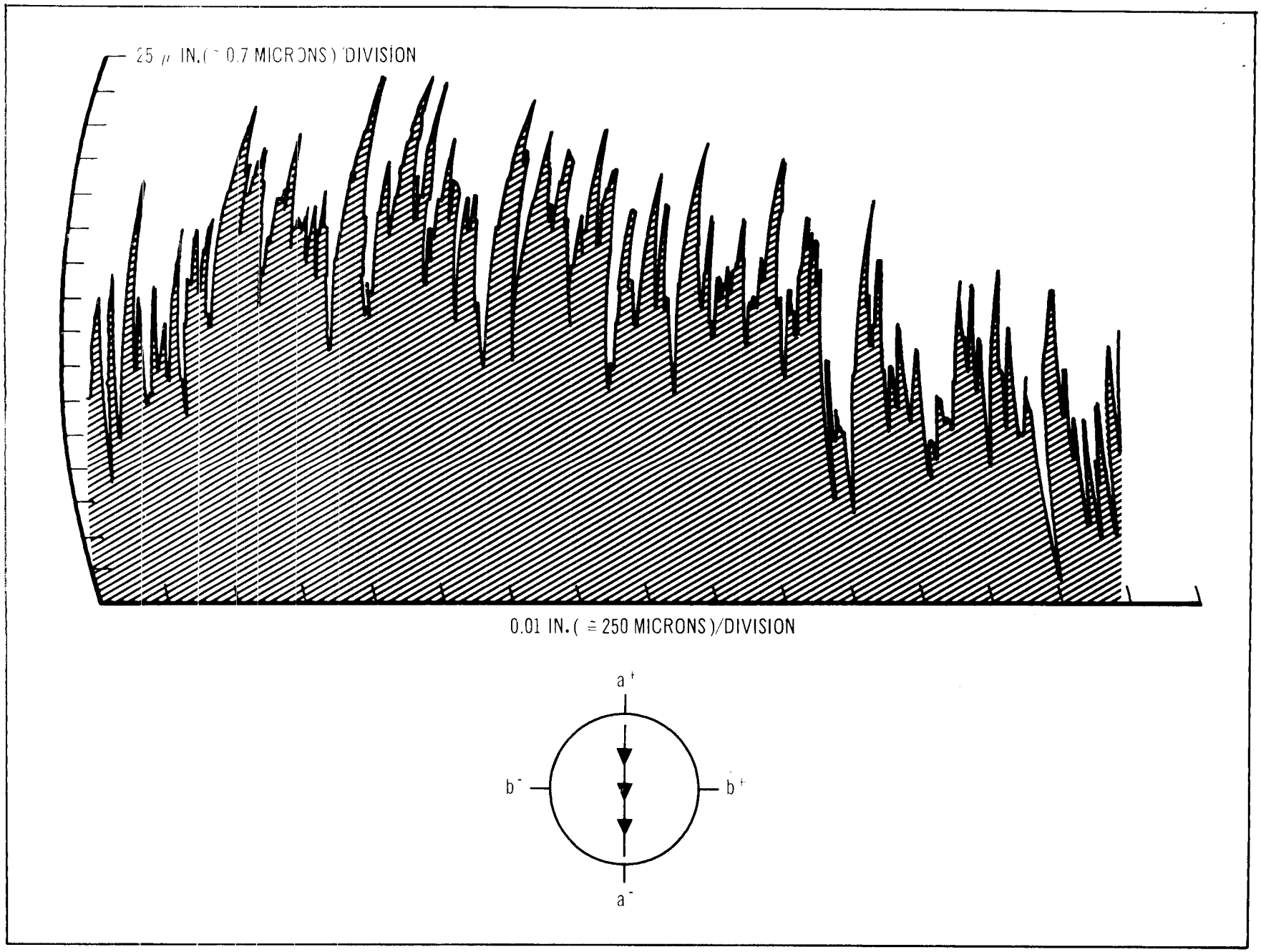

Figure 23. Orthoclase (001) [O (II) 2B] Surface Roughness Along a-Axis

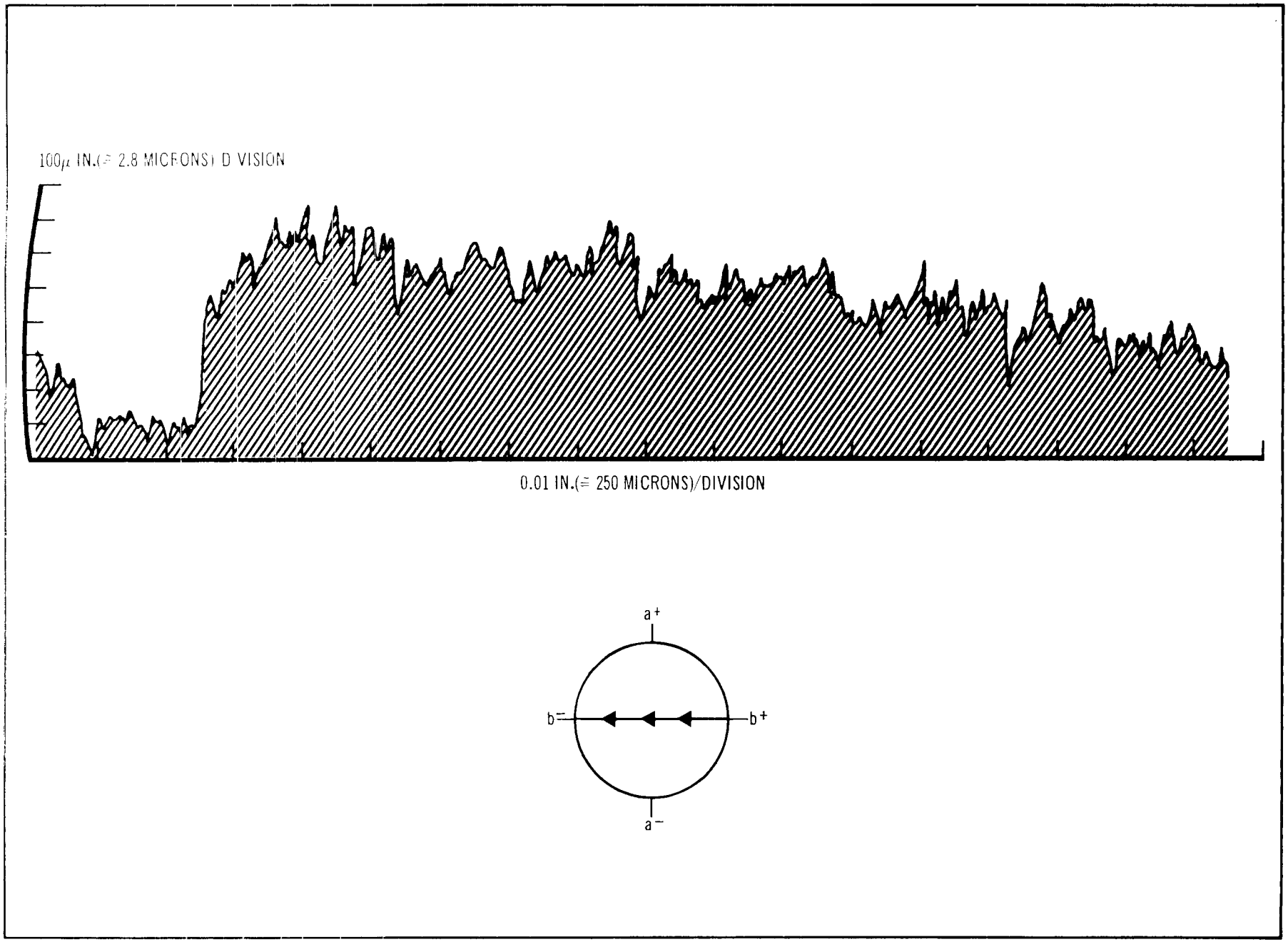

Figure 24. Orthoclase (001) [O (II) 2B] Surface Roughness Along b-Axis

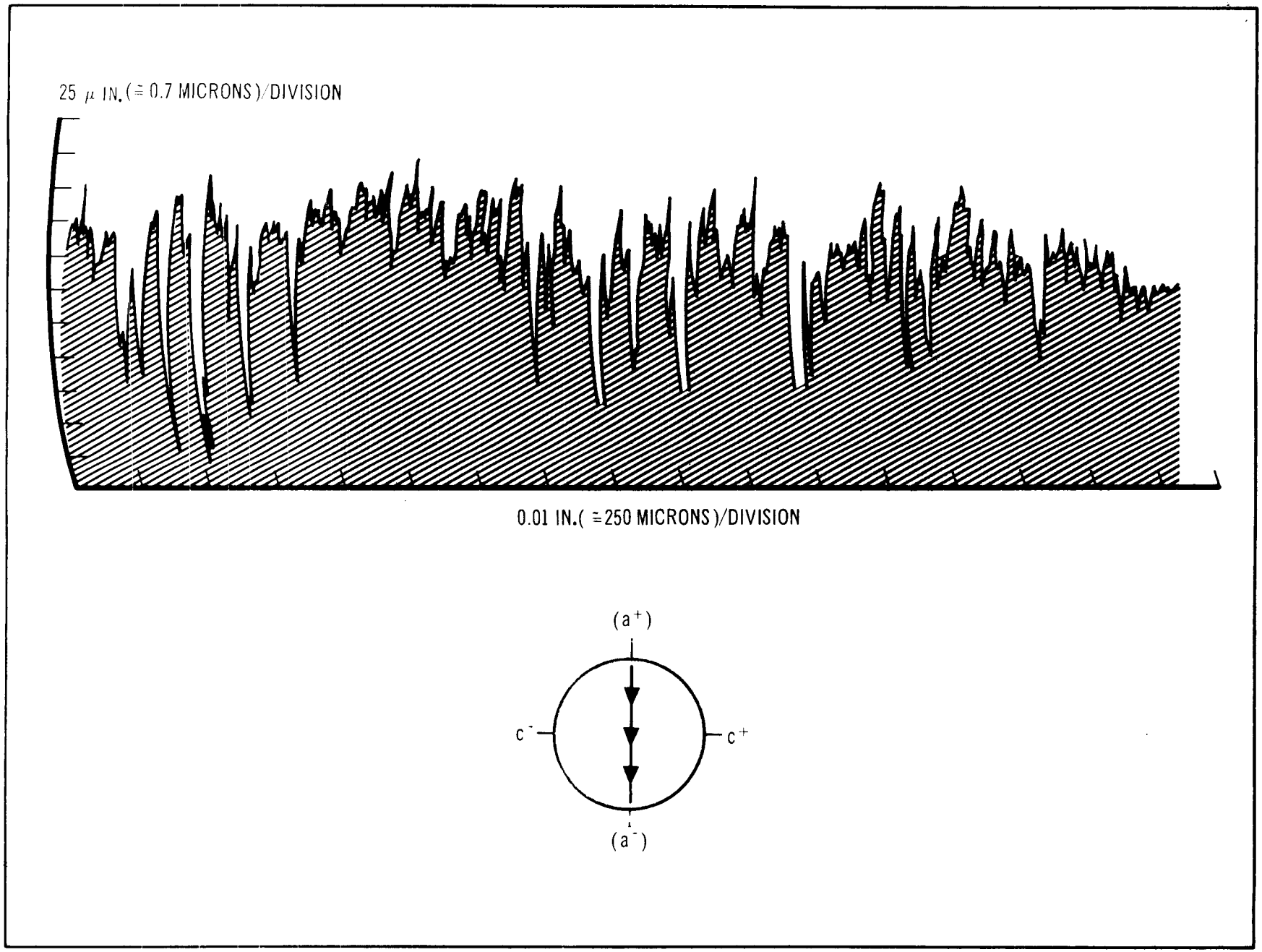

Figure 25. Hypersthene (110) [H3 (||) NP] Surface Roughness Along a-Axis Projection

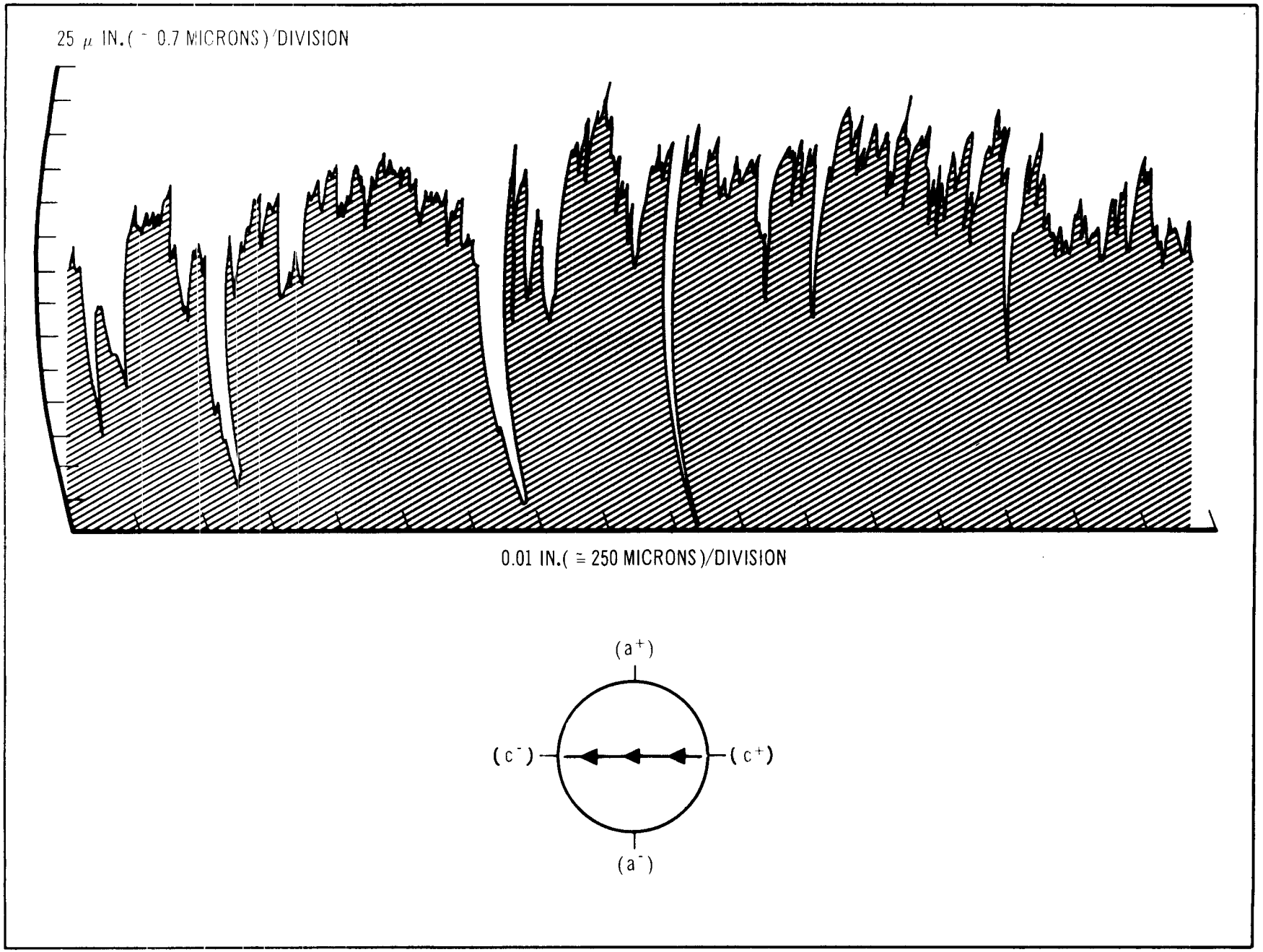

Figure 26. Hypersthene (110) [H3 (II) NP] Surface Roughness Along c-Axis

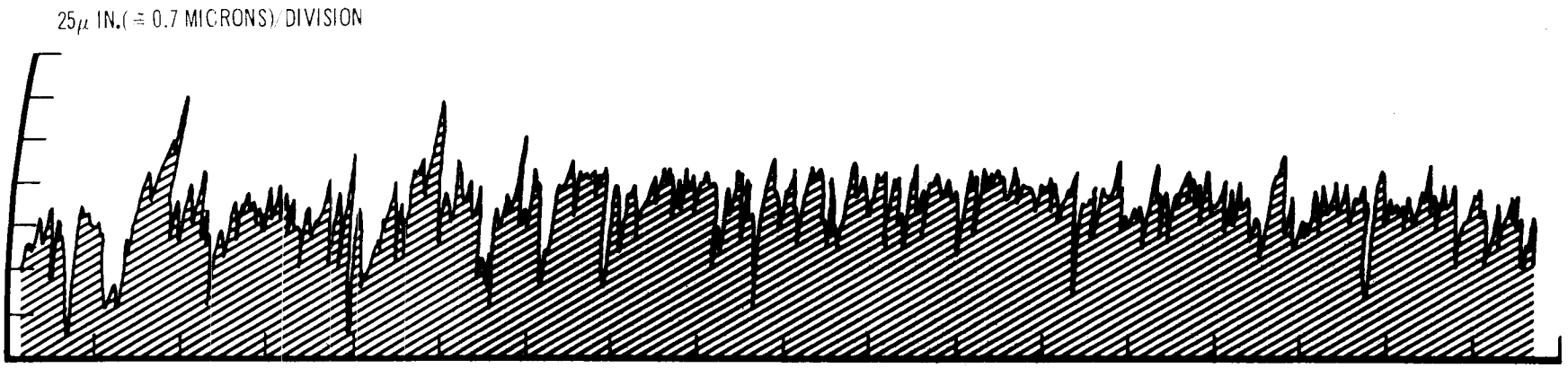

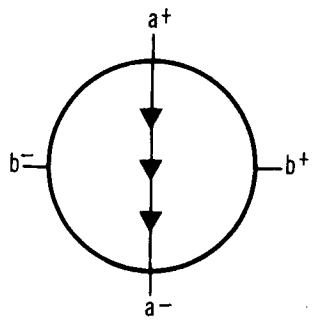

Figure 27. Albite (001) [A (II)NP] Surface Roughness along a-Axis

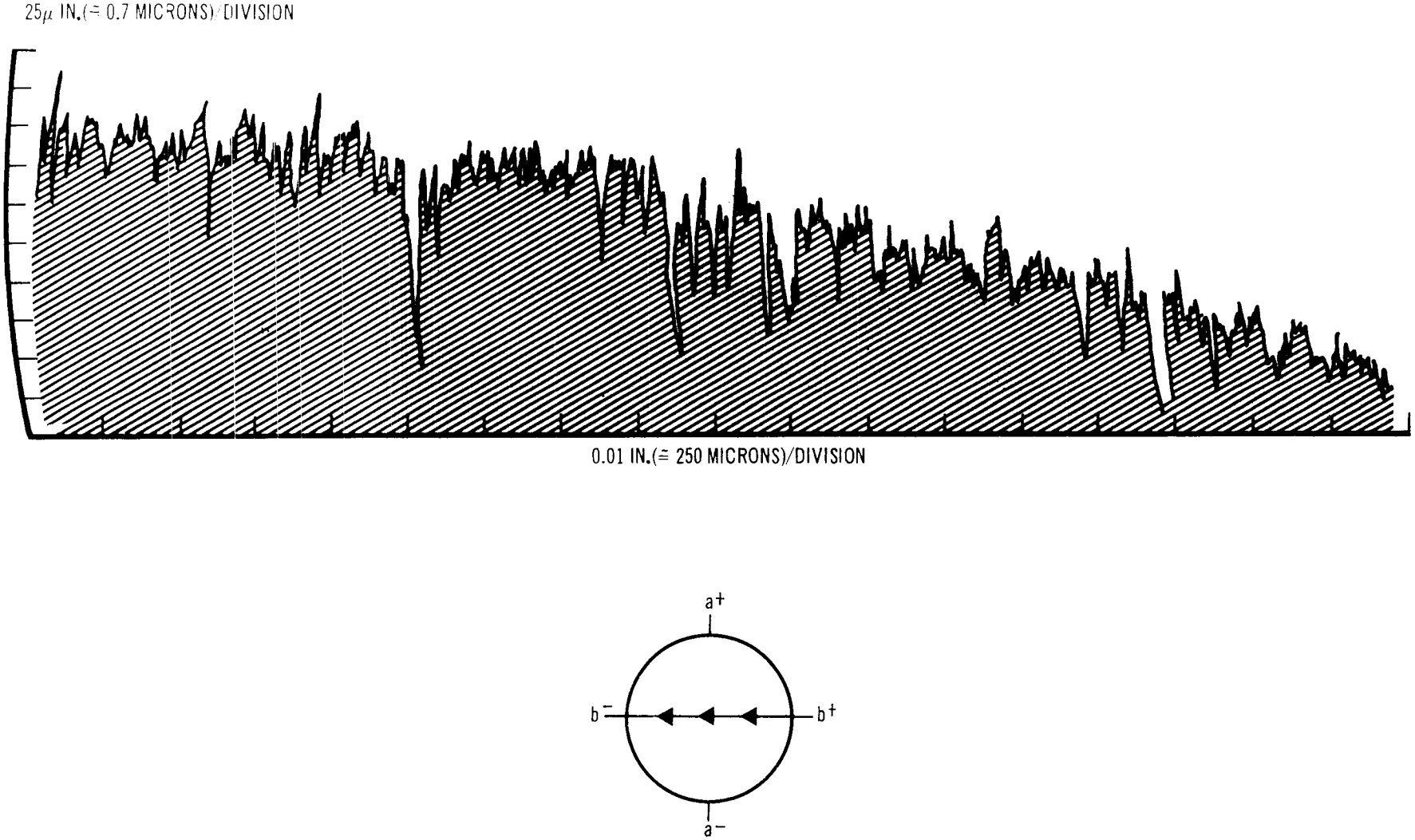

Figure 28. Albite (001) [A (||) NP] Surface Roughness Along b-Axis

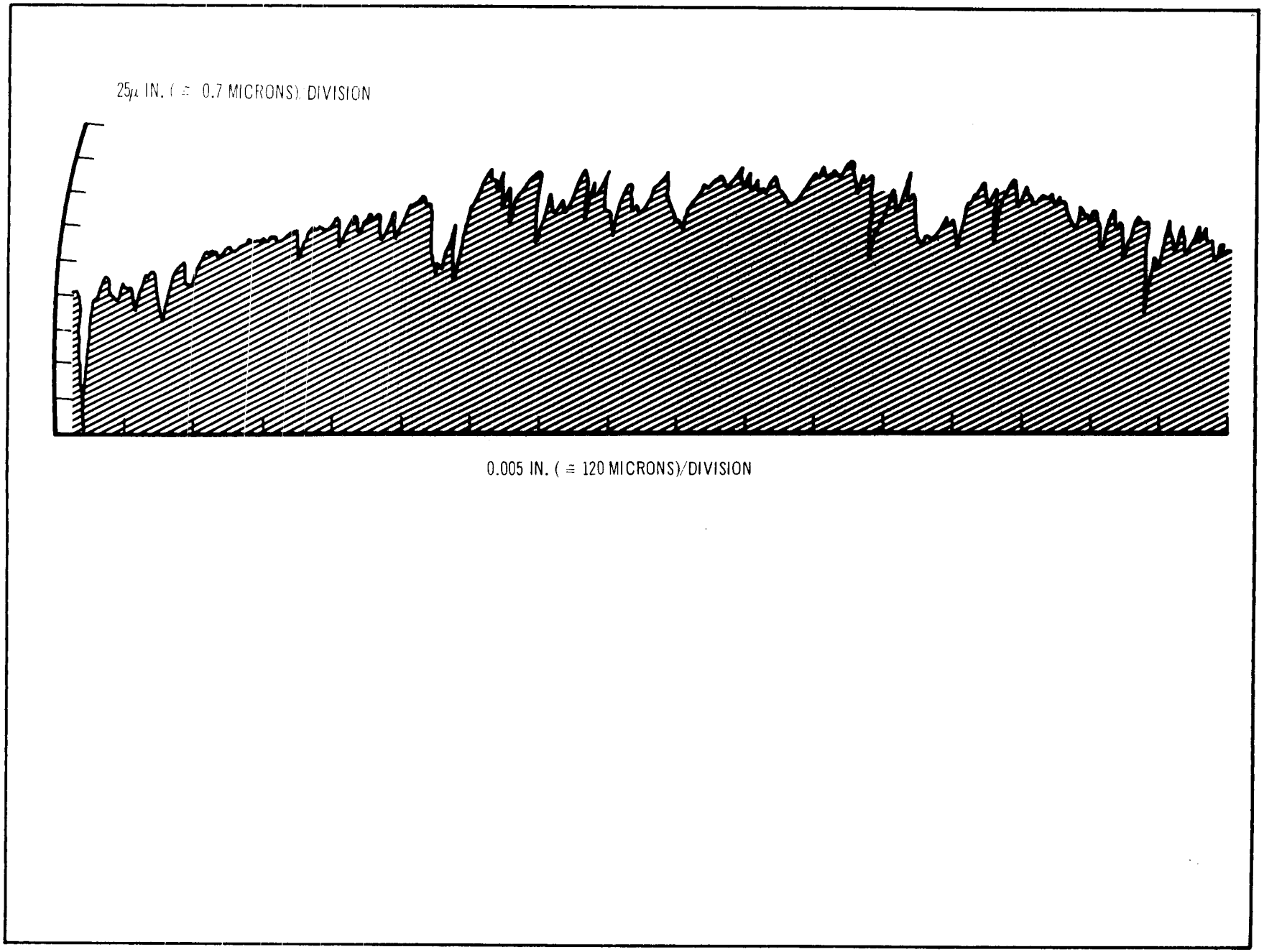

Figure 29. Aluminum Surface Roughness Profile

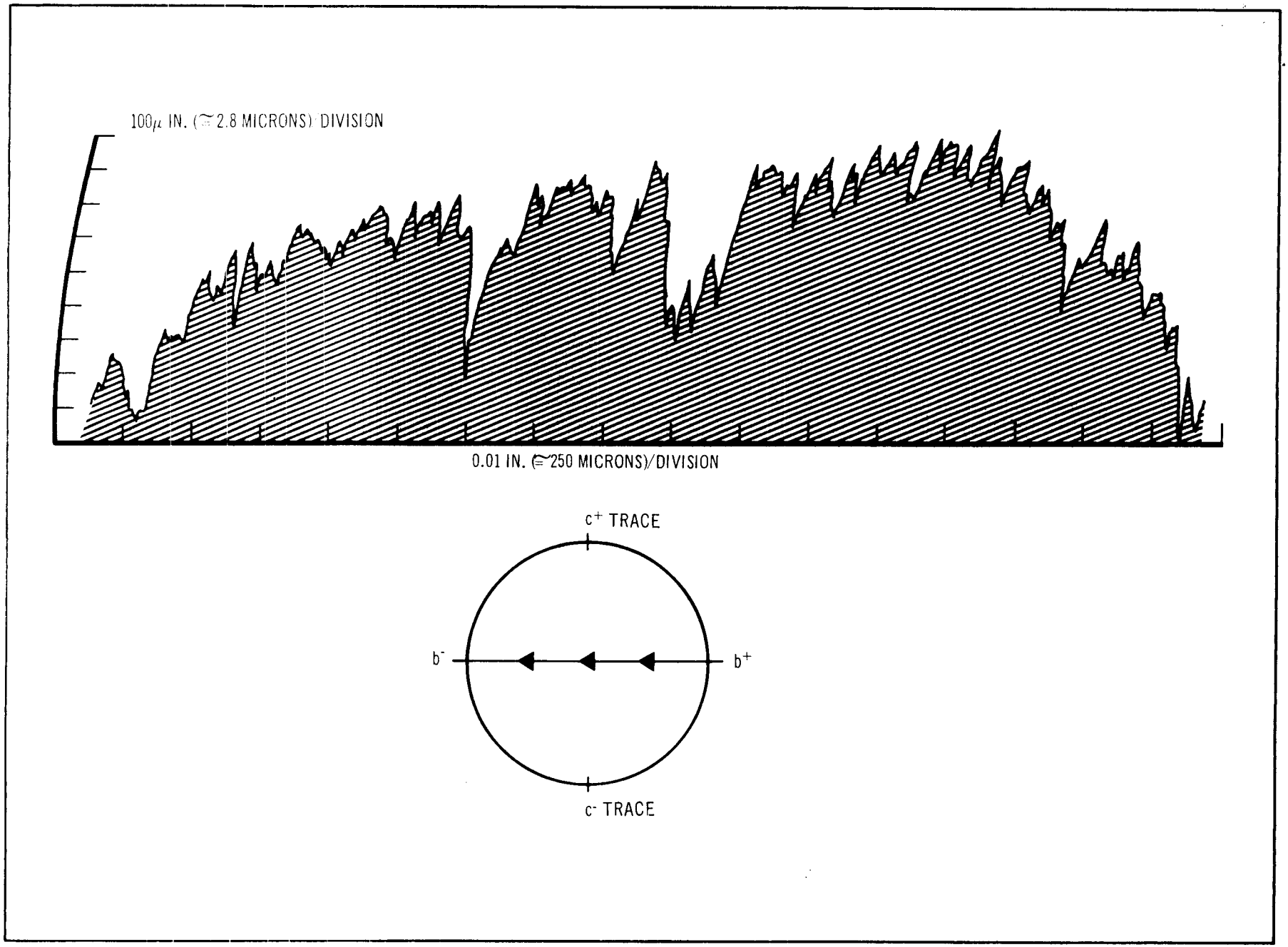

Figure 30. Hornblende (101) [Hb (⊥) IT] Surface Roughness Along b-Axis

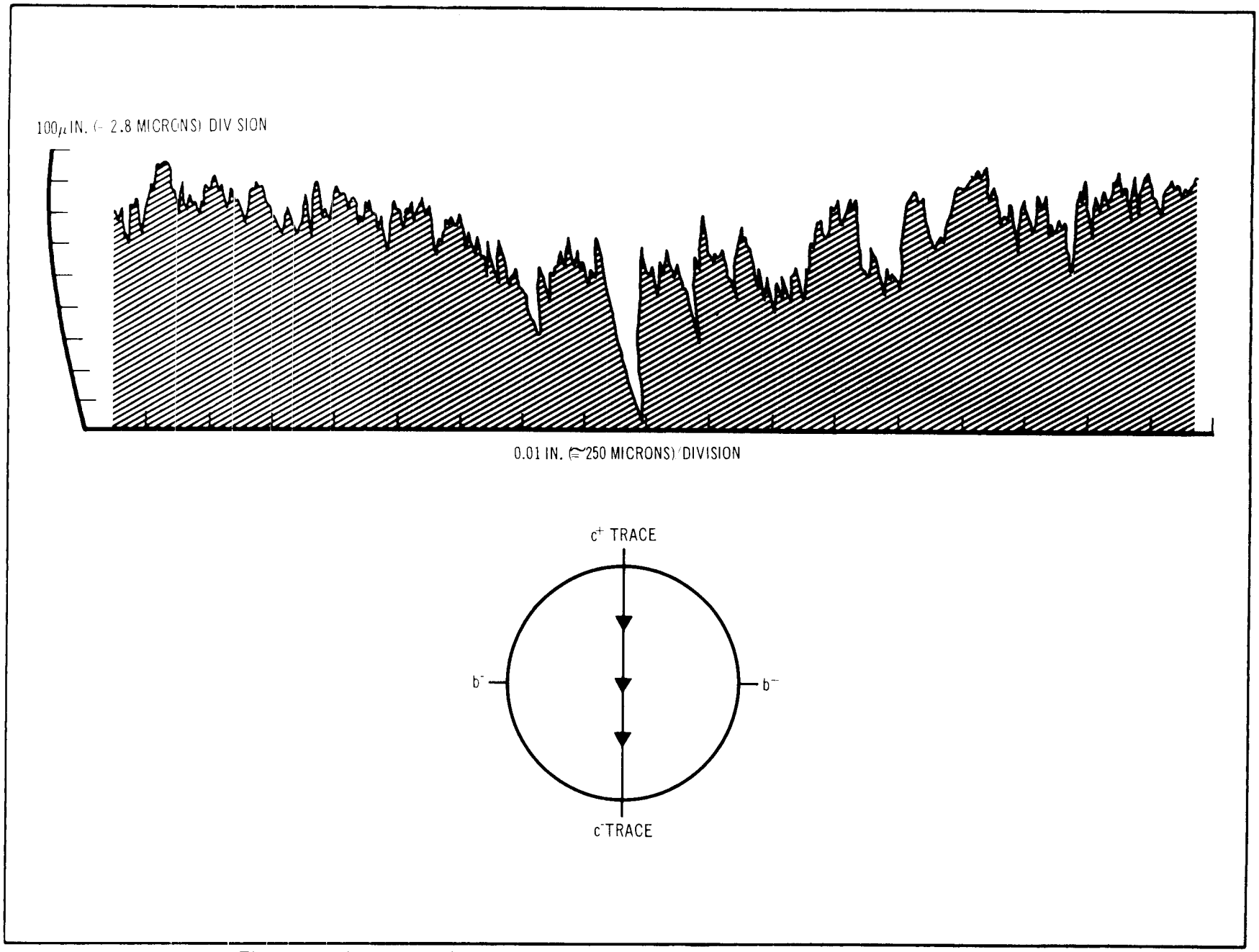

Figure 31. Hornblende (101) [Hb (⊥) IT] Surface Roughness Along c-Axis

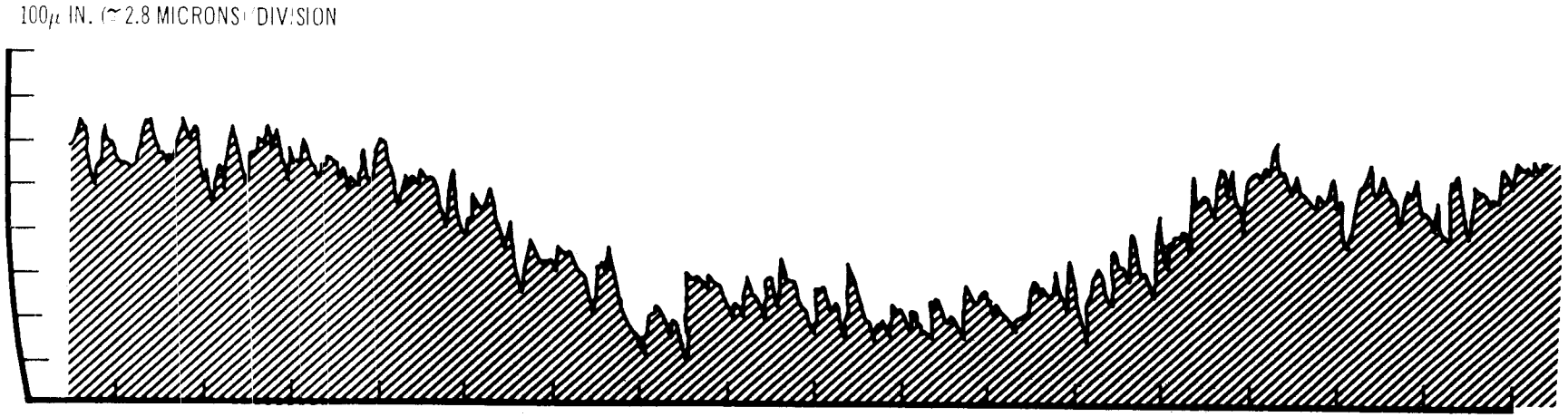

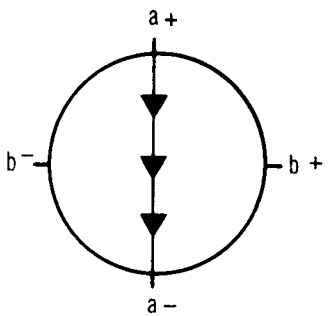

Figure 32. Bytownite (001) [B (II) NP] Surface Roughness Along a-Axis

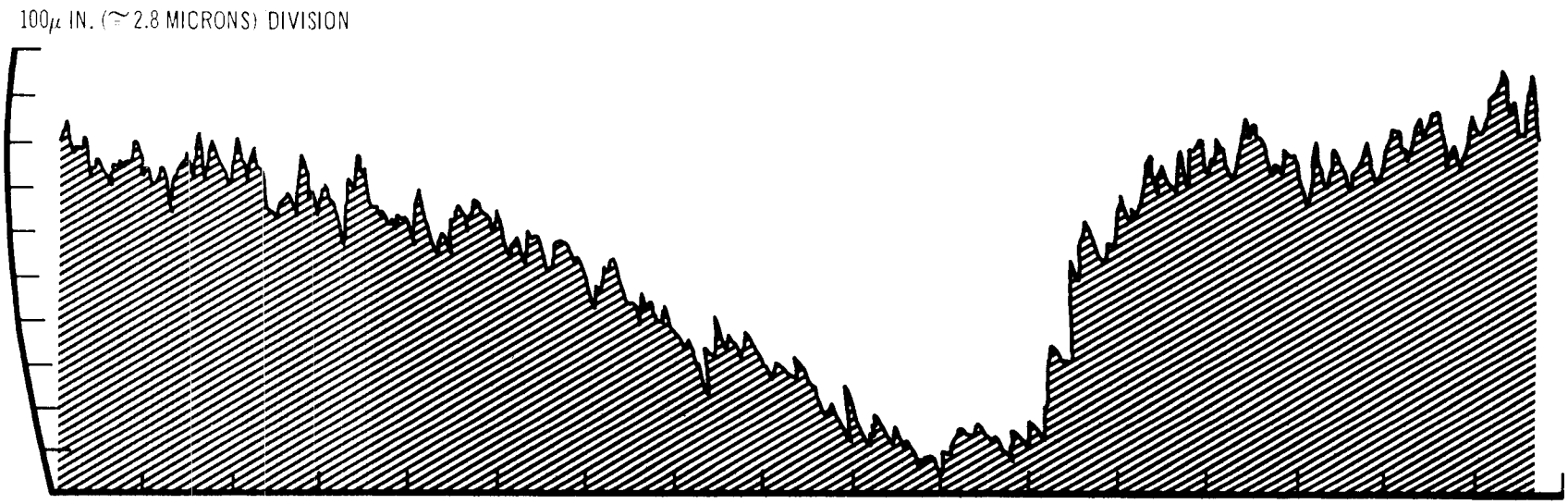

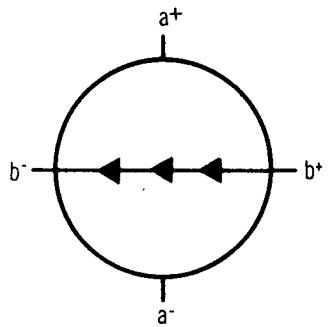

Figure 33. Bytownite (001) [B(||)NP] Surface Roughness Along **b**-Axis

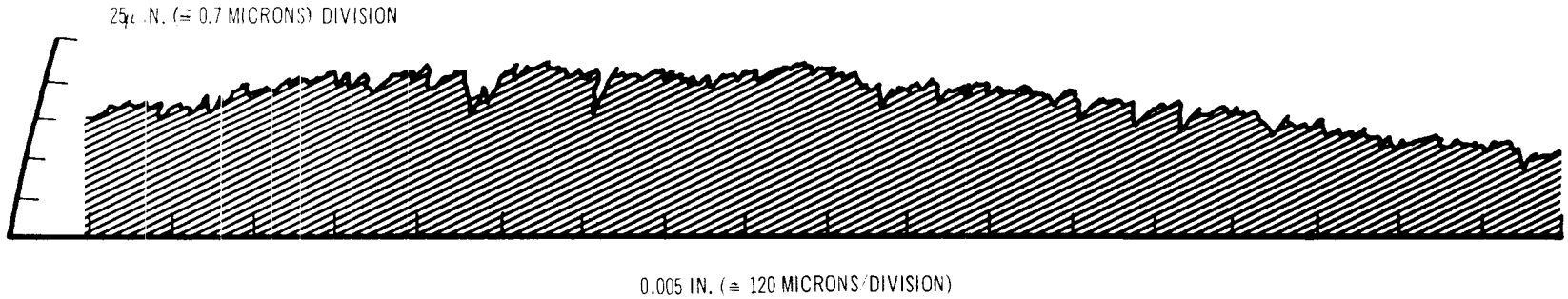

Figure 34. Titanium Alloy Surface Roughness Profile

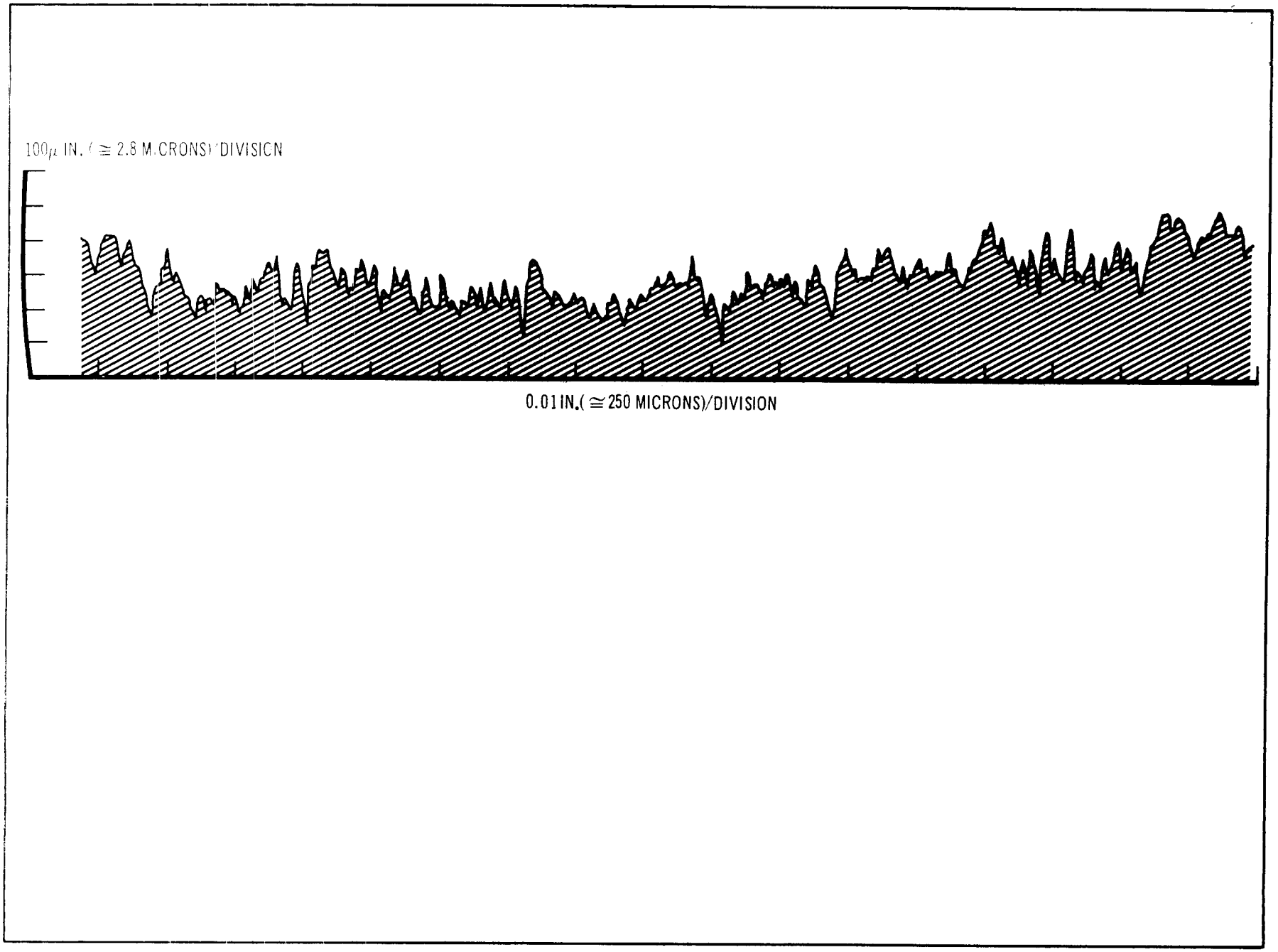

Figure 35. Beryllium Surface Roughness Profile

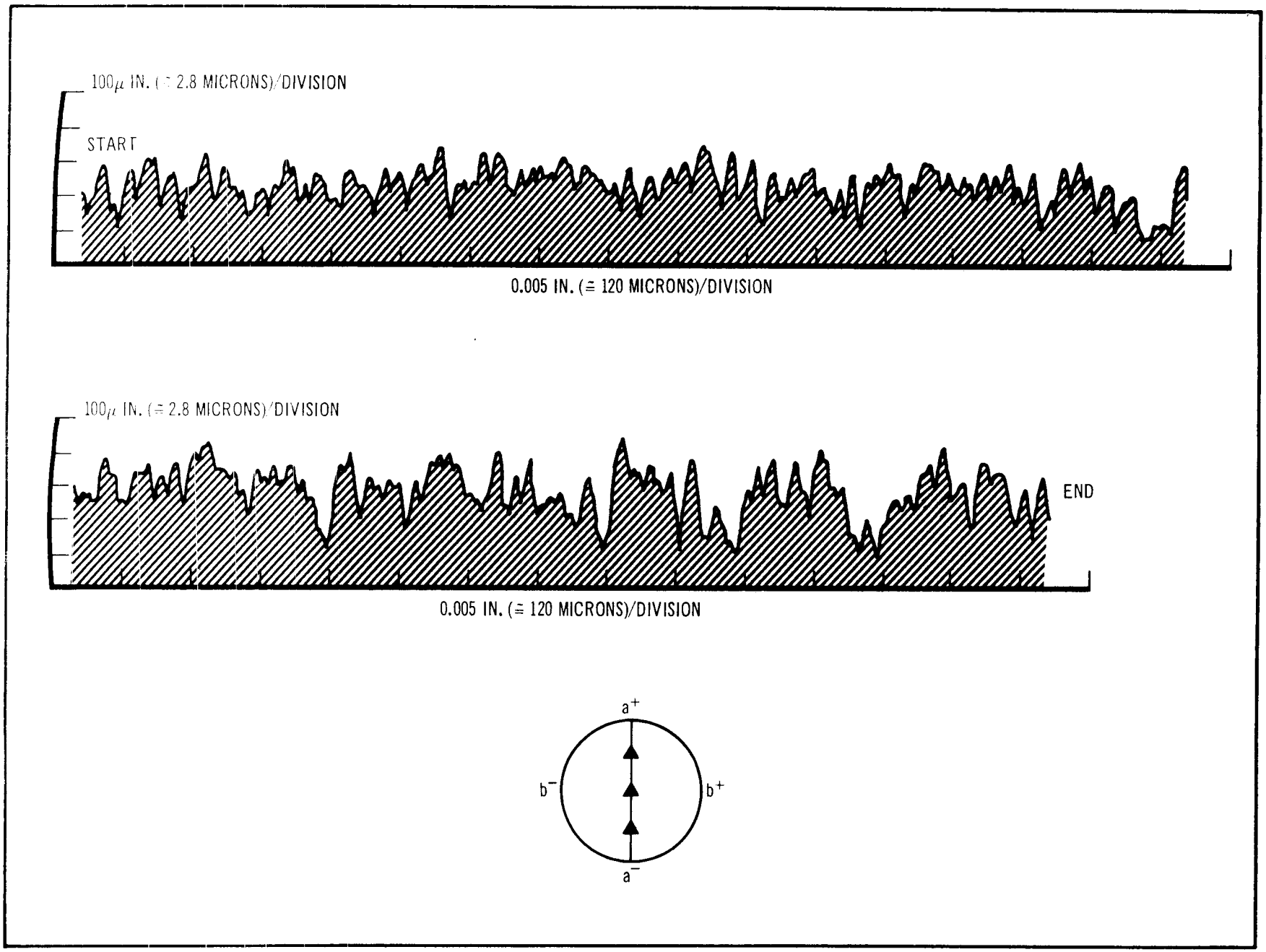

Figure 36. Orthoclase (001) [0(11) IB] Surface Roughness Along a-Axis

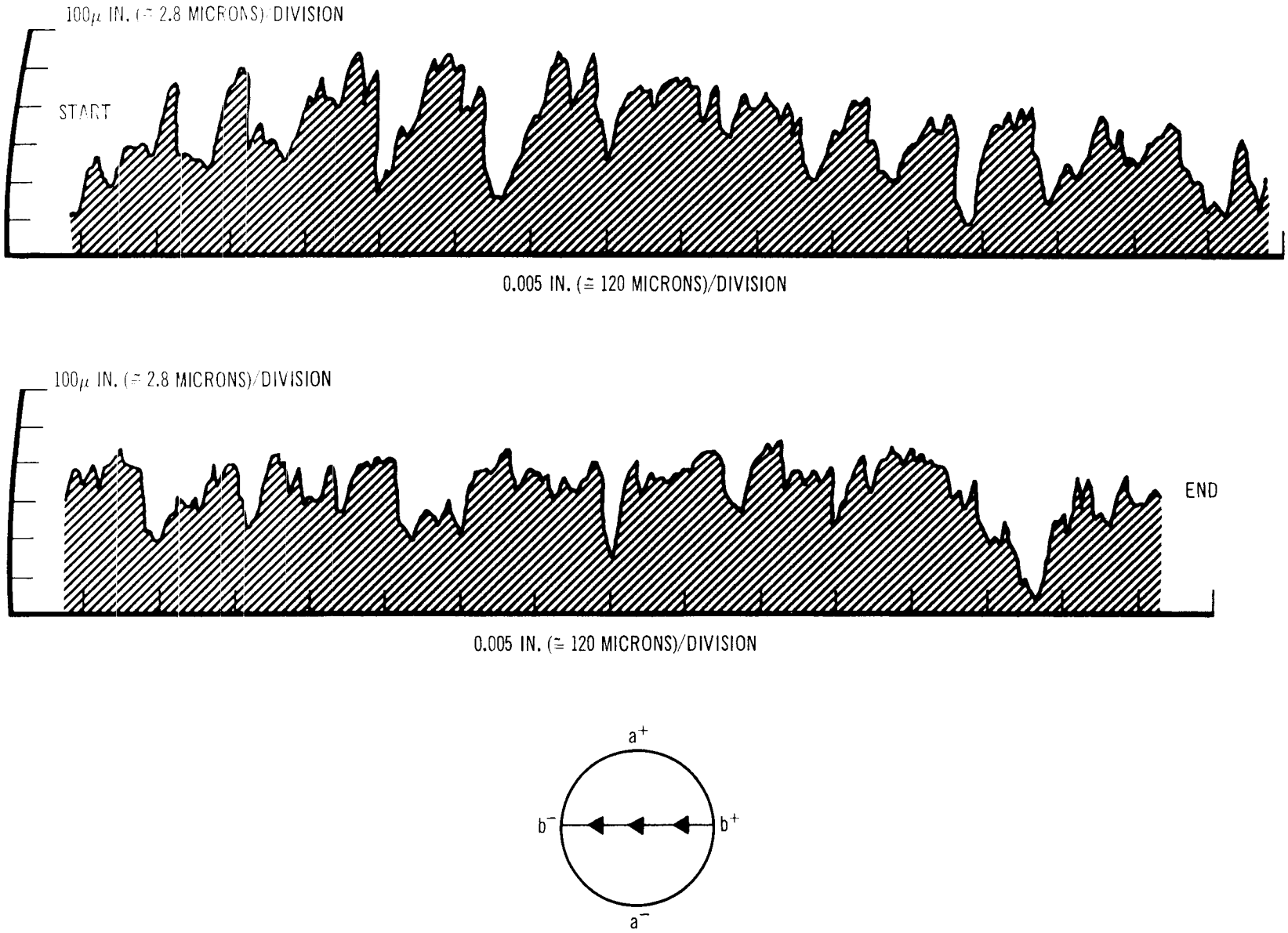

Figure 37. Orthoclase (001) [0(11) 1B] Surface Roughness Along b-Axis

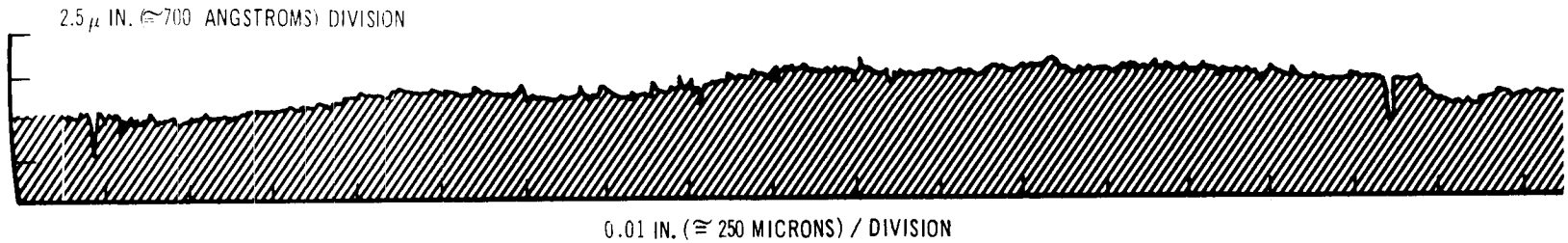

Figure 38. No.1723 Glass Surface Roughness Profile

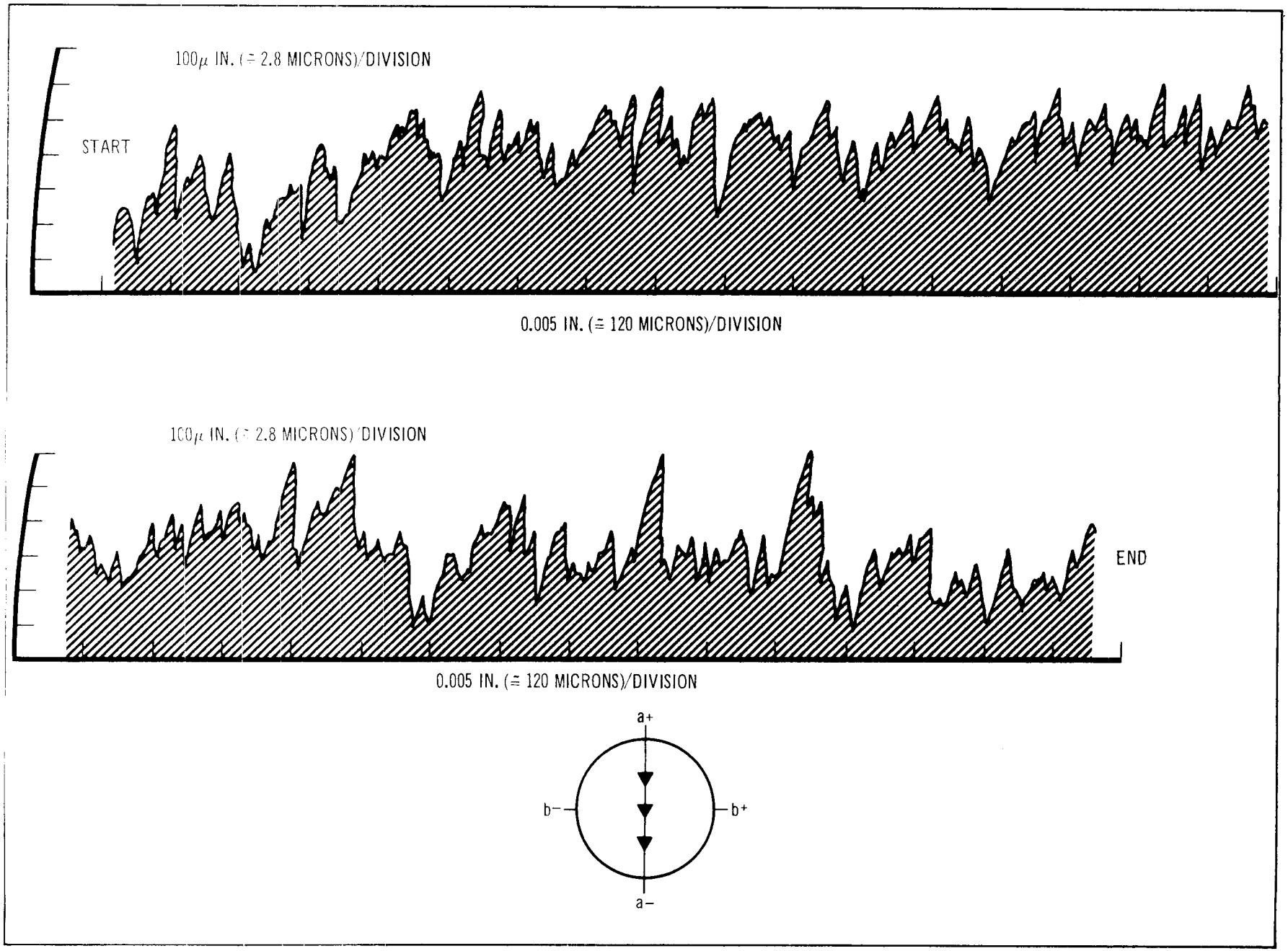

Figure 39. Orthoclase (001) [0 (11) 1T] Surface Roughness Along a-Axis

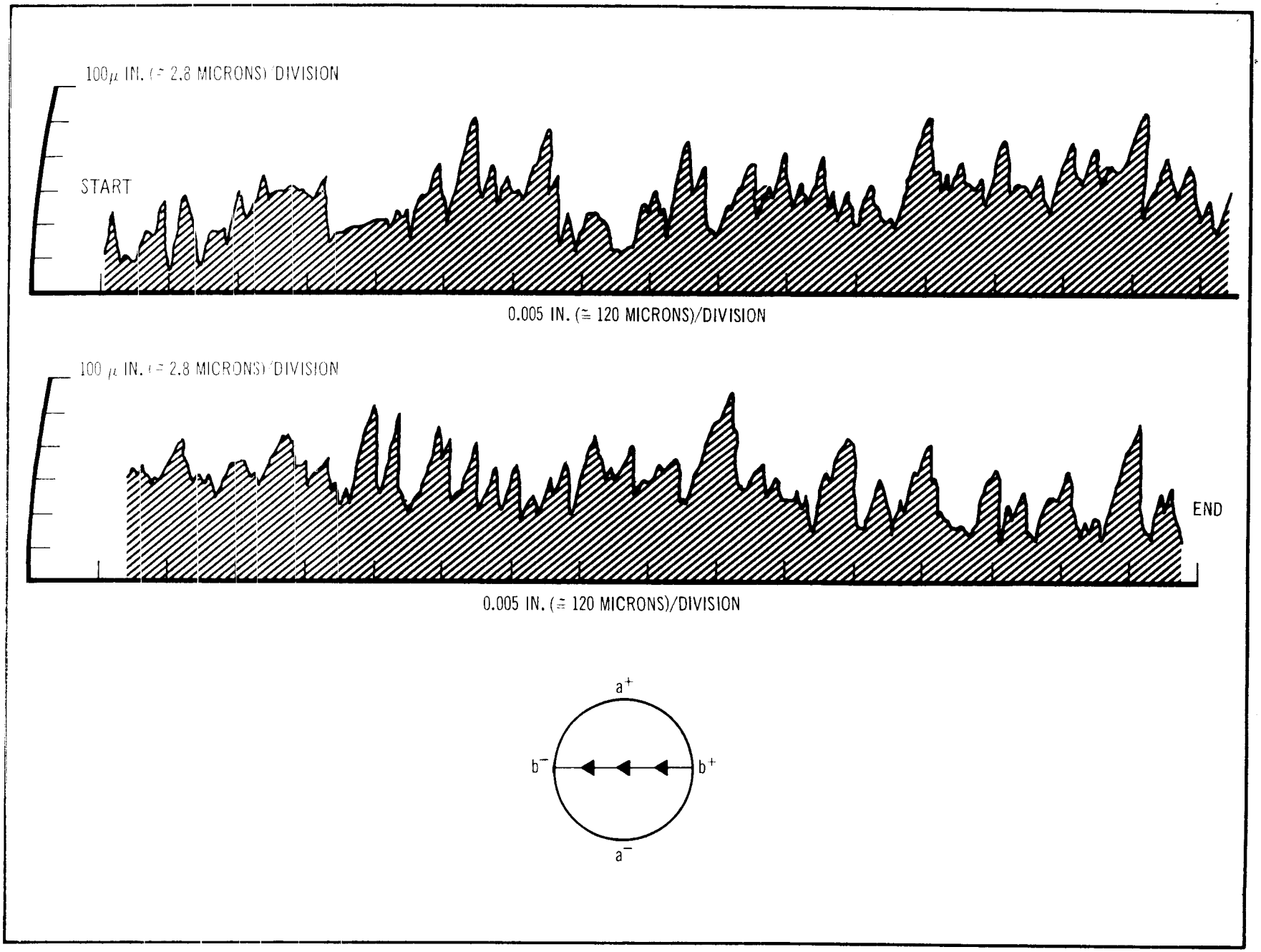

Figure 40. Orthoclase (001) [0(11) 1T] Surface Roughness Along b-Axis

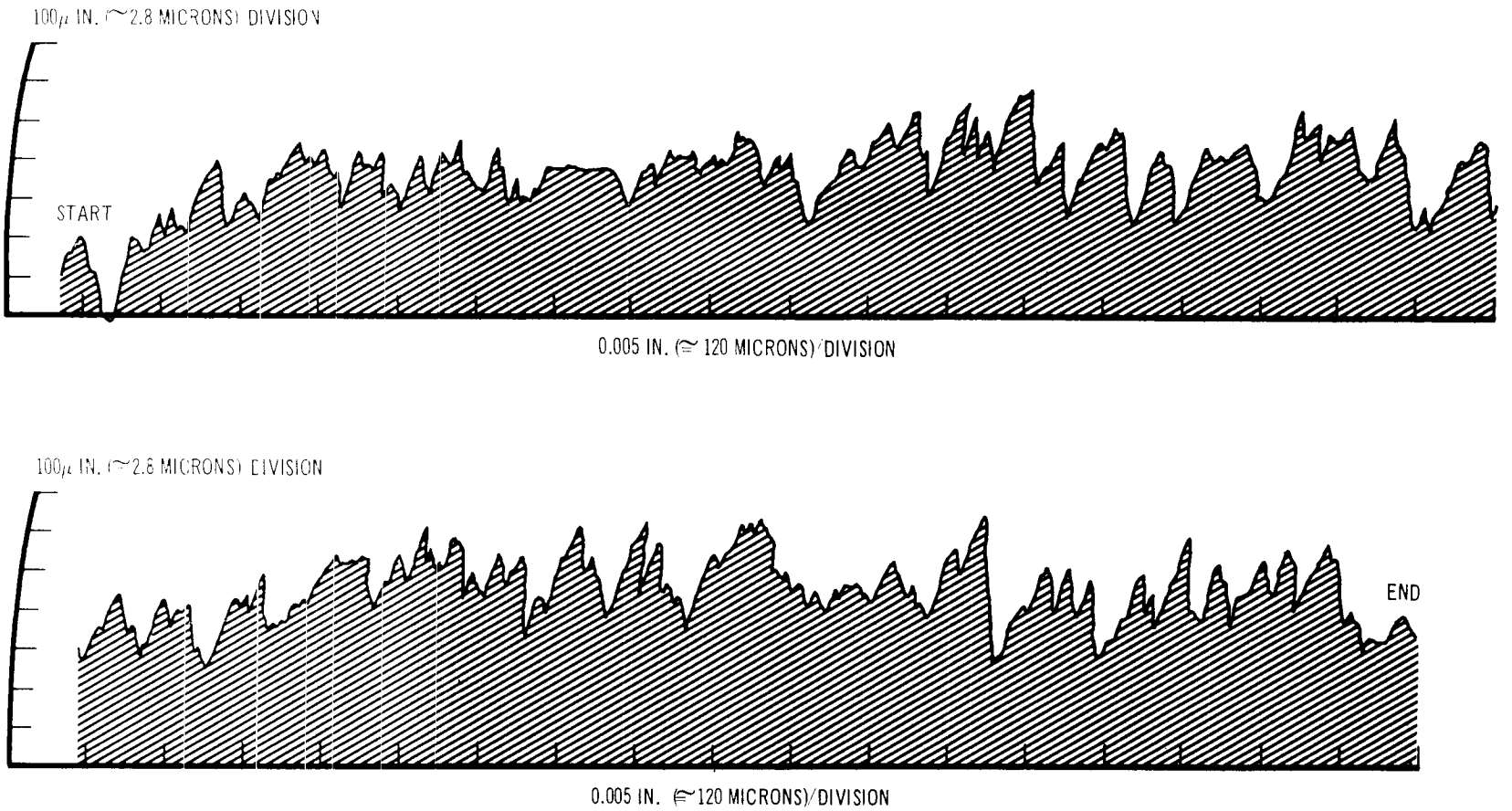

Figure 41. Ceramic (Alumina) Surface Roughness Profile

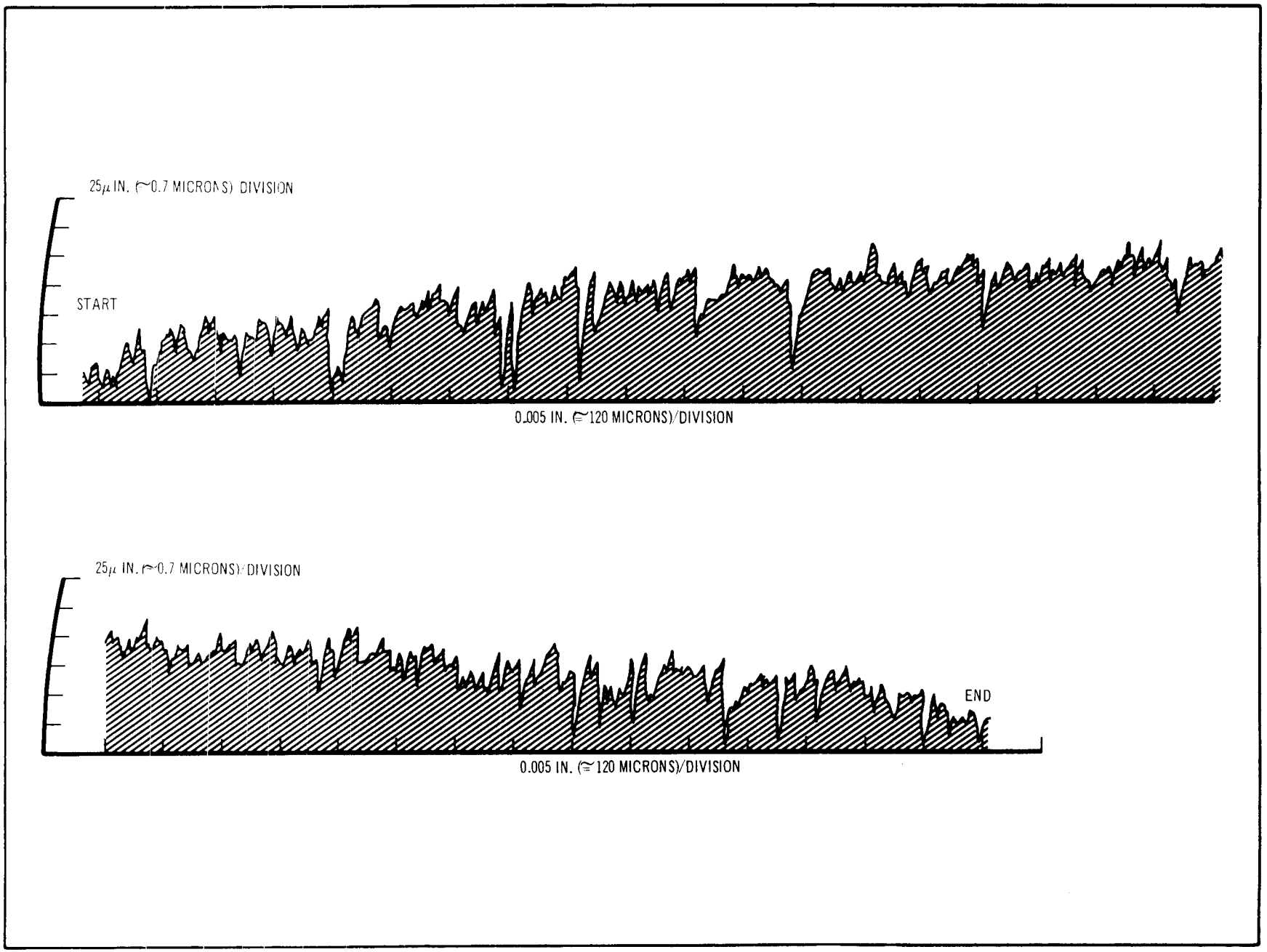

Figure 42. Obsidian [OB (IT)] Surface Roughness Profile

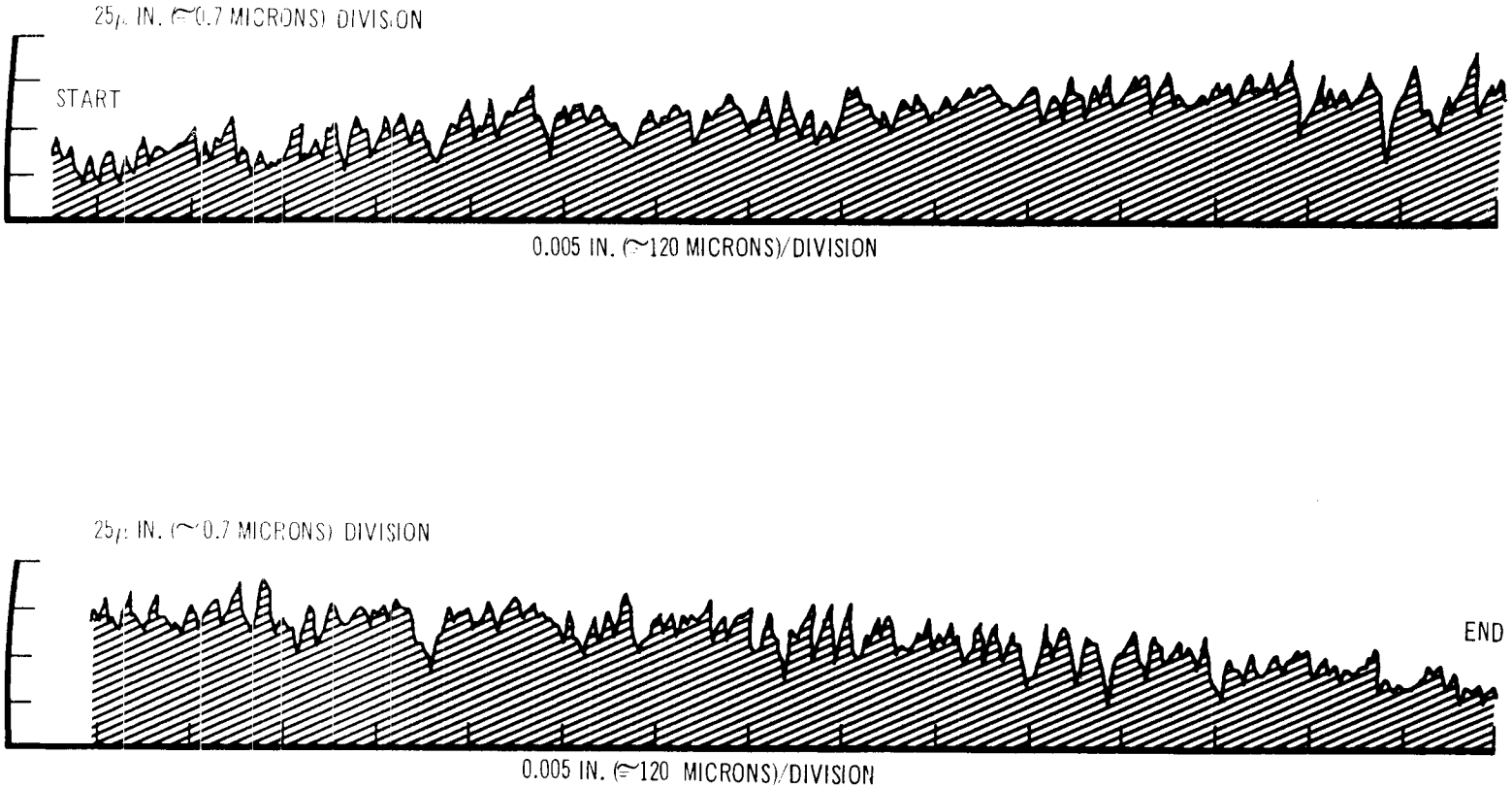

Figure 43. Obsidian [OB (IB)] Surface Roughness

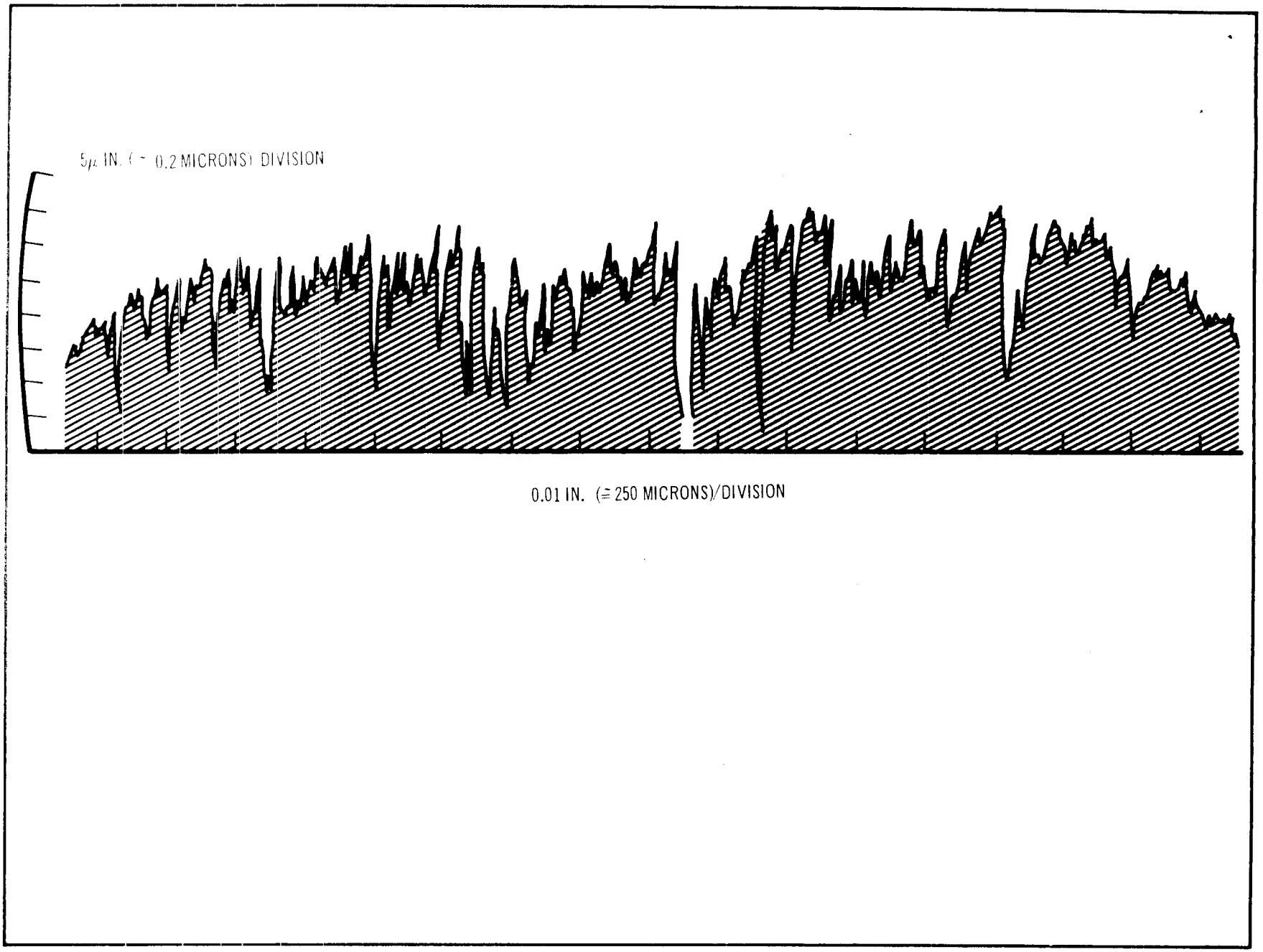

Figure 44. Stainless Steel Surface Roughness Profile

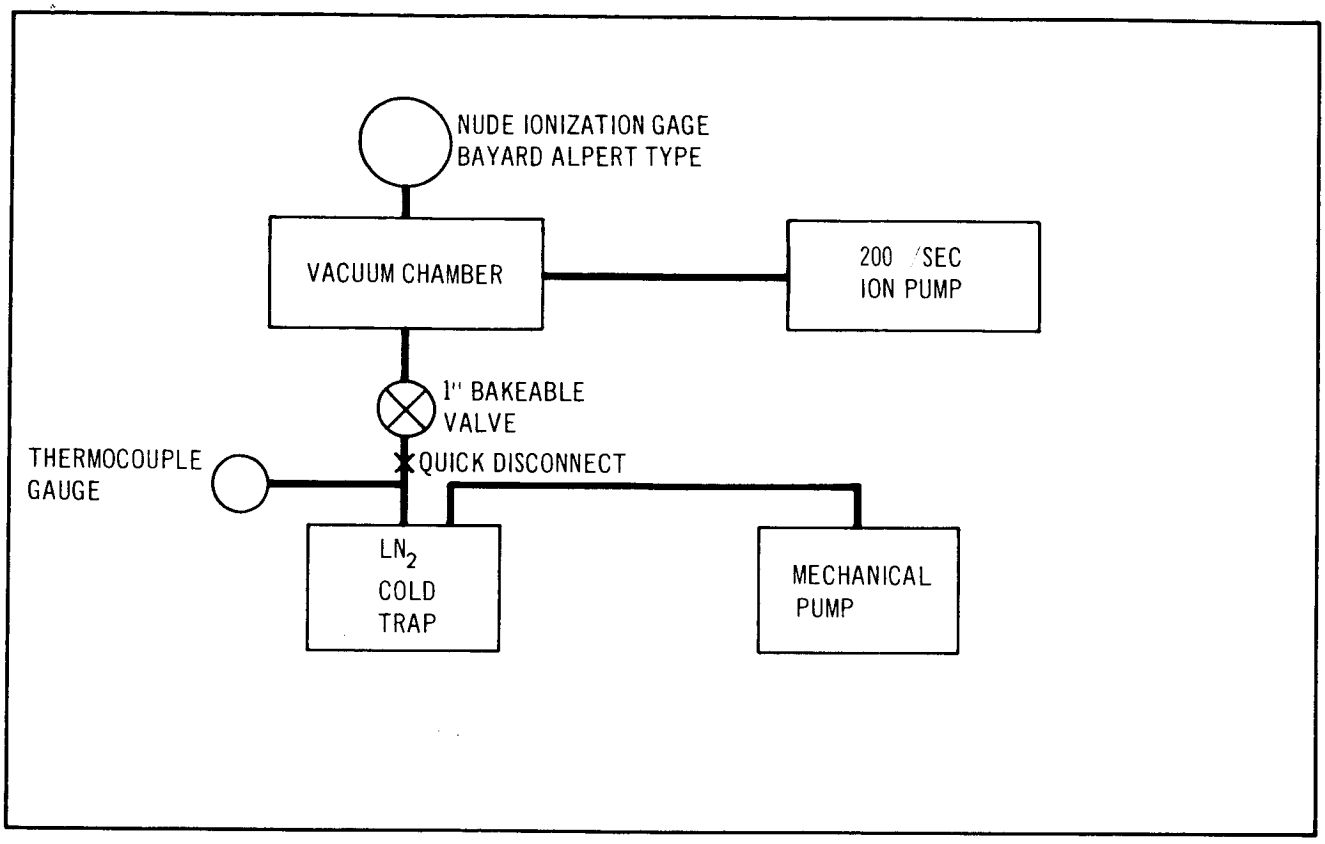

Figure 45. Schematic of Vacuum System

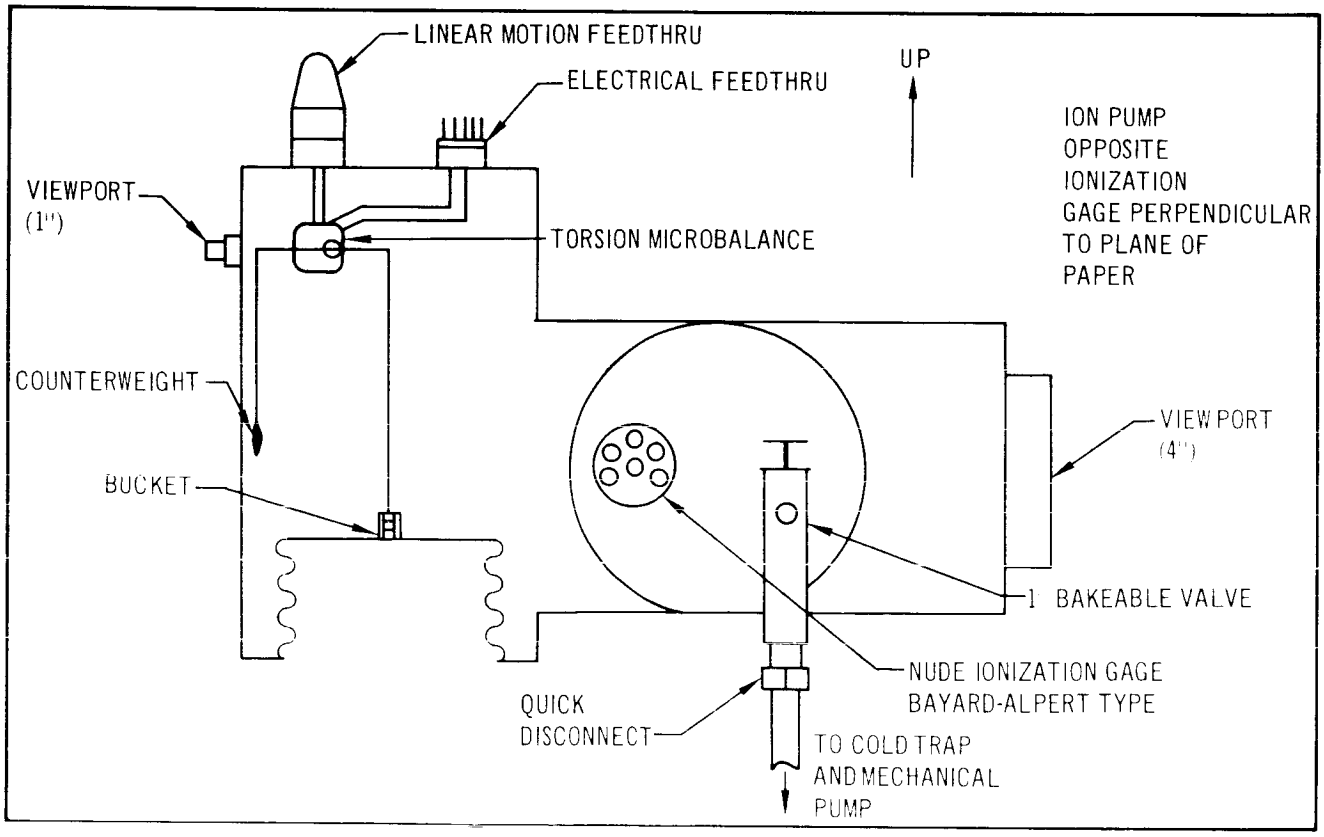

Figure 46. Ultra-High Vacuum Chamber

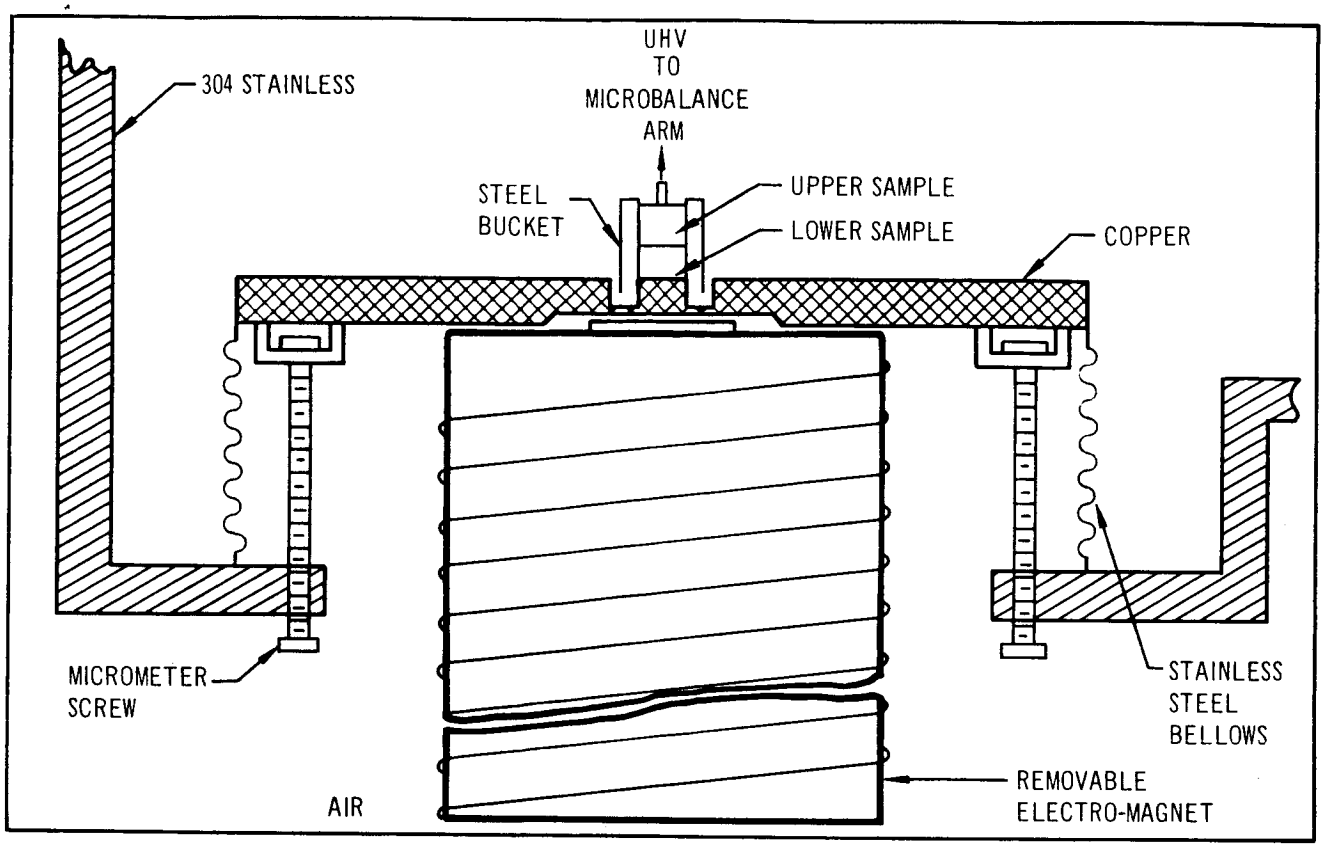

Figure 47. Load Application System

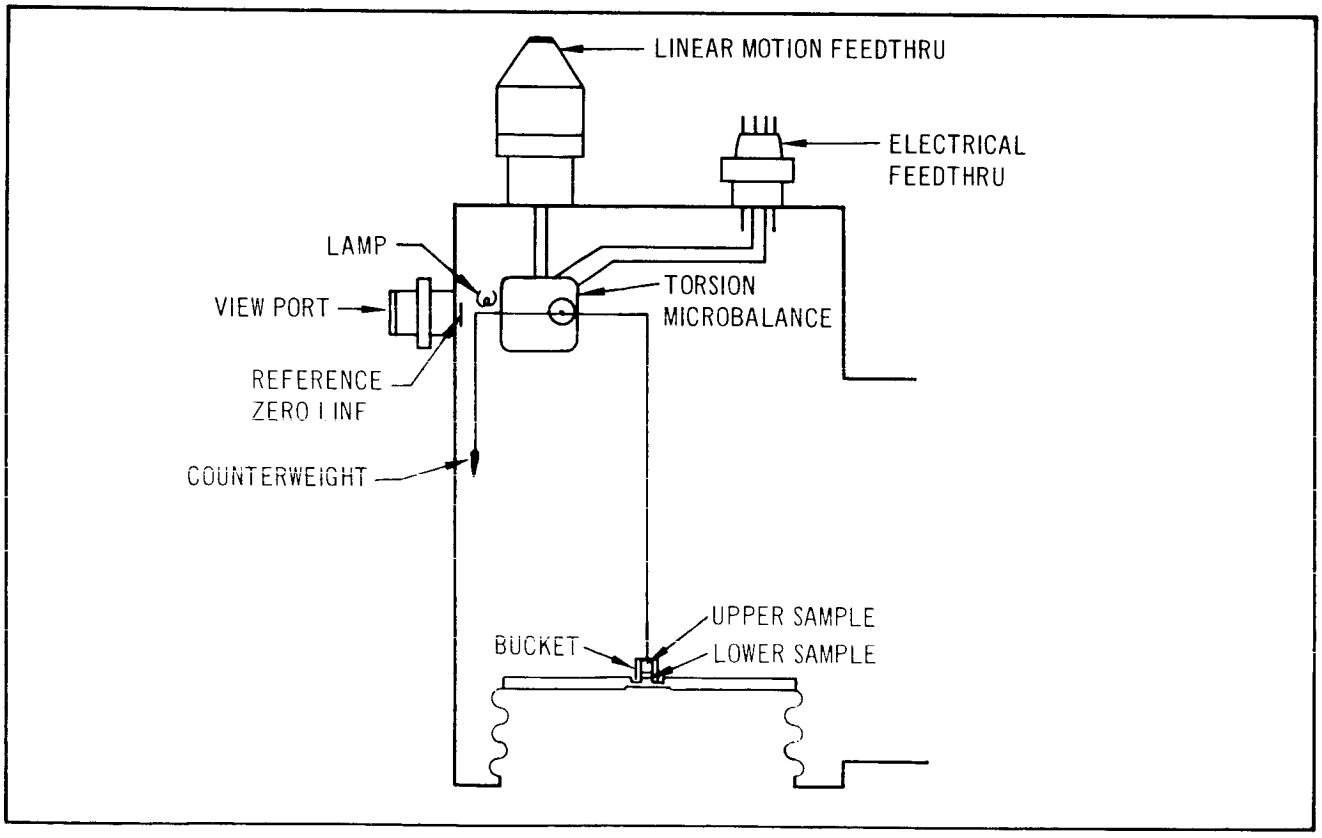

Figure 48. Adhesion Measuring System

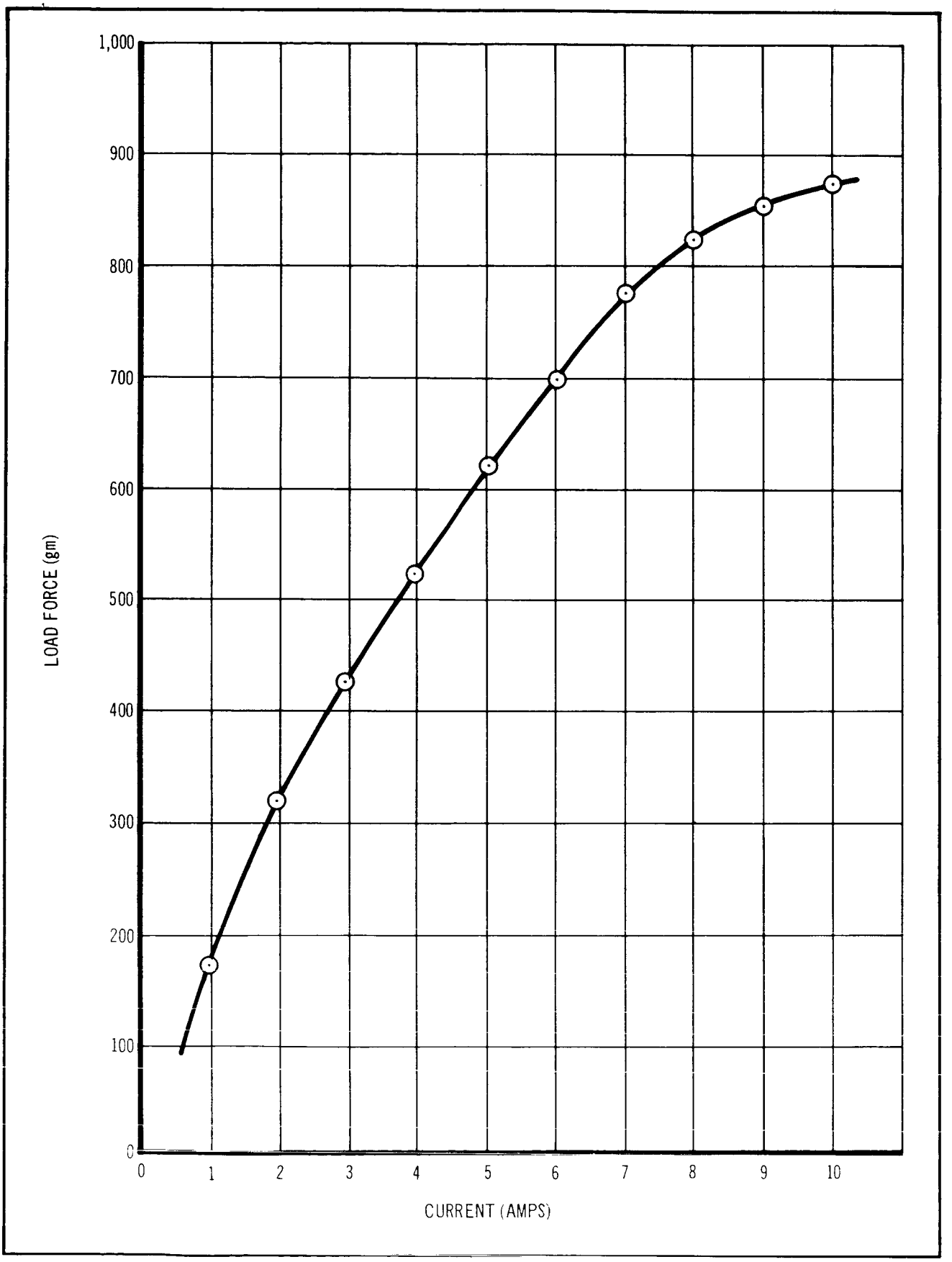

Figure 49. Load Calibration for Electromagnet

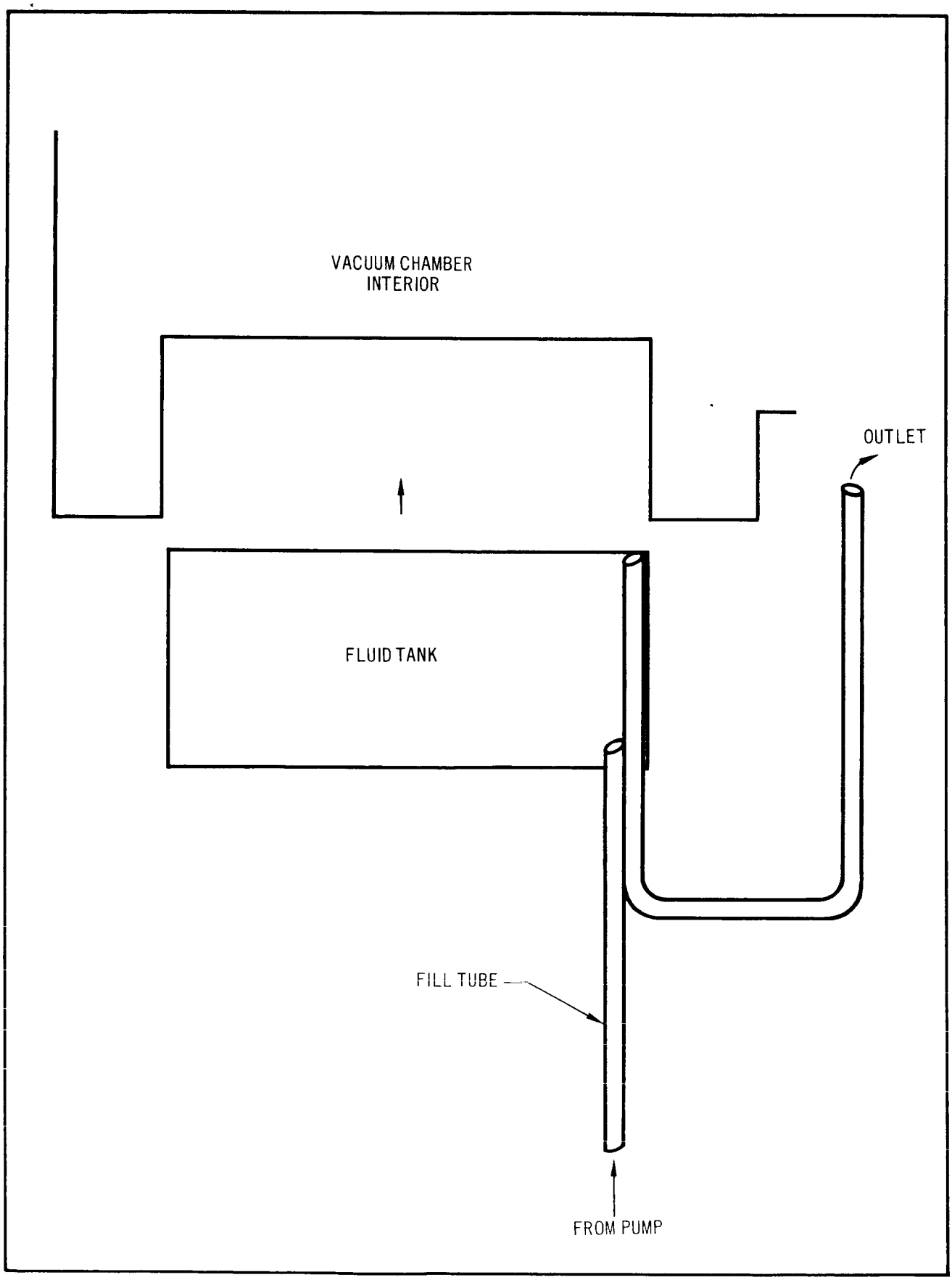

Figure 50. Temperature Control System

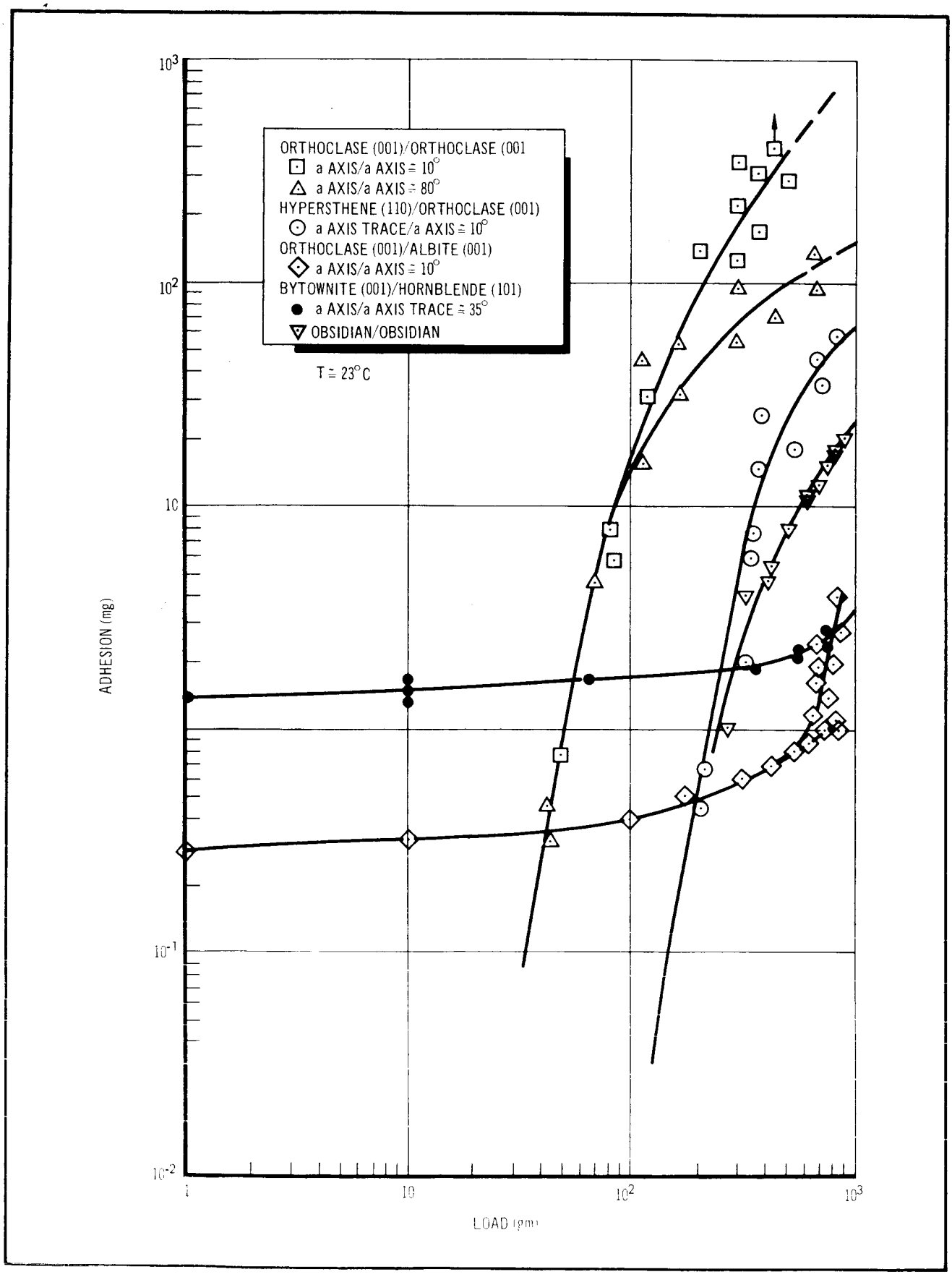

Figure 51. Adhesion Force vs Load for Silicates

Figure 52. Orthoclase (001) Surface After Contact with Hypersthene (110 (Reflected Light)

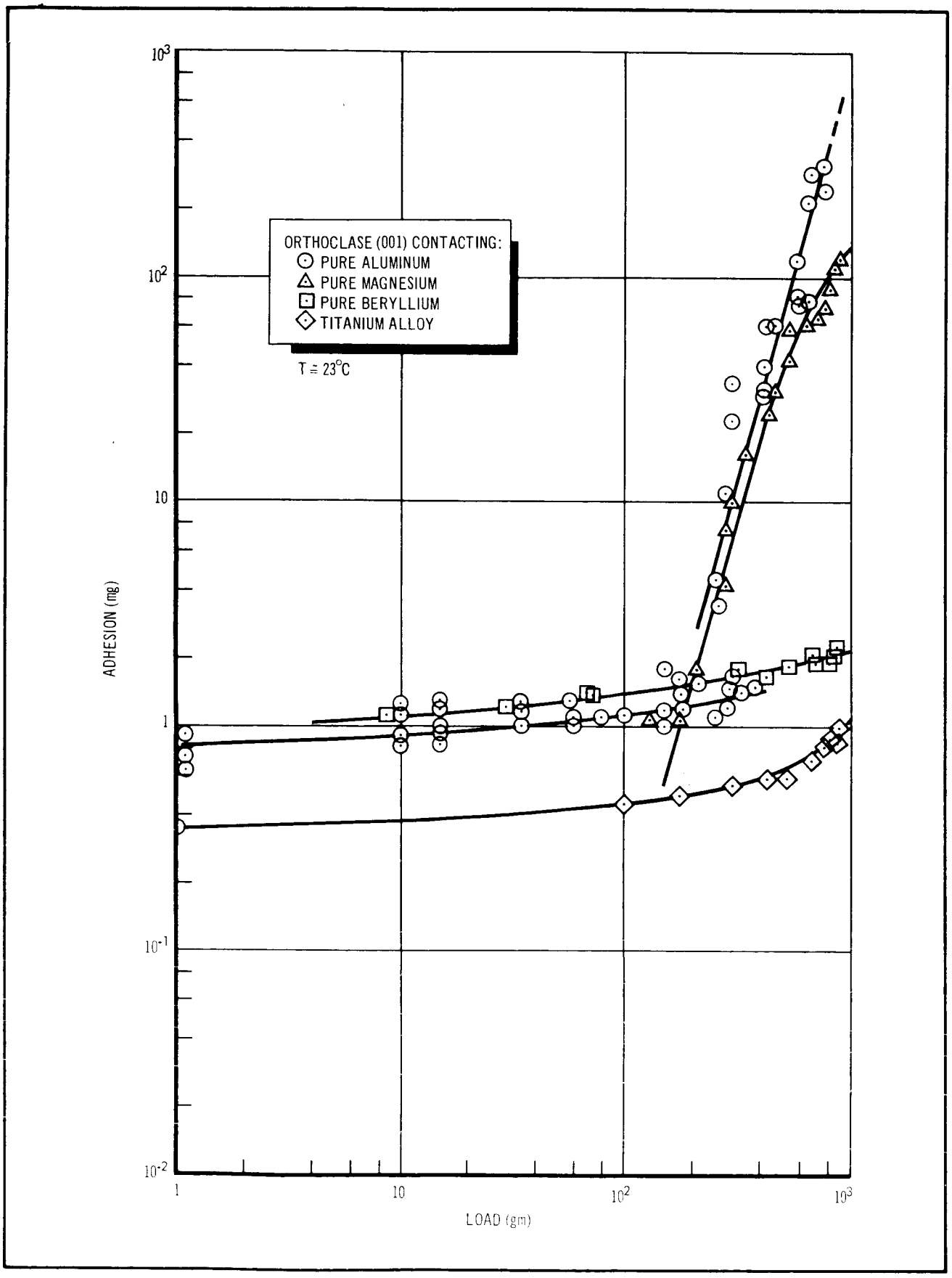

Figure 53. Adhesion Force vs Load for Silicates Contacting Metals – Metal Oxides

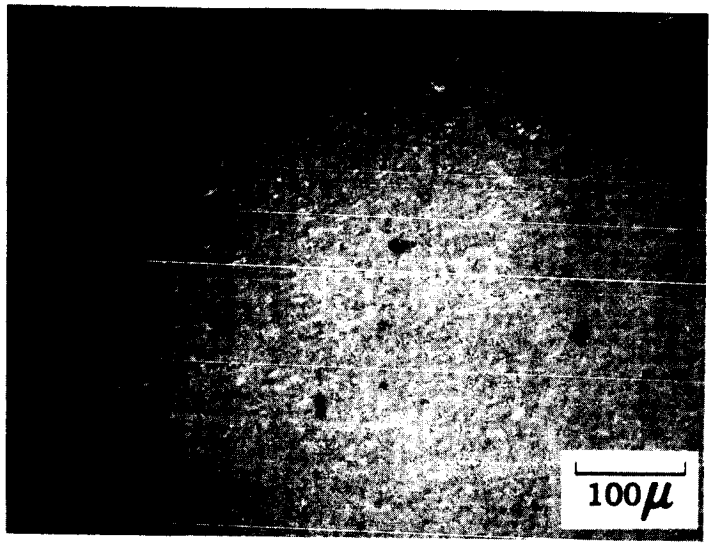

Figure 54. Orthoclase (001) Surface After Contact with Aluminum (Transmitted Light)

Figure 55. Magnesium Surface After Contact with Orthoclase (001) (Reflected Light)

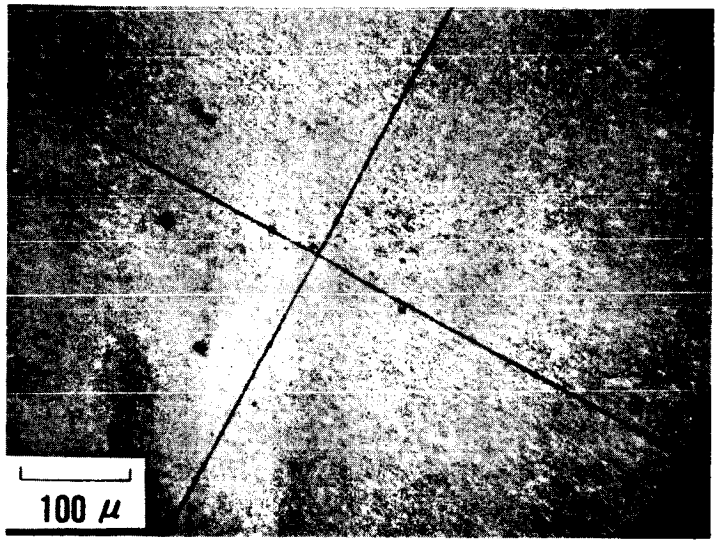

Figure 56. Orthoclase (001) Surface After Contact with Titanium (Reflected Light)

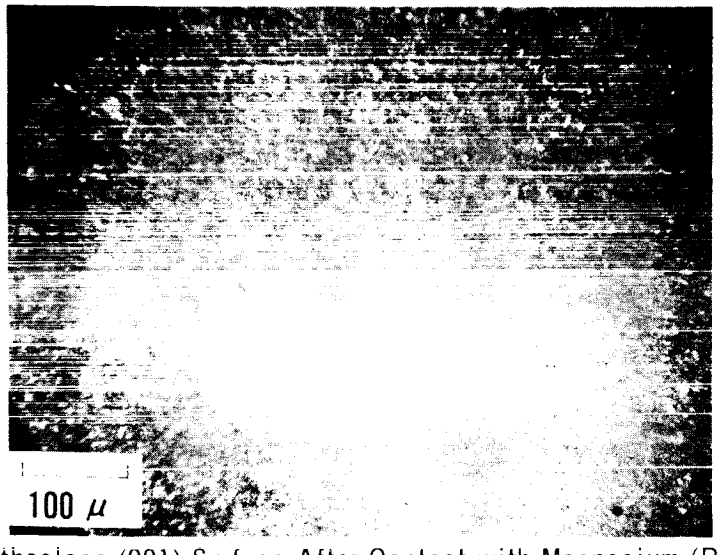

Figure 57. Orthoclase (001) Surface After Contact with Magnesium (Reflected Light)

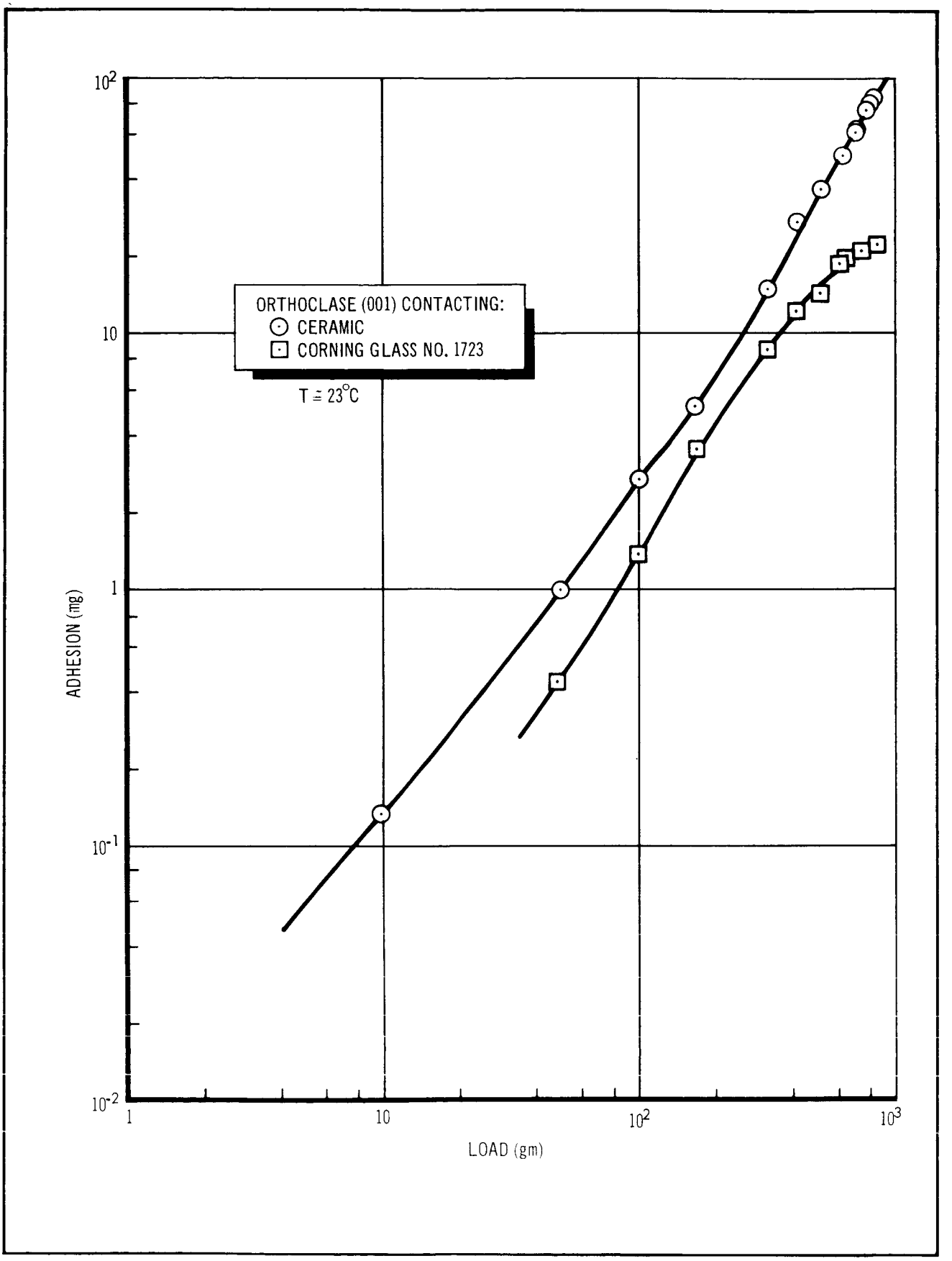

Figure 58. Adhesion Force vs Load for Silicates Contracting Ceramics and Glass

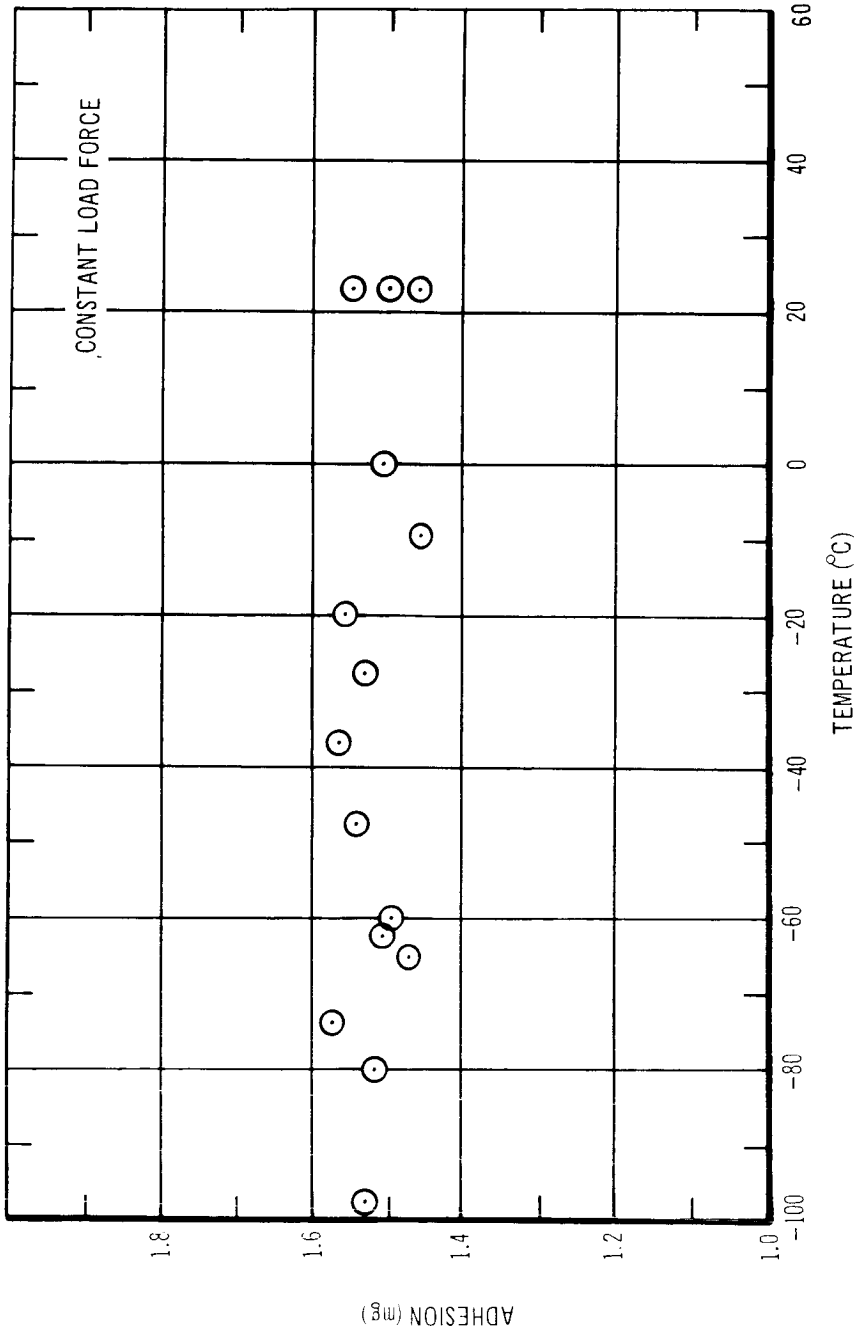

Figure 59. Adhesion Versus Temperature for Hornblende Contacting Bytownite

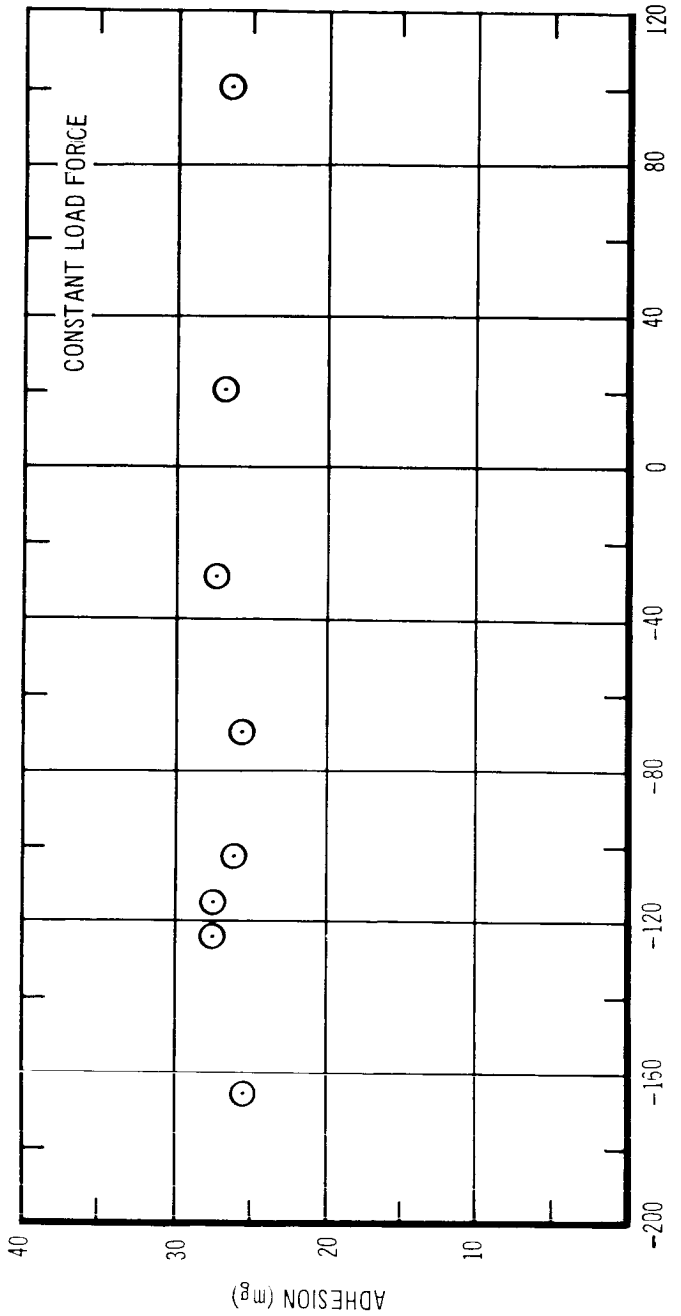

Figure 60. Adhesion Versus Temperature for Orthoclase Contracting Orthoclase